UNIVERSIDADE DE LISBOA
FACULDADE DE CIÊNCIAS
DEPARTAMENTO DE QUÍMICA E BIOQUÍMICA

Changes in synaptic plasticity and lipid raft composition in a rat model of temporal lobe epilepsy

Andreia Bento de Oliveira

Mestrado em Bioquímica
Especialização em Bioquímica

Dissertação orientada por:
Doutora Diana Cunha-Reis
Doutor Rodrigo de Almeida

2018

The most exciting phrase to hear in science, the one that heralds new discoveries, is not “Eureka!” but “That’s funny…”.

Isaac Asimov

Table of contents

Acknowledgments/Agradecimentos

Em primeiro lugar quero agradecer à minha orientadora, Doutora Diana Cunha-Reis, por me ter aceite para trabalhar neste seu projeto, no qual espero não ter desiludido. Um obrigada por acompanhar os meus primeiros passos rumo à investigação e por toda a ajuda, disponibilidade, e por todos os conselhos profissionais. Trabalhar consigo permitiu-me saber o que é ser uma boa investigadora e colega de laboratório, algo ao qual espero ser fiel no futuro. Um muito obrigada por tudo.

Nunca esquecendo o Professor Rodrigo de Almeida, por toda a ajuda e simpatia. Principalmente por me ter apresentado à Biofísica de Biomembranas que se tornou uma paixão. Ainda, por me ter aceite no seu grupo sem qualquer reserva. Não me poderia ter sentido mais incluída, e devido a isso estar-lhe-ei para sempre grata.

Ao restante grupo de Biofísica Molecular, Carla, António, Sr. Doutor Joaquim e Carolina, por toda a ajuda e acolhimento que prestaram a esta naba. Principalmente por todos os momentos de descontração (musical ou *baseboliana*) entre trabalho. Não poderia ter encontrado um grupo melhor para partilhar a minha loucura científica. Um carinho especial à Filipa, por todas as gargalhadas, amizade e inúmeras boleias (físicas e principalmente emocionais) sem as quais não teria conseguido manter a minha saúde.

Aos bioquímicos do meu coração (que pirosice): Ana, Rita e Guilherme por entenderem melhor que ninguém os desabafos em relação a pessoas que dizem "a" enzima. Por partilharem comigo noites de verdadeira loucura, nada científicas, cheias de intriga, ficção e revelações extraordinárias enquanto jogávamos os bons jogos de tabuleiro.

Às minhas meninas Joana e Iara, pela amizade e gargalhadas partilhadas já há 5 anos (bolas isso é muito tempo!). Obrigada por estimularem o meu intelecto com as vossas conversas sobre ciência, voluntariado e anatomia humana bicuda.

À minha árvore genealógica que apesar da dificuldade em perceberem o que é ser investigador, foi a crescer ao vosso lado que moldou o meu espírito crítico, e o empenho pelo trabalho que caracteriza a nossa família, e a mim também.

Por fim, ao meu pilar nisto tudo, que apesar de estar a passar por stresses próprios, sempre esteve lá para me ajudar, apoiar, ouvir. Percorremos a adversidade em conjunto, a comer bem, a dormir pouco, a fingir que conseguíamos emagrecer. Dedico este último parágrafo à minha *Sushi*, a gata do meu namorado. Ah, e a ele também claro, coitado. Obrigada Fernando, obrigada por me respeitares como mulher, amiga, cientista e cozinheira.

A todos e a quem me possa ter esquecido, um obrigada, por aturarem esta maluca.

Abstract

Temporal lobe epilepsy (TLE) is the most common form of epilepsy. In many cases, patients with TLE are resistant to antiepileptic drugs. Therefore, it is imperative to unravel the underlying molecular mechanisms that are the cause and/or consequence of the disease to find new strategies to fight it.

Synaptic plasticity is the ability of synapses to strengthen or weaken the communication efficiency in response to transient variations in their activity. Studies in the pilocarpine rat model of TLE indicate that neuronal hyperactivity in epilepsy is associated with abnormal synaptic plasticity, involving molecular changes in α-amino-3-hydroxy-5-methyl-4-isoxazole propionic acid receptors (AMPARs), in voltage-gated potassium channels Kv4.2, and post-synaptic proteins, post-synaptic protein 95 (PSD-95) and gephyrin.

Remodelling of lipid raft composition is believed to contribute to altered cognition and synaptic plasticity observed upon ageing and neurodegenerative diseases. However, it is still unknown if such changes contribute to the cognitive decline and altered synaptic plasticity observed in TLE.

In this thesis, an initial study was performed to evaluate changes in Kv4.2. channel levels and its phosphorylation in Thr_{602}, Thr_{607} and Ser_{438} observed in non-pathological long-term-potentiation (LTP; a type of synaptic plasticity) induced by a moderate θ-burst stimulation and their relation to PSD-95 and synaptosomal nerve-associated protein 25 (SNAP-25) levels was evaluated by western-blot in hippocampal membranes obtained from stimulated and control slices. As expected, PSD-95 and SNAP-25 levels did not change, but the levels of Kv4.2 channel and its phosphorylation at Ser_{438} and Thr_{602} increased following LTP induction, while phosphorylation at Thr_{607} did not change. These results suggest a possible role for Kv4.2 channels in LTP expression even with mild θ-burst stimulation patterns, through phosphorylation at Ser_{438} and Thr_{602} residues.

The main objective of this work was to unravel molecular mechanisms underlying TLE regarding the role of lipid raft changes in abnormal synaptic plasticity observed in TLE. For that, several approaches were used to characterize the chronic period of the Li^{2+}-pilocarpine model of TLE in the rat. First, histochemistry was performed in hippocampal slices from 12-month-old Wistar rats exhibiting long-term spontaneous recurrent seizures (SRSs) and *Sham* controls to evaluate anatomical changes in this tissue. In SRS animals, NeuN immunolabelling revealed a decrease in neurons in the pyramidal cell layer of CA1 and CA3 and in the *hilus* of the *dentate gyrus* (DG). Changes in the architecture of the granule cell layer of the DG were also detected for NeuN immunolabelling and Nissl-staining. Finally, using Timm-staining it was possible to detect mossy fibre sprouting. These findings show that the DG is the hippocampal region that suffers more damage in this model.

Molecular changes related to synaptic plasticity were studied by performing western-blot in hippocampal membranes isolated from SRS and *Sham* rats to evaluate: GluA1 and GluA2 AMPARs subunit levels, GluA1 phosphorylation in Ser_{831} and Ser_{845} and Kv4.2 channel expression; in addition, molecular changes related to profound changes in synaptic architecture were studied by targeting postsynaptic proteins PSD-95 and gephyrin and the presynaptic marker SNAP-25; finally, changes in planar lipid rafts and *caveolae* scaffolding proteins, flotillin-1 and caveolin-1 respectively, were monitored. The GluA1 and GluA2 subunit and PSD-95 levels decreased while the GluA1/GluA2 ratio, GluA1 phosphorylation in Ser_{831} and Ser_{845}, along with gephyrin and caveolin-1 levels increased in SRS animals. SNAP-25, Kv4.2 channel and flotillin-1 levels did not change.

To initiate the biophysical study of lipid rafts in model membranes obtained from synaptic lipids from the Li^{2+}-pilocarpine rat model of TLE, the biophysical imaging and quantification of lipid rafts in giant unilamellar vesicles obtained from binary and ternary artificial lipid mixtures was performed. Giant unilamellar vesicles preparation by electroformation was optimized with success.

Changes found for AMPARs subunit stoichiometry and phosphorylation contribute to an increase in synaptic transmission that surely contributes to enhancement of neuronal excitability, and to progression of the disease. A decrease in PSD-95 and gephyrin suggests that excitatory transmission is down-regulated and inhibitory transmission is up-regulated, contributing to lower neuronal excitability, hinting on an adaptive molecular mechanism that is trying to counteract the hyperexcitability that characterizes epilepsy. The increase found for caveolin-1 suggests a new role for this protein in TLE, that is probably neuroprotection, as it occurs in other diseases.

Key words: Temporal lobe epilepsy, Synaptic plasticity, Lipid rafts.

Resumo

A epilepsia do lobo temporal (do inglês, TLE) é o tipo de epilepsia mais comum. Na maioria dos casos os pacientes com TLE são resistentes ao tratamento com fármacos antiepiléticos. É importante compreender os mecanismos moleculares subjacentes à doença, de modo a encontrar novas estratégias para combatê-la.

Estudos no modelo da pilocarpina em rato indicaram que a hiperexcitabilidade na TLE experimental está associada a plasticidade sináptica anómala, através de alterações moleculares que consequentemente afetam a excitabilidade neuronal.

A plasticidade sináptica é a capacidade que as sinapses apresentam de reforçar ou atenuar o seu rendimento em resposta a variações transientes na sua actividade que resultam de estímulos fisiológicos. A nível molecular, este mecanismo é caracterizado por alterações bidirecionais no número e actividade de alguns receptores de neurotransmissores e canais. Na potenciação de longo prazo (do inglês, LTP), o tipo de plasticidade sináptica mais estudado e conhecido no hipocampo, algumas destas alterações incluem o aumento dos receptores de ácido α-amino-3-hidroxi-5-metil-4-isoxazolo propiónico (Rs AMPA) no neurónio pós-sináptico, que aumenta a eficiência da comunicação glutamatérgica, e diminuição da corrente K^+ do tipo A (I_A), mediada por canais de potássio dependentes de voltagem 4.2 (Kv4.2), que reduz a excitabilidade dendrítica.

A modulação dos Rs AMPA pode afetar a excitabilidade neuronal através de alterações na estequiometria das subunidades e da fosforilação das mesmas. Estas alterações estão ambas implicadas na expressão da LTP no hipocampo assim como nas alterações patológicas em modelos de TLE em roedores. O aumento da excitabilidade neuronal está relacionado com a presença de Rs AMPA sem a subunidade GluA2, permeáveis ao ião Ca^{2+}, e com a fosforilação da subunidade GluA1 na Ser_{831} e na Ser_{845}, através do aumento dos Rs AMPA com maior condutância, na região sináptica.

Alterações na expressão e modulação do canal Kv4.2 foram observadas tanto na LTP como na TLE. Sendo o principal mediador da corrente I_A, a sua regulação afeta a excitabilidade dendrítica, que dela depende. Uma forma de modular o canal é através da fosforilação nos resíduos Thr_{602}, Thr_{607} e Ser_{438}.

A densidade pós-sináptica (do inglês, PSD) tem um importante papel na regulação de cascatas de sinalização que ajustam a composição molecular das entidades pós-sinápticas necessárias para manter a plasticidade sináptica. Duas proteínas da PSD associadas à TLE são a proteínas pós-sináptica 95 (PSD-95), que é expressa exclusivamente em sinapses glutamatérgicas (excitatórias), e a gefirina que se encontra exclusivamente em sinapses glicinergicas e GABAergicas (inibitórias).

No sistema nervoso podem ser encontradas tanto jangadas lipídicas planares como caveolas, associadas às proteínas específicas, flotilinas e caveolinas, respectivamente. Estas jangadas são microdomínios membranares ordenados, ricos em colesterol e esfingolípidos e que estão associados a diferentes funções celulares. Estudos recentes sugerem que estes microdomínios podem estar envolvidos na plasticidade sináptica, fornecendo a estrutura necessária à organização e compartimentalização de diferentes eventos moleculares na neurotransmissão, tendo também um papel na sua regulação dinâmica de forma a aumentar ou diminuir a eficiência da comunicação sináptica. A remodelação da composição das jangadas lipídicas ocorre durante o desenvolvimento e contribui para alterações cognitivas e de plasticidade sináptica observadas durante o envelhecimento e doenças neurodegenerativas. No entanto, ainda não é claro se tais alterações contribuem para o declínio cognitivo e para as alterações na plasticidade sináptica encontradas na TLE.

O principal objectivo deste trabalho foi avaliar as alterações nos marcadores da plasticidade sináptica e na composição sináptica de jangadas lipídicas num modelo de TLE induzida por lítio-pilocarpina no rato, de forma a desvendar os mecanismos moleculares subjacentes à doença.

Num primeiro passo avaliaram-se por *western-blot* as alterações nos níveis e na fosforilação do canal Kv4.2 nos resíduos de Thr_{602}, Thr_{607} e Ser_{438}, relativamente à PSD-95 e à proteína pre-sináptica SNAP-25, em membranas de hipocampo obtidas de fatias nas quais se induziu LTP com um estímulo θ-*burst* moderado, que mimetiza a actividade neuronal fisiológica na região CA1 do hipocampo durante a aprendizagem e memória.

Apesar dos níveis da proteína pós-sináptica, PSD-95 e da pré-sináptica, SNAP-25 não se alterarem em resposta à estimulação com θ-*burst* moderado, como era esperado, os níveis do canal Kv4.2 e da sua fosforilação nos resíduos de Ser_{438} e Thr_{602} aumentaram. Estes resultados sugerem um papel da regulação do canal Kv4.2 na LTP, através da fosforilação nos resíduos de Ser_{438} e Thr_{602}.

Para a caracterização do modelo de Li^{2+}-pilocarpina no período crónico da TLE, foram primeiro realizados ensaios de histoquímica em fatias de hipocampo de ratos Wistar com 12 meses que exibiam convulsões espontâneas recorrentes (SRSs) induzidas pelo método do Li^{2+}-pilocarpina e com controlos *Sham*. Nos ratos modelos da TLE de Li^{2+}-pilocarpina, usando o marcador NeuN foi possível observar uma diminuição de neurónios na camada de células piramidais da região CA1 e CA3 e do *hilus* do giro dentado (DG). Foi vista também uma alteração de disposição dos neurónios da camada de células granulares do DG também observadas em resultados da coloração de Nissl. Por fim, com a coloração de Timm foi possível detetar *sprouting* axonal no DG nos ratos modelo da TLE, concordante com o observado em trabalhos anteriores. Neste estudo confirmamos então que o DG é a região do hipocampo que sofre maior dano neste modelo, o que é concordante com o observado no DG de pacientes com TLE.

As alterações moleculares associadas à plasticidade sináptica foram avaliadas por *western-blot* em membranas de hipocampo obtidas de ratos modelo da TLE e *Sham* tendo como alvo: a subunidade GluA1 e GluA2 dos Rs AMPA, a fosforilação da subunidade GluA1 nos resíduos de Ser_{831} e na Ser_{845} e a expressão do canal Kv4.2. Para avaliar alterações estruturais nas sinapses estudaram-se as proteínas da PSD, PSD-95 e gefirina e o marcador pré-sináptico SNAP-25. Por fim, estudou-se a expressão das proteínas específicas de jangadas lipídicas, flotilina-1 e caveolina-1.

Os níveis de subunidade GluA1 e GluA2 diminuíram em ratos modelo da TLE, enquanto que a razão GluA1/GluA2 e a fosforilação da subunidade GluA1 na Ser_{831} e na Ser_{845} aumentaram. Estas alterações contribuem para um aumento da transmissão glutamatérgica que certamente contribui para o aumento da excitabilidade neuronal, e para a progressão da doença.

Os níveis de SNAP-25 não se alteraram nos ratos modelo da TLE de Li^{2+}-pilocarpina. Face aos níveis desta proteína a expressão relativa de PSD-95 diminuiu enquanto que a da gefirina aumentou. Uma vez que o PSD-95 e a gefirina são específicos para sinapses glutamatérgicas e GABAérgicas/glicinérgicas, respetivamente, estes resultados evidenciam que há mecanismos associados à transmissão glutamatérgica que estão diminuídos neste modelo enquanto que outros associados à transmissão GABAérgica/glicinérgica estão aumentados. Isto, por sua vez, sugere um aumento da transmissão inibitória e diminuição da excitatória, o que na totalidade diminui a excitabilidade neuronal. Esta alteração das proteínas da PSD poderá ser um mecanismo de adaptação molecular para contrariar a hiperexcitabilidade causada em parte pelas alterações descritas para os Rs AMPA, garantindo a sobrevivência do animal.

A expressão do canal Kv4.2 não se alterou nos animais modelo da TLE, no entanto observa-se uma tendência para aumento e o estudo de um número mais elevado de animais poderá tornar mais clara esta questão.

Finalmente, os níveis de flotilina-1 não se alteraram no modelo de TLE em rato enquanto que os níveis de caveolina-1 aumentaram, sugerindo que a caveolina-1 e alterações nas jangadas lipídicas têm um papel na fisiopatologia da TLE. Face à sua ação noutros modelos de doença no SNC, este papel será provavelmente neuroprotector.

Para iniciar o estudo biofísico de jangadas lipídicas em membranas modelo preparadas com lípidos sinápticos do rato modelo da TLE de Li^{2+}-pilocarpina, foram realizadas a deteção e quantificação biofísica de jangadas lipídicas em vesículas gigantes unilamelares preparadas com misturas de lípidos artificiais. A otimização da preparação de vesículas gigantes unilamelares por eletroformação foi efetuada com sucesso.

Este trabalho revela alterações moleculares nunca descritas tanto para a LTP como para o período crónico da TLE no modelo de Li^{2+}-pilocarpina em rato. No entanto, serão necessários estudos adicionais para melhor compreender o que é causa ou consequência da doença e, mais importante, o que pode ser feito para tratar ou prevenir a TLE.

Palavras chave: Epilepsia do lobo temporal, Plasticidade sináptica, Jangadas lipídicas.

List of Figures

List of Tables

Abbreviations and Symbols

aCSF	artificial cerebrospinal fluid
AMPAR	α-amino-3-hydroxy-5-methyl-4-isoxazole propionic acid receptors
APS	ammonium persulfate
BSA	bovine serum albumin
CA1	*cornu Ammonis* area 1
CA3	*cornu Ammonis* area 3
Ca^{2+}	calcium ion
CaMKII	Ca^{2+}/calmodulin-dependent protein kinase II
Chol	cholesterol
CNS	Central nervous system
CTD	carboxy-terminal domain
CTR	control
DG	*dentate gyrus*
DOPC	1,2-dioleoyl-*sn*-glycero-3-phosphocholine (DOPC),
DPPC	1,2-dipalmitoyl-*sn*-glycero-3-phosphocholine
EDTA	ethylenediamine tetraacetic acid
EEG	electroencephalograms
EPSP	excitatory post-synaptic potential
ERK	extracellular signal-regulated kinases
fEPSP	field excitatory post-synaptic potential
GABA	γ-aminobutyric acid
Glu	glutamate
GluA1 Ser_{818}	Serine residue 818 of the GluA1 subunit
GluA1$PSer_{831}$	GluA1 phosphorylated on Serine 831
GluA1$PSer_{845}$	GluA1 phosphorylated on Serine 845
GPHN	gephyrin gene
GPI	glycosylphosphatidylinositol
GUV	giant unilamellar vesicle
HEPES	4-(2-hydroxyethyl)-1-piperazineethanesulfonic acid
HRP	horseradish peroxidase
I_A	A-type K^+ current
i.m.	intramuscular
i.p.	intraperitoneal
KA	kainic acid
Kv4.2	voltage-gated potassium channel 4.2
Kv 4.2 Thr_{38}	Threonine residue 38 of the Kv4.2 channel
Kv4.2$PSer_{438}$	Kv4.2 phosphorylated on Serine 438
Kv 4.2 Ser_{552}	Serine residue 552 of the Kv4.2 channel
Kv 4.2 Ser_{616}	Serine residue 616 of the Kv4.2 channel
Kv4.2$PThr_{602}$	Kv4.2 phosphorylated on Threonine 602
Kv4.2$PThr_{607}$	Kv4.2 phosphorylated on Threonine 607
l_d	liquid-disordered
Li^{2+}-Pilo	Lithium-pilocarpine
l_o	liquid-ordered
LTD	long-term depression

LTP	long-term potentiation
MAPK	mitogen-activated protein kinases
Mg^{2+}	magnesium ion
mPFC	medial prefrontal cortex
MRI	magnetic resonance imaging
MTLE	mesial temporal lobe epilepsy
N.A.	numerical aperture
Na^{+}	sodium ion
NeuN	Neuronal nuclear protein
NMDA	*N*-methyl-D-aspartate
NTD	N-terminal domain
PKA	protein kinase A
PKC	protein kinase C
PMSF	Phenylmethanesulfonyl fluoride
PSD	post-synaptic density
PSD-95	post-synaptic density protein 95
PVDF	polyvinylidene fluoride
Rhod-DOPE	N-(lyssamine Rhodamine B sulfonyl)-1,2-dioleoyl-*sn*-glycero-3-phosphoethanolamine
SDS	sodium dodecyl sulfate
SE	*status epilepticus*
SEM	Standard error of the mean
SNAP-25	synaptosomal-associated protein 25
SNARE	soluble n-ethylmaleimide-sensitive factor attachment protein receptor
s_o	solid-ordered
SRS	spontaneous recurrent seizures
TBS	θ-burst stimulation
TBST	Tris-buffered saline with Tween 20
TEMED	tetramethylethylenediamine
TLE	temporal lobe epilepsy
TM	transmembrane domain
Tris	2-amino-2-(hydroxymethyl)propane-1,3-diol

1. Introduction

1.1. Epilepsy

Epilepsy is one of the most common neurological diseases[1], and is characterized by recurrent unpredictable seizures involving the synchronized firing of multiple neurons. It is associated with a chronic imbalance between excitatory and inhibitory transmission. Besides genetic changes, which make up a minor cause for the disease, epilepsy is believed to be a secondary consequence of brain insults such as acute seizures caused by toxic or febrile stimuli, stroke, head trauma, or cerebral infections[2]. According to the *Epilepsy Foundation*, approximately 60% of all living people with epilepsy have temporal lobe epilepsy (TLE), making it the most common form of focal epilepsy in humans[3,4]. Some of the changes found in patients with TLE include abnormal electroencephalograms (EEGs), memory impairment, hippocampal atrophy and sclerosis, as seen in Figure 1.1. At the cellular level changes include neuronal loss, gliosis and axonal sprouting, but also abnormal morphology. With the progression of the disease, alterations can spread to the rest of the brain, as seen in Figure 1.1 where besides the hippocampus, the whole right temporal cortex shows atrophy.

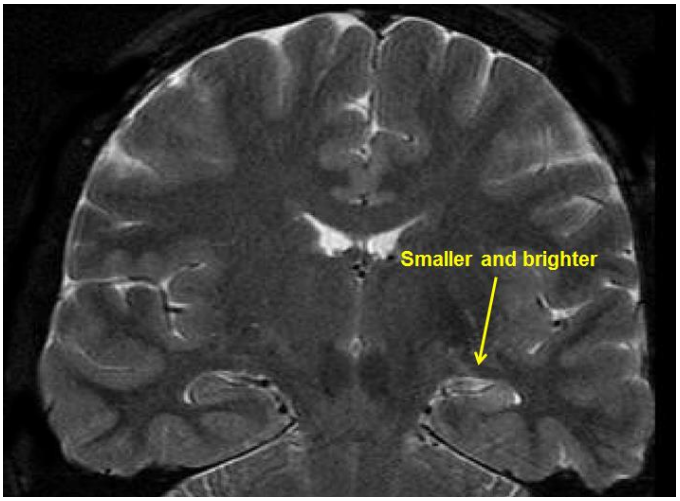

Figure 1.1. Magnetic resonance imaging (MRI) brain scan from a patient with mesial TLE (MTLE). MTLE is associated with hippocampal atrophy and sclerosis, which includes neuronal loss and gliosis, but also loss of internal architecture. In this case an asymmetry of the brain is detected which is due to the temporal cortex atrophy.[4]

Epilepsy is a major public health concern since 50 million people worldwide are epileptic[1], and currently there are no disease-modifying therapies. Possible treatments include antiepileptic drugs, ketogenic diet, neurosurgical resection, and electrical stimulation of the nervous system[5]. In the particular case of TLE, about one third of the patients do not respond to therapy with antiepileptic drugs having to resort to hippocampal and/or amygdala resection surgery, from which 70% of the patients become seizure-free[4]. This drug resistance and the attempt to avoid cerebral surgery are the main reasons why it is imperative to explore the molecular mechanisms underlying TLE and find new strategies to fight it.

Multiple experimental approaches have been developed to study TLE disease mechanisms. *In vitro* models usually consist of mammalian neuronal cell cultures or brain slices from animals, that are subjected to epileptic crisis (usually monitored using electrophysiological recordings), and can be acutely isolated or organotypic slices[6]. A wide range of species have been used to study epilepsy in an *in vivo* fashion, but the most common animals used to model TLE are the rodents *Rattus norvegicus* or *Mus musculus* (see ref [7] for review), due to their small size, rapid breeding and the possibility to use advanced genetic tools. Several procedures can be used to induce chronic seizures in these animals, such as: 1) electrical stimulation which includes the kindling model; 2) administration of chemoconvulsants

such as kainic acid (KA) or pilocarpine; and, less frequently, 3) brain hypoxia or ischaemia models. In addition, genetic models of seizure-prone rodents have been used.

The properties of some antiepileptic drugs available today, *e.g.* phenobarbital, to which some patients are resistant, were found using simple acute seizure models[5]. One possible hypothesis is that the drug resistance found in epileptic patients is due to the fact that the acute models do not mimic the chronic state of the patients, characterized by spontaneous recurrent seizures (SRSs)[5]. Therefore, chronic models, also called SRS models are being used to better understand the disease and search for novel therapeutic approaches.

In the lithium-pilocarpine (Li^{2+}-Pilo) rat model of SRSs, pathological features including histological, behavioral, electroencephalographic (EEG) and pharmacological responses to antiepileptic and other drugs, resemble those observed in patients with MTLE, making it a good model of the human disease. The injection of pilocarpine induces an initial crisis of epileptic seizures or *status epilepticus* (SE), that lasts for up to a few hours. After typically 15 to 44 days with no observable seizures, a time called latent period, the animal starts to exhibit SRSs[8,9].

Abnormal synaptic plasticity has been found in animal models of epilepsy[3,10,11] and in epileptic patients[12], not only during epileptogenesis (the process by which the brain develops epilepsy[13]) but also in the chronic period of the disease. This altered plasticity relies on changes in α-amino-3-hydroxy-5-methyl-4-isoxazole propionic acid receptors (AMPARs) and the voltage-gated potassium channels 4.2 (Kv4.2 channel), among others.

To better understand this association between disease and synaptic plasticity, it is important to first define synaptic plasticity itself.

1.2. Synaptic plasticity

Synaptic plasticity is a cellular process that confers synapses the ability to strengthen or weaken their communication in response to transient variations in their activity. These changes can endure for short or long periods and are considered crucial cellular mechanisms in learning and memory formation. Synaptic plasticity can involve changes at the molecular level, such as bidirectional scaling in the number and activity of some neurotransmitters receptors and channels[14], or more profound structural cellular changes, like the formation of new synaptic contacts.

In vitro, synaptic plasticity involves cellular changes in synaptic communication that can occur in a broad range of time frames and through different molecular processes depending on the stimulation pattern[15–17]. The two most studied forms of synaptic plasticity in the hippocampus are long-term potentiation (LTP) and long-term depression (LTD), since the lasting duration of the molecular and cellular changes observed suggests that these are crucial cellular mechanisms in hippocampal memory storage[14].

Using 2-amino-5-phosphonopentanoate, a competitive *N*-methyl-D-aspartate (NMDA) receptor antagonist, it was found that, LTP at hippocampal glutamatergic synapses is triggered by the activation of NMDA receptors[18]. The sustained depolarization of the postsynaptic membrane releases magnesium ions (Mg^{2+}) that block NMDA receptors channels, allowing calcium ions (Ca^{2+}) to enter the cell (Figure 1.2 - B)[19]. The influx of Ca^{2+} ions leads to autophosphorylation of enzyme Ca^{2+}/calmodulin-dependent protein kinase II (CaMKII) causing its persistent activation[15,20]. This enzyme, in turn, catalyzes the phosphorylation of AMPARs[21,22].

The increase of intracellular Ca^{2+} and the consequent activation of CaMKII triggers the molecular events that drive synaptic plasticity (Figure 1.2) such as the recruitment of AMPARs to the synaptic region of the postsynaptic neuron, which then becomes easier to stimulate showing an increase in excitatory post-synaptic potentials (EPSPs)[23]. Simultaneously, there is an increase in dendritic excitability caused by the decrease of A-type K^+ current (I_A) mediated by Kv4.2 channel (see section

1.4)[24]. Other changes also include an increase in neurotransmitter release, an increase in postsynaptic ribosomes, changes in calcium compartmentalization, and growth of the actin cytoskeleton[25,26].

Other structural synaptic changes were found following LTP induction with θ-burst stimulation (TBS). The neck of dendritic spines (input neuronal protrusions) becomes wider and shorter, while the volume of the spine head increases, which facilitates protein traffic from dendrites into the spines, and enhances the synaptic contact area, leading to increased efficacy of synaptic transmission[27]. These spine changes are accompanied by modifications in the postsynaptic density (PSD)[28]. The PSD suffers a dynamic reorganization that modulates glutamate receptors (excitatory transmission) through linking these receptors to downstream signaling molecules that guarantee LTP expression[29].

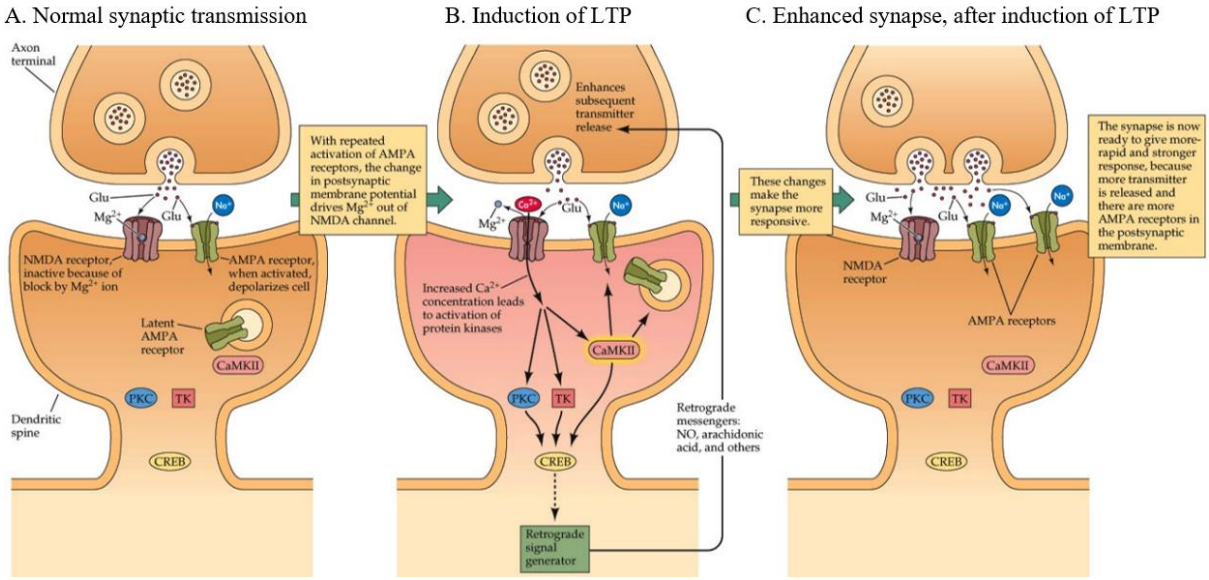

Figure 1.2. **Induction of LTP depends on NMDA receptors and AMPARs.** In normal synaptic transmission (**A**), NMDA receptors have Mg^{2+} that blocks Ca^{2+} influx through the channel of this receptors. Sustained depolarization of the postsynaptic membrane (caused by high-frequency or TBS) drives Mg^{2+} out of the channel allowing Ca^{2+} influx (**B**), triggering synaptic changes such as the increase of AMPARs in the postsynaptic membrane (**C**).[30]

Although many studies have focused on LTP, there is still a lot to uncover. One distinct problem is the fact that when this type of synaptic plasticity is being investigated the procedures followed, specifically stimulation that induces LTP, are not kept the same between studies, making it hard to learn how this mechanism is expressed and maintained physiologically.

1.3. AMPA receptors

AMPARs (Figure 1.3) mediate most of the excitatory glutamatergic neurotransmission across chemical synapses in the central nervous system (CNS), and changes in their activity, phosphorylation state, subcellular targeting and expression levels have been associated with physiological synaptic plasticity and TLE pathology.

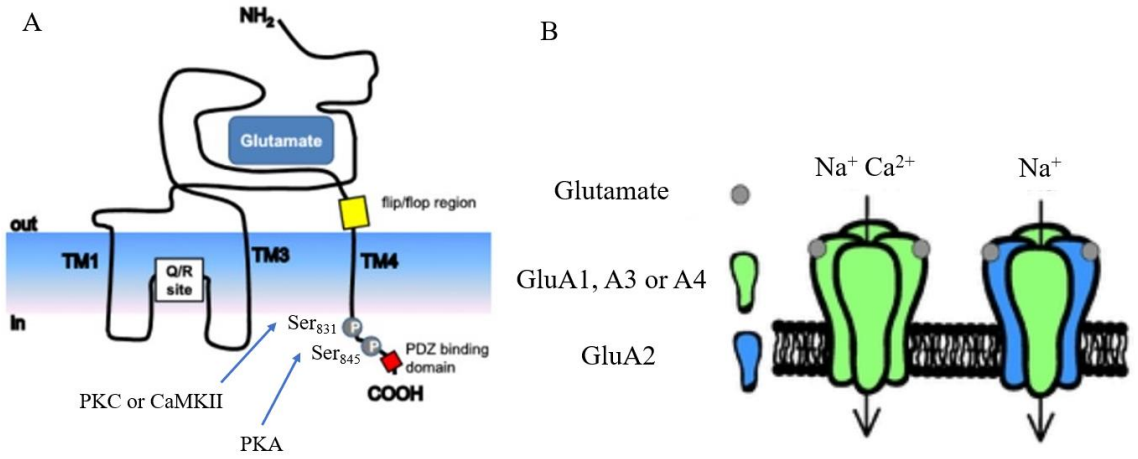

Figure 1.3. Overview of the AMPARs structure (A) and subunit composition (B). Each subunit contains four different hydrophobic domains (TM) that transverse the membrane. When the receptor is assembled with GluA2, the channel is not permeable to Ca^{2+}, but without GluA2 the channel is permeable to Ca^{2+}.[31,32]

AMPARs are transmembrane homo or hetero-tetrameric ionotropic receptors assembled from four different subunits, GluA1-4 [33] that share 68-74% amino acid sequence identity[34]. These differ in the C-terminus where some post-translation modifications can occur, such as phosphorylation[31]. In the adult hippocampus, there are two major populations of AMPARs: those assembled with GluA1 and GluA2 or those assembled with GluA3 and GluA2 subunits[35]. Only a small pool of AMPARs lack GluA2, being composed by GluA1 and GluA3 or solely by GluA1 subunits (homomeric receptors)[35].

Subunit stoichiometry is important in the modulation of gating kinetics, ion permeability and responsiveness to an array of small-molecule channel modulators[36]. When the receptor lacks the GluA2 subunit, the core channel displays a strong, inwardly rectifying current-voltage relation as well as Ca^{2+} permeability, but not when GluA2 is present (Figure 1.3 - B)[37,38].

Knockdown of hippocampal GluA2 subunit promotes hyperexcitability, leading to a decrease in seizure threshold and seizure-like behavior[39], thus increasing the risk of epileptogenesis[40,41].

AMPARs permeable to Ca^{2+} (lacking the GluA2 subunit), have been implicated in the expression of hippocampal LTP through protein kinase A (PKA)-dependent mechanisms[42], which occur only when LTP is induced with strong and repeated TBS patterns. Following LTP induction a transient insertion of AMPARs without GluA2 in synapses, was observed[42,43], suggesting that GluA2-lacking AMPARs might have a part in the expression of LTP. However, LTP can also occur without any detectable changes in AMPAR subunits stoichiometry[44], which suggests that other mechanisms and changes might also play a role in mediating and consolidating LTP.

After 85 days of SE induction with pilocarpine, mRNA levels of GluA2 are increased in the *dentate gyrus (*DG) of the rat hippocampus, but decreased in the CA1 area of the rat hippocampus[45]. An increase in the mRNA levels of GluA2 in the DG of the rat hippocampus was also detected, 2 weeks after SE induced with Li^{2+}-Pilo[46].

Studies also relate GluA2 subunits-lacking AMPAR with TLE. One week after SE induction by Li^{2+}-Pilo (latent period), three-week-old Wistar rats show no changes in the GluA1/GluA2 ratio in the hippocampus, but three days after SE the same ratio is increased in the medial prefrontal cortex (mPFC)[3].

1.3.1. Receptor phosphorylation

Besides subunit stoichiometry, other mechanisms regulate AMPARs. GluA1 can undertake certain post-translation modifications such as phosphorylation in serine residues 818 (Ser_{818}), 831 (Ser_{831}) and 845 (Ser_{845}), which have been implicated in LTP expression. Also, GluA2 phosphorylation at serine residue 880 catalyzed by protein kinase C (PKC) has been associated with LTD, another synaptic

plasticity mechanism. For instance, the use of specific antibodies for phosphorylated GluA1 on Ser_{831} or on Ser_{845}, showed that both residues are phosphorylated when LTP is induced in the CA1 region of the hippocampus with four episodes of TBS, each consisting of ten trains delivered at 5Hz of four pulses at 100Hz[47], a very strong stimulation paradigm.

Our group studied GluA1 phosphorylation when the induction of LTP was carried using only one episode of TBS, each comprising only five trains of stimuli. Under these conditions, the phosphorylation of GluA1 subunits occurred only at Ser_{831} without changes in the GluA1 levels or phosphorylation at Ser_{845} (Figure 1.4)[48]. This difference is a consequence of the different stimulation paradigms applied and is consistent with the observations of Park *et al*., reporting that LTP induced by TBS is only PKA-dependent when stronger and repeated TBS patterns are used[49]. Thus, only under these conditions phosphorylation at both Ser residues will happen, which suggests that these events are important in different phases of LTP: both Ser_{831} and Ser_{845} phosphorylation are required for late LTP, but only Ser_{831} phosphorylation is associated with the initial phase of LTP.

Ser_{831} phosphorylation can be catalyzed by PKC[50] or by CaMKII[21,22], an enzyme that, as mentioned before, has a role in LTP induction. This modification can lead to an increase of the time that AMPARs occupy the higher conductance states[51], correlating to the increased conductance of synaptic AMPARs during LTP. This phosphorylation also drives AMPARs to the synaptic region[52,53].

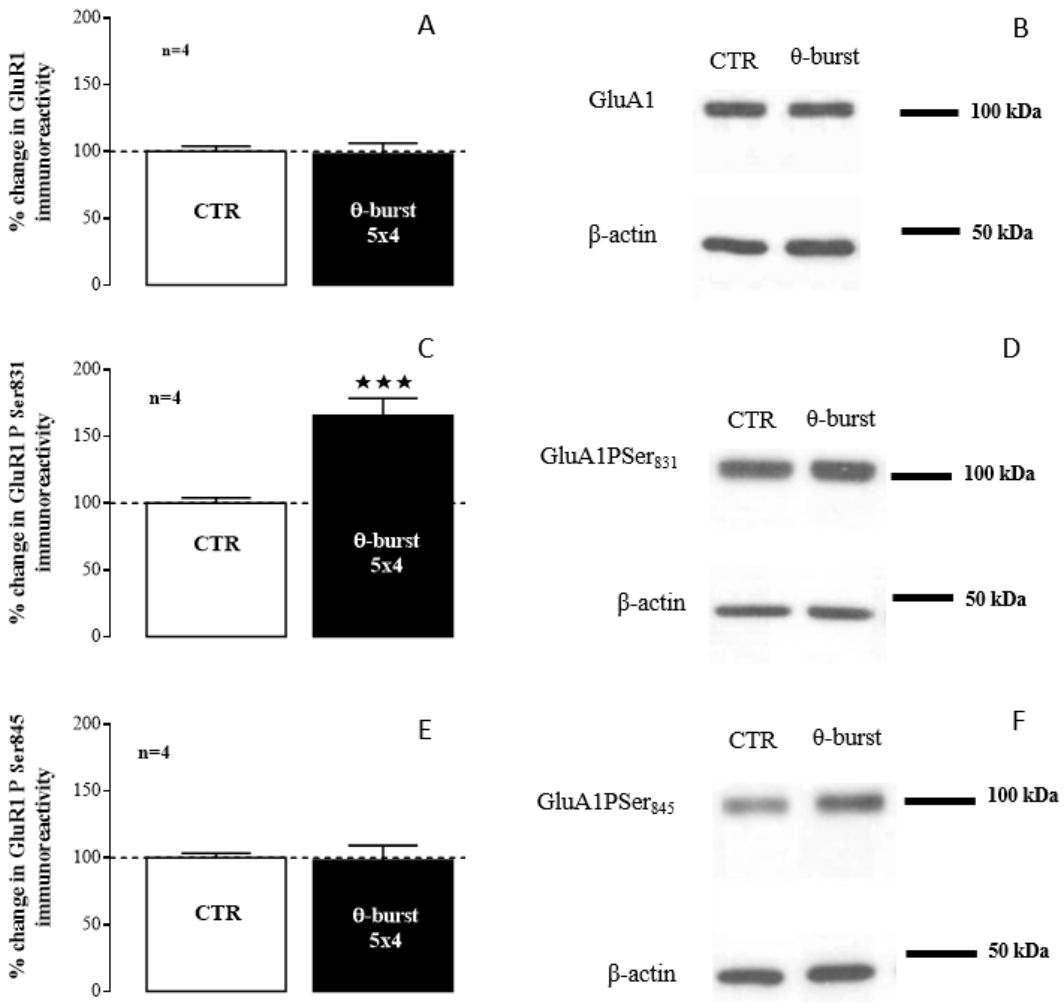

Figure 1.4. GluA1 levels and phosphorylation following LTP induction with moderate TBS. Representative western-blots (**B, D, F**) and averaged changes observed in reactivity (**A, C, E**) in western-blots probing for GluA1 levels and phosphorylation on Ser_{845} and Ser_{831}. Levels of GluA1 phosphorylated in Ser_{831} (**C, D**) were increased following LTP induction with TBS, but not total GluA1 levels or its phosphorylation on Ser_{845}. CTR: control. ⋆ ⋆ ⋆p -value < 0.001, Student's t-test [48].

Phosphorylation of Ser_{845} of GluA1 subunit is catalyzed by PKA[50], which induces the insertion of AMPARs from the intracellular pool to the extra-synaptic region of the plasma membrane[52,53]. This modification also increases the open-probability of the receptor[54].

Phosphorylation at these two Ser residues has also been related to TLE pathology. Lopes *et al* showed that 50 days after SE was induced with pilocarpine (chronic period), levels of GluA1 phosphorylated in Ser_{845} were reduced in the rat hippocampus, without any changes in GluA1 phosphorylated in Ser_{831} or in GluA1 expression levels[55]. In another study, rats showing SRSs 60 days after SE induction with pilocarpine (chronic period) exhibited a decrease in GluA1 phosphorylation in Ser_{845} in the dorsal hippocampus, and a decrease of GluA1 phosphorylation in Ser_{831} in the ventral hippocampus[8].

1.4. Kv4.2 channel

Across the neuron membrane, a variety of channels can be found, each contributing to different ionic currents. The largest and most diverse group of these ion channels is the potassium channel family, that has an important role in controlling neuronal excitability and plasticity[56]. As mentioned above, the I_A current plays an important role in the enhancement of dendritic excitability associated with LTP. The main mediator of this current in hippocampal neurons is the Kv4.2 channel[57].

Kv4.2 belongs to the superfamily of potassium channels with six hydrophobic transmembrane domains (Figure 1.5)[58] and is mostly expressed in the distal dendrites of neurons[59,60]. In response to a depolarization, the channel pore opens due to a conformational change triggered by the voltage sensor found in the fourth TM domain[61].

Channel properties and function can be regulated by post-translational phosphorylation. There are a few highly conserved sites that can be phosphorylated by ERK (extracellular signal-regulated kinases) and other kinases of the MAPK (mitogen-activated protein kinases) family like the threonine 602 residue (Thr_{602}) and threonine 607 (Thr_{607})[62,63]. When this happens, I_A decreases, and internalization of the channel occurs[63]. ERK family can also catalyze the phosphorylation of Ser_{616}, which suppresses the channel's activity[64].

PKA also phosphorylates some sites in Kv4.2 channel, such as the threonine 38 residue (Thr_{38}) or serine 552 residue (Ser_{552}). The consequences of phosphorylation on Thr_{38} are unknown, but phosphorylation of Ser_{552} causes internalization of the channel[65].

Another possible phosphorylation site is Ser_{438}, that can be phosphorylated by CaMKII, causing an increase of cell-surface expression of Kv4.2 channel[66].

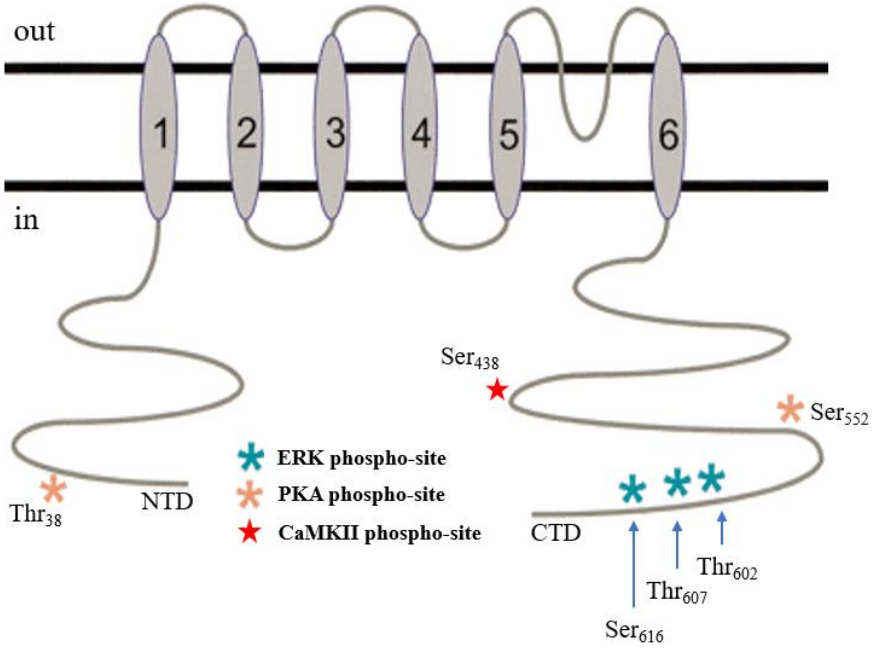

Figure 1.5. Overview of Kv4.2 channel structure. The channel is composed of six TM domains, with an extracellular P-domain between the fifth and the sixth. It also has three ERK phosphorylation sites (blue stars), Ser_{616}, Thr_{607} and Thr_{602}; two PKA phosphorylation sites (orange stars), Thr_{38} and Ser_{552}; and one CaMKII phosphorylation site (red star), Ser_{438}. CTD: carboxy-terminal domain; NTD: N-terminal domain. Adapted from [62].

Induction of LTP reduces the levels of Kv4.2 on the membrane of dendrites (Figure 1.6 - B) which is accompanied by a shift in the voltage-dependence of I_A. This suggests that control of the trafficking of the channel, which depends on modifications such as phosphorylation, could underlie a mechanism of LTP expression[67,68].

The first evidence that Kv channels could have a role in epilepsy came from the observation that Kv channel blockers induce convulsions in mice[69]. Studies in chronic TLE models have showed changes in Kv4.2 expression at several stages of disease progression. In animals with SRSs induced with pilocarpine, an increased excitability of neuronal pyramidal cell dendrites in hippocampal CA1 region was correlated with decreased dendritic availability of Kv4.2 channels and an increase in the phosphorylation of Kv4.2 channel at ERK-sites that is probably mediated by ERK itself[70].

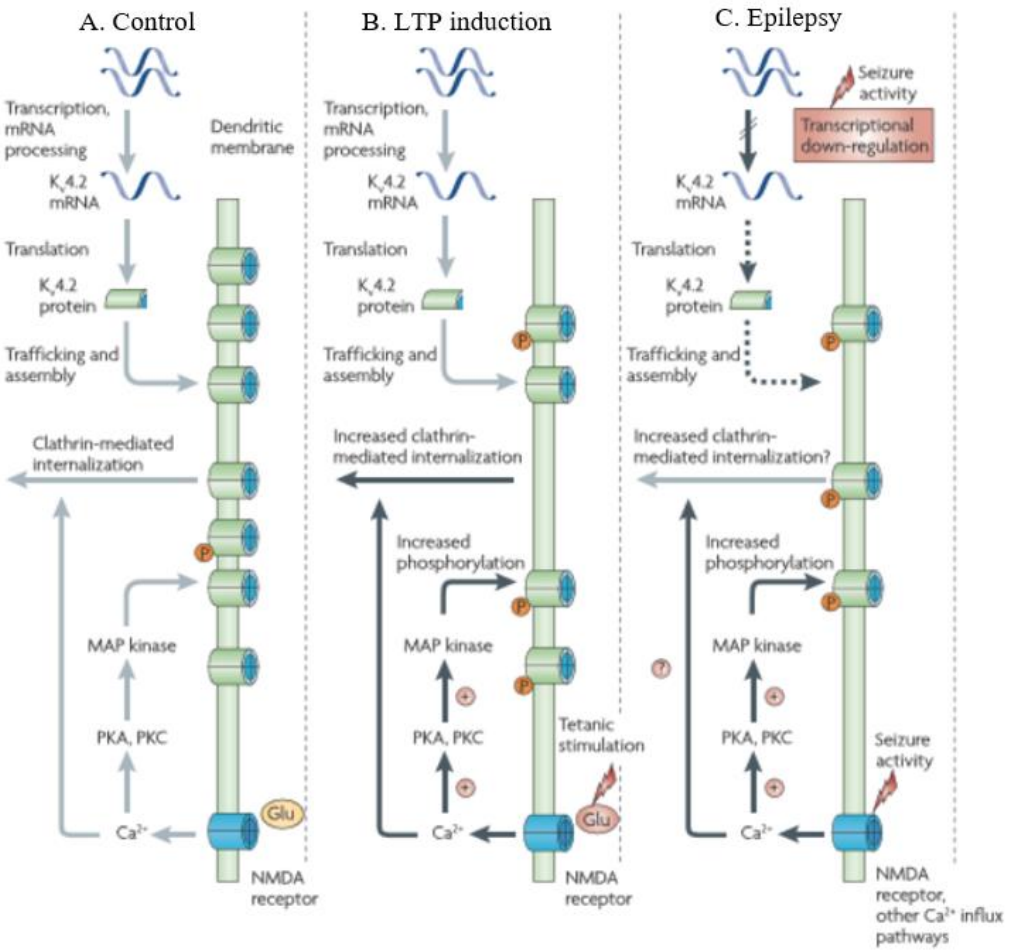

Figure 1.6. Regulation of dendritic Kv4.2 channels by physiological activity and in epilepsy. Under control conditions (**A**) clathrin-mediated internalization, trafficking to the membrane and production of the Kv4.2 channel regulate the density of the channel in the dendritic membrane. The activity of the channel is also controlled by PKA, PKC, and MAPK dependent-signaling. When LTP is induced (**B**) MAPK dependent-signaling activity and clathrin-mediated internalization are increased. Phosphorylation of the channel is also increased in SE of the pilocarpine model of epilepsy (**C**) but some of the mechanisms on the internalization of the channel are still unclear. In this situation, there is also a transcriptional downregulation of the channel.[57]

In another study, in the Li^{2+}-Pilo model of TLE, western-blot and immunohistochemistry studies have shown an increase in Kv4.2 expression that starts 6 hours after SE and continues to increase until 2 days after the first grade of seizures (latent period). This is followed by a decrease in Kv4.2 expression during the chronic period (50 days after SE). These changes were more prominent in the CA1 and CA3 regions of the hippocampus[11].

Besides the changes in phosphorylation and availability/trafficking of the channel on the membrane, a transcriptional down-regulation has also been reported in epilepsy (Figure 1.6 - C)[70].

1.5. Pre-synaptic protein: SNAP-25

The synaptosomal-associated protein 25 (SNAP-25) is a component of the trans-SNARE (soluble n-ethylmaleimide-sensitive factor attachment protein receptor) complex, playing an important role at presynaptic vesicle fusion in neurotransmitter release[71]. Neurotransmitter release is regulated, amongst other mechanisms, by SNAP-25 palmitoylation. When SNAP-25 is palmitoylated, the protein partitions to the cell membrane allowing the SNARE complex to dissociate during vesicle fusion[72]. Palmitoylation is the post-translational modification in which a fatty acid palmitate (or less frequently other fatty acid) is attached covalently to a protein in a cysteine residue (and less frequently to serine and threonine)[73].

A few observations relate SNAP-25 with synaptic plasticity but no changes have been reported in TLE. Increased mRNA levels of SNAP-25 were associated with the expression of LTP in the granule cells of the DG of the rat hippocampus[74]. Also, SNAP-25 is phosphorylated by PKC when LTP is induced with a high-frequency TBS[75].

1.6. Post-synaptic density proteins: PSD-95 and gephyrin

The post-synaptic density (PSD; Figure 1.7) is a complex net of interacting proteins at the synapse that lies just underneath and in close connection with the post-synaptic membrane, opposed to the active zone of the presynaptic neuron. Its composition includes neurotransmitter receptors, effector proteins, enzymes, scaffold proteins and structural proteins[29].

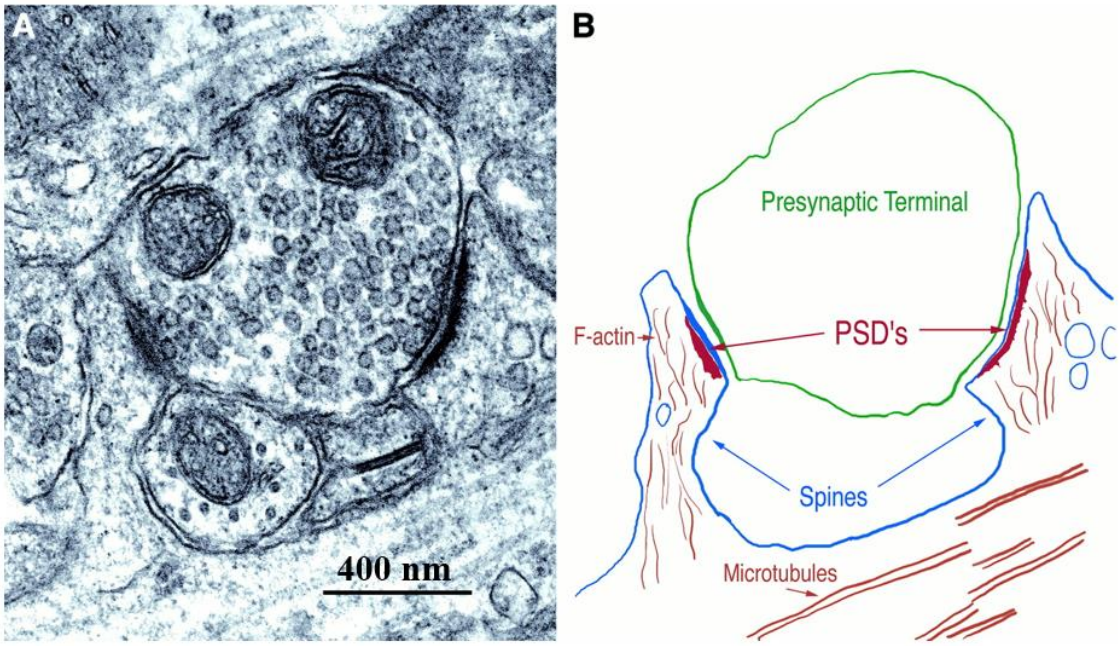

Figure 1.7. The PSD, opposing presynaptic terminals forming glutamatergic synapses with two dendritic spines. The protein complex is visible with electron microscopy as a thickening of approximately 30 nm in the postsynaptic membrane (**A**). In (**B**) a tracing of the structures shown in (**A**), with its most important structures identified, is depicted [76].

The molecules that compose the post-synaptic density have important roles, one of them being the regulation of downstream signaling pathways that adjust the molecular composition of the post-synaptic entities necessary to sustain synaptic plasticity[77].

An important protein found in these structures is post-synaptic density protein 95 (PSD-95), which is exclusively found in glutamatergic post-synaptic densities, associating with glutamate receptors and cytoskeletal elements[78,79].

PSD-95 has a role in synaptic stabilization and plasticity, through post-translational modifications such as phosphorylation and palmitoylation. PSD-95 palmitoylation on its N-terminus acts as an anchor for the protein in the postsynaptic membrane and is important for protein clustering at the PSD[80,81]. In fact, the PSD-95 palmitoylation cycle regulates AMPAR trafficking: high neuronal activity leads to PSD-95 depalmitoylation which induces its dissociation from PSD. Consequently, glutamate receptors are internalized and synaptic strength decreases. With lower neuronal activity, PSD-95 suffers palmitoylation promoting PSD-95 and glutamate receptors trafficking to the postsynaptic membrane[80,82]. Expression of PSD-95 lacking palmitoylation sites inhibits the incorporation of AMPARs into synapses during LTP[83].

The hippocampus of rats with SRS-induced by KA, showed down-regulation of PSD-95 expression 6 weeks post-SE, that correlates with a behavioral deficit. This decrease in PSD-95 expression, alongside other factors, likely contributes to behavioral impairments such as spatial learning memory deficit, anxiety and increased locomotor activity[10].

Like PSD-95 in excitatory synapses, gephyrin is found exclusively in inhibitory glycinergic and GABAergic synapses. This 93 kDa protein anchors glycine receptors and type A GABA ($GABA_A$) receptors, to the cytoskeleton[84–86], ensuring the stability that guarantees that the appropriate number of these receptors are localized at the post-synaptic membrane. Despite this stability, gephyrin scaffold sustains several forms of synaptic plasticity due to rapid changes in its composition[77].

Although not as well studied as PSD-95 regarding synaptic plasticity, gephyrin is believed to sustain it through the regulation of $GABA_A$ receptor internalization and function, *i.e.* by regulating the strength of GABAergic transmission. This regulation depends on changes in gephyrin through post-translational modifications, such as phosphorylation and/or palmitoylation, and interaction with signaling molecules that modulate downstream signaling cascades related to synaptic plasticity in GABAergic synapses[87].

Patients with TLE showed aberrant alternative splicing in the gephyrin gene (*GPHN*), which lead to a gephyrin variant that clusters differently with $GABA_A$ receptors[88]. Also, a decrease in gephyrin expression was detected in the hippocampus of rats from 24 hours to 2 months after the first grade of seizures induced with Li^{2+}-Pilo[89].

1.7. Summary of the changes found in TLE regarding the proteins mentioned

Several studies have been conducted to study what molecular changes happen in TLE, both in human tissue and in rodent models of TLE. Some of the changes in proteins involved in synaptic plasticity studied in the present work, can be found in human tissue (Table 1.1). Changes in these proteins observed in different rodent models of TLE are summarized in Table 1.2. Results for human tissue are very similar to the ones obtained for rat models. Interestingly, for the rat models, the results not only vary between brain regions or even hippocampus areas, but also along different periods of the disease.

Table 1.1. Protein changes found in patients with TLE. The diseased tissues were compared with non-seizure autopsies. Note that for some studies not all differences found in each study are described, only the ones that are relevant for the present work. ↑ represents an increase; ↓ represents a decrease.

Author and year	Situation	Assay	Details	Result
Blümcke *et al*. 1996 [90]	Hippocampal tissue from patients with intractable TLE	protein	CA1	↓ GluA2
			Granular cell layer of the DG	↑GluA2
Mathern *et al*. 1998 [91]	Hippocampi from TLE patients (with and without hippocampal sclerosis)	mRNA		↑ GluA1/GluA2
Palomero-Gallagher *et al*. 2012 [92]	Neocortical biopsies from patients with pharmacoresistant focal TLE	protein		↑ AMPAR
Fang *et al*. 2011 [89]	Temporal neocortex samples from patients who underwent surgery to treat drug-refractory TLE	protein		↓ Gephyrin
Ying *et al.* 2004 [93]	Brain tissue from four patients with medically intractable neocortical epilepsy	protein		↑ PSD-95

Table 1.2. Protein changes found in rodent models of TLE. Note that for some studies not all differences found in each study are described, only the ones that are relevant for the present work. ↑ represents an increase; ↓ represents a decrease; - represents no changes.

Author and Year	Model	Assay	Region of the brain	Period	Result
Condorelli *et al*. 1994 [94]	Li^{2+}-Pilo	mRNA	Hippocampus	SE: 24 hours after treatment with pilocarpine	↓ GluA1
					- GluA2 and GluA3
			Hippocampus DG	SE: 12 hours after treatment with pilocarpine	↓ GluA1
					↑GluA3
			Hippocampus CA1	SE: 12-24 hours after treatment with pilocarpine	↓ GluA1
					↓ GluA3
Mathern *et al*. 1998 [45]	Pilocarpine	mRNA	Hippocampus DG	Chronic period: 85 days after SE	↑GluA2
			Hippocampus CA1		↓GluA2
Porter *et al*. 2006 [46]	Li^{2+}-Pilo	mRNA	Hippocampus DG	2 weeks after SE	↑GluA2
					↓GluA3
Rajasekaran *et al*. 2012 [95]	Pilocarpine	protein	Hippocampus	SE: 10 or 60 min after the first seizures	↓GluA2 surface expression
Malkin *et al*. 2016 [3]	Li^{2+}-Pilo	mRNA	Hippocampus	Latent period: 1 day after treatment with pilocarpine	↓ GluA1
					↓GluA2
			mPFC	Latent period: 3 days after pilocarpine treatment	↑GluA1
				1st to the 7th day after treatment with pilocarpine	↓GluA2
				Latent period: 3rd day after treatment with pilocarpine	↑GluA1/GluA2
Lorgen *et al*. 2017 [96]	KA	protein	Hippocampus	8 weeks after SE	↓ GluA2
Russo *et al*. 2013 [97]	Pilocarpine	protein	Hippocampus	3 hours after SE	↑GluA2
					↓ GluA1
					↓ GluA1PSer831
Lopes *et al*. 2013 [55]	Pilocarpine	protein	Cortex	1, 3 and 12 hours after SE	↑GluA1PSer845
			Hippocampus		↑GluA1PSer831
				Chronic period: 50 days after SE	↓GluA1PSer845
			Cortex	Latent period: 5 days after SE	↓ GluA1
			Hippocampus	Chronic period: 50 days after SE	- GluA1 and GluA1PSer831
Lopes *et al*. 2015 [8]	Pilocarpine	protein	Dorsal hippocampus	Chronic period: 60 days after treatment with pilocarpine	↓GluA1PSer845
			Ventral hippocampus		↓GluA1PSer831
Su *et al*. 2008 [11]	Li^{2+}-Pilo	protein	Hippocampus	Latent period: 2 days after SE	↑ Kv4.2 channel
				Chronic period: 50 days after SE	↓ Kv4.2 channel
Sun *et al*. 2009 [10]	KA	protein	Hippocampus	Chronic period: 4 and 6 weeks after SE	↓ PSD-95
Fang *et al*. 2011 [89]	Li^{2+}-Pilo	protein	Temporal lobe	from 24 hours to 2 months after the first seizures	↓Gephyrin

1.8. Lipid rafts

Since the fluid mosaic model of membrane structure was proposed by Singer and Nicolson in 1972[98], several new aspects of membrane organization have been uncovered (Figure 1.8), such as the transmembrane asymmetry of glycerophospholipids, but also the lateral heterogeneity (*i.e.*, non-randomness) in lipid and protein distribution (see [99] for review). In fact, the membrane is currently viewed as being composed by different functional domains which are distinct not only in their lipid and protein composition, but also in their biophysical properties, such as membrane lateral diffusion coefficient and thickness, and in the fact that they operate in a large range of time and length scales[100].

This lateral organization is highly relevant for the neuronal membrane due to all the roles associated to it, some of them already mentioned above, and especially, but not only, in synapses. The existence of lateral interactions between the high diversity of neural membrane components, with different degrees of affinity between them, drives and stabilizes the existence of different domains[101]. These domains are involved in the regulation of signaling pathways and other neurophysiological processes. Therefore, disturbance of this dynamic network in the membrane of neurons is associated with several pathologies, especially neurodegenerative diseases[102].

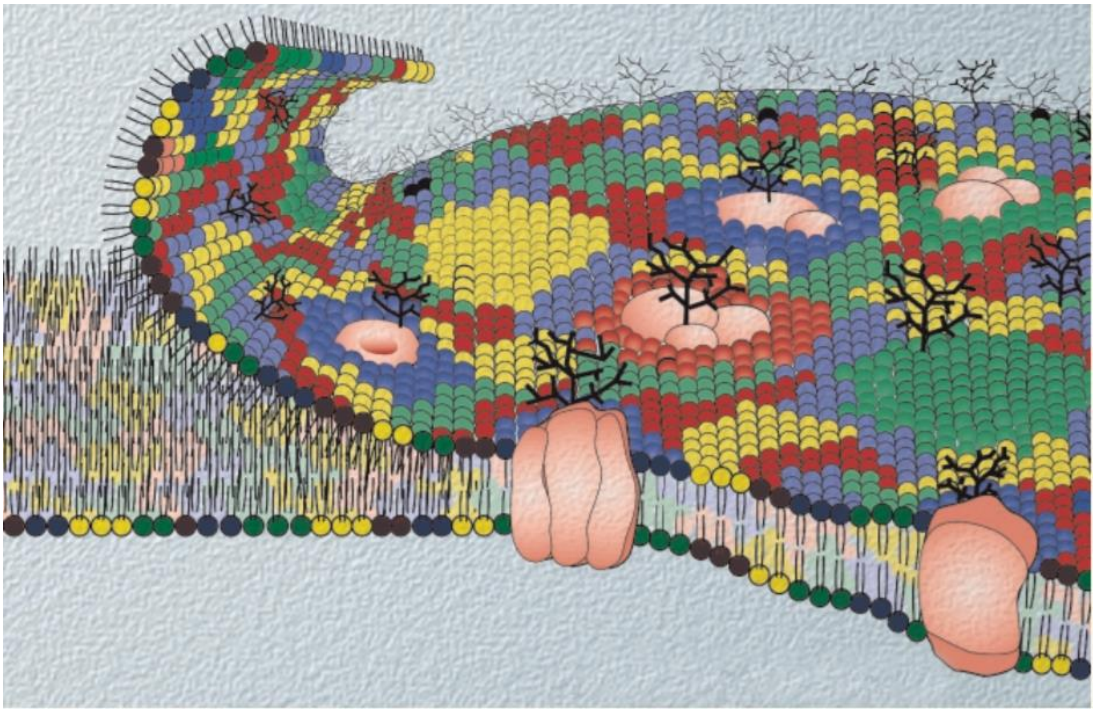

Figure 1.8. Schematic representation of the fluid mosaic membrane proposed by Singer and Nicolson modified to highlight the diversity of lipid components and their heterogeneous transversal and lateral distribution. Two types of domains are illustrated: those that are formed due to the segregation of different lipid components, and lipid annulus surrounding transmembrane proteins. Different colors correspond to different lipid species. The pink bulks represent proteins, and the black branches carbohydrates.[103]

The term lipid raft was first used by Simons and Ikonen in 1997 to describe the existence of membrane domains that were more rigid (liquid-ordered; l_o) formed by the dynamic aggregation of sphingolipids and cholesterol, that move along the liquid-disordered (l_d) lipid bilayer, in a way similar to a raft on water[104]. Many studies have been conducted since then with the purpose of better understanding these domains. Regarding lipid raft composition in mammalian cells, it was found that besides cholesterol, these domains are also rich in a specific sphingolipid, sphingomyelin, and in glycosylphosphatidylinositol (GPI)-anchored proteins. From the *Keystone Symposium on lipid rafts and cell function* that happened in 2006 emerged the consensus definition of a membrane raft that is still

presently accepted. In addition to the already mentioned characteristics, this definition also includes the possibility of small rafts to be stabilized in order "to form larger platforms through protein-protein and protein-lipid interactions"[105]. The importance of these domains is evidenced by the functions that have been attributed to them so far, that include organization of signaling molecules for the assembly of signaling platforms or trafficking, and regulation of membrane fluidity.

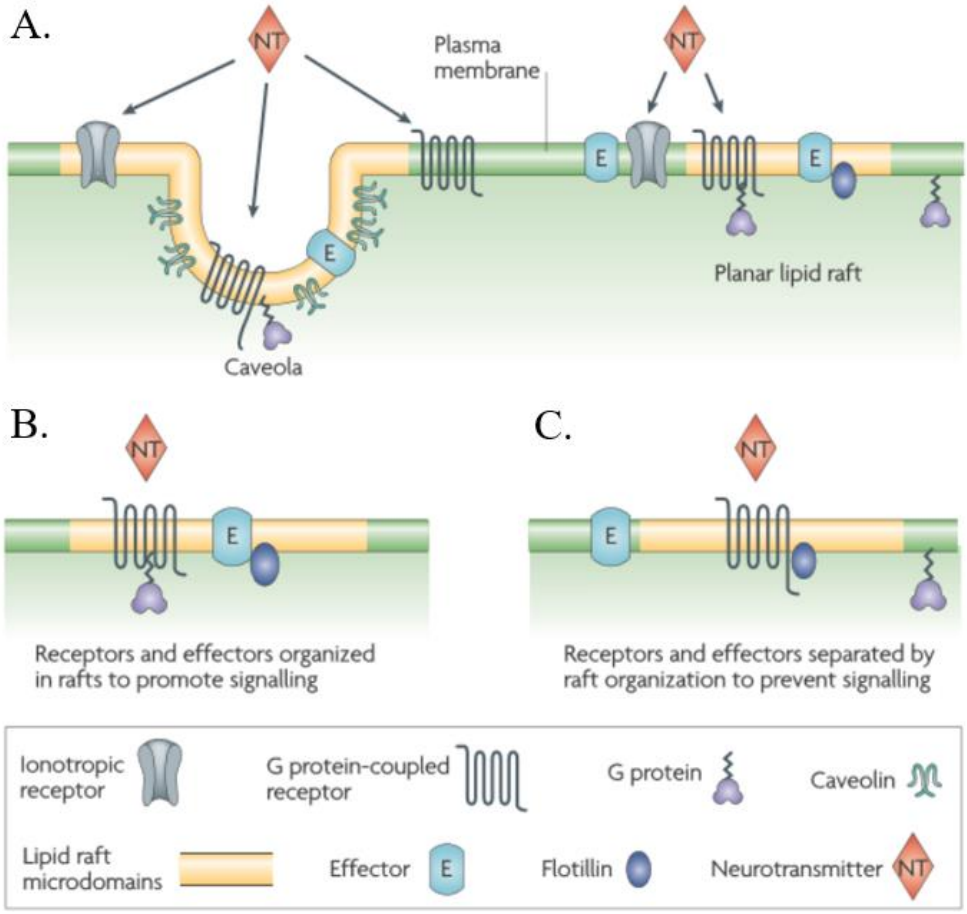

Figure 1.9. Lipids raft organization and possible roles in neurotransmitter signaling. *Caveolae* and planar lipid rafts (**A**) are two types of ordered microdomains found in the CNS. These domains are believed to spatially organize different membrane molecules to promote (**B**) or prevent (**C**) signal transduction[106].

In the CNS, lipid rafts have been associated with modulation of synaptic signaling by regulating neurotransmission and receptor trafficking[107]. The lipid raft signaling hypothesis proposes that these domains organize the spatial distribution of signaling molecules at the membrane in order to promote kinetically favorable interactions that are necessary for signal transduction (Figure 1.9 - B). The opposite might also happen, *i.e.* the inhibition of interactions by separation of the signaling molecules which results in a dampening of the signaling response (Figure 1.9 - C)[106]. Two different types of lipid rafts have been associated with these functions: planar lipid rafts and *caveolae* (Figure 1.9 - A)[106]. *Caveolae* are flask-shaped membrane invaginations that have caveolins as protein markers. In a similar way, flotillins are marker proteins found in planar lipid rafts. Both proteins are thought to promote stability of these domains. Localization within these microdomains affects the binding affinity of neurotransmitters to ionotropic receptors, such as AMPARs[108–110]. However, it is still unclear exactly how location within lipid rafts affects AMPAR properties.

Palmitoylation is one of the mechanisms responsible for proteins recruitment to lipid rafts[104]. PSD-95, along other proteins important for synaptic signaling, can be found in these domains in a palmitoylation-dependent fashion. During rat postnatal development an increase in PSD-95 palmitoylation and lipid-raft constituent lipids were observed, which likely facilitate the formation of

lipid rafts[81]. In fact, remodeling of lipid raft composition in the CNS occurs during development and is believed to contribute to altered cognition and synaptic plasticity observed upon ageing and neurodegenerative diseases[106,111]. However, it is still unknown if such changes contribute to the cognitive decline and altered synaptic plasticity observed in TLE, and more studies are needed to better understand this issue.

1.8.1. Membrane model systems

The use of membrane model systems, such as Giant unilamellar vesicles (GUVs), is a good approach to study in detail a limited number of molecular interactions, to determine, amongst the overwhelming complexity surrounding biomembranes, which of those interactions are involved in a given biological process, and if they are altered in pathologies such as TLE. As stated above, cellular membranes can have different domains with different biophysical properties, such as fluidity. These properties vary according to the environment and composition of the membrane itself and are reminiscent of the lipid phases found in membrane model systems[100]. The existing lamellar phases, *i.e.*, those in which the lipids are organized into a lipid bilayer, as in biomembranes, under close to physiological conditions are l_d, l_o and solid-ordered (s_o), here listed from more fluid to more ordered and compact[112]. It is usually considered that biological membrane domains, are in a fluid state, and therefore are considered either l_d –like or l_o –like domains, although evidence in the past decade has emerged for the existence also of s_o–like domains in living cells under physiological conditions, at least in yeast[113]. Lipid phases and domains have been studied by a variety of spectroscopic and microscopic techniques[112]. One of those has been fluorescence spectroscopy and microscopy, which relies on the use of sensitive molecular probes that have a certain preference in partitioning to specific domains, *e.g.* N-(lyssamine Rhodamine B sulfonyl)-1,2-dioleoyl-*sn*-glycero-3-phosphoethanolamine (Rhod-DOPE) prefers to partition into l_d over l_o and is largely excluded from s_o domains[114].

As membrane model systems, GUVs are liposomes with around 20 to 100 μm of diameter used to study, among others, how lipid composition affects shape and stability of domains. By using a fluorescent probe, domains with sizes on the μm range can be visualized by fluorescence microscopy, preferably using a laser-scanning confocal microscope[115,116].

From phase diagrams such as the one present in Figure 1.10, it is possible to estimate the percentage of each phase in the vesicle for each mixture, by using the tie-line which contains the proportion of components used in the experiment and the lever rule[112]. To obtain tie-lines in ternary systems usually it is necessary to physically separate the phases in coexistence and to determine the composition of each phase. To obtain the tie-lines in ternary lipid systems, namely from GUV imaging, information regarding the composition of each domain observed in the vesicles studied, especially the percentage of each component, would be needed[117]. This information can be indirectly estimated from spectroscopic measurements in which the spectra or quantitative parameters obtained can be separated in to the individual contribution of each phase, such as fluorescence lifetime components of fluorescent probes or Nuclear magnetic resonance (NMR), namely ^{2}H-NMR of a lipid component with perdeuterated acyl chain versus ^{1}H-NMR of the other lipid. Moreover, there are thermodynamic rules that restrict the different possible directions for the tie-lines. All together these theoretical and experimental approaches allowed to obtain ternary phase diagrams and several tie-lines, particularly in the l_d/l_o coexistence region with a high accuracy, with uncertainty in the order of 2 mol% or less. These phase diagrams are now a well-established and fundamental framework in membrane biophysical studies concerning membrane domains and lipid rafts.[114]

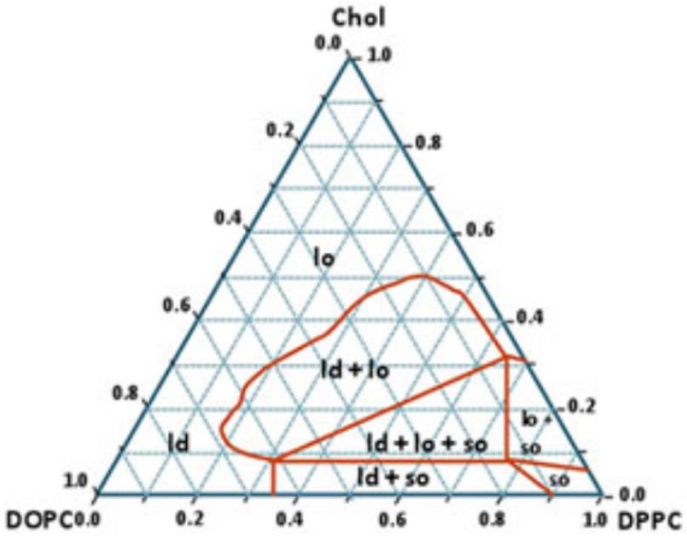

Figure 1.10. Miscibility phase diagram for DPPC, DOPC and cholesterol at 24°C. Regions of different phase coexistence are defined by red boundaries as shown: the $l_d + l_o$, $l_d + s_o$ and $l_o + s_o$ areas indicate the respectively l_d/l_o, l_d/s_o, l_o/s_o phase coexistence. The $l_d + l_o + s_o$ area indicates the three-phase coexistence situation.[114]

2. Aims

The main objective of this work was to unravel molecular mechanisms underlying TLE which are yet to be discovered, regarding the role of lipid raft changes in abnormal synaptic plasticity observed in TLE.

For this purpose, it is important first to understand what happens in physiological synaptic plasticity, namely LTP. Therefore, the first aim of this work was to study the changes in Kv4.2 channel phosphorylation in Ser_{438}, Thr_{602} and Thr_{607}, but also PSD-95 and SNAP-25, when LTP is induced with a moderate TBS.

To understand the relation of altered lipid raft domains in TLE with abnormal synaptic plasticity, the hippocampus of Li^{2+}-Pilo rat model of TLE was studied to evaluate:

- Histological changes in hippocampal tissue regarding cell death and axonal sprouting;
- Changes in the expression and phosphorylation of synaptic plasticity markers, AMPAR subunits GluA1 and GluA2, and Kv4.2 channel;
- The changes in presynaptic and PSD markers, by studying the expression of PSD-95, gephyrin and SNAP-25;
- And finally, the levels of flotillin-1 and caveolin-1.

To initiate the biophysical study of lipid rafts in model membranes obtained from synaptic lipids from the Li^{2+}-Pilo rat model of TLE the biophysical imaging and quantification of lipid rafts in giant unilamellar vesicles obtained from lipid mixtures was first performed.

3. Methods

All solutions were made using Milli-Q H_2O (MilliQ® Gradient, Millipore) to reduce the possibility of contaminations.

All reagents are from VWR, Merck or Fluka unless otherwise stated.

When needed pH was asserted using a pH meter Crison micropH2001.

3.1. Animals

The tissues available for this study were obtained from animal and *in vitro* studies performed at Instituto de Medicina Molecular and at the Rodent facility of the Faculty of Medicine of Lisbon (FML) where Li^{2+}-Pilo treatment and brain dissection procedures were performed, as described below, by Doctor Diana Cunha-Reis or collaborators.

Male Wistar rats were purchased from Harlan Iberica and were then kept under controlled environmental conditions (25°C, 50-60 % humidity, 12 hours light/dark cycle, light on at 6:00 hours) with free access to standard laboratory chow and tap water.

All animal handling and experimental procedures were in accordance with standards established in the Guide for Care and Use of Laboratory Animals, Portuguese and European law on animal welfare and were approved by the Ethical Committee of FML.

3.2. Brain dissection and hippocampus isolation

Brain dissection procedures and isolation of the hippocampus were performed by D. Cunha-Reis under my careful observation in more than one occasion. Animals were killed by decapitation and the brain removed by exposing the *cranium*, cutting through the scalp of the rat with a scissors. Then the initial part of the spine that remained after the beheading, was removed, allowing the cut between the parietal and temporal bones, which were removed with the help of forceps, exposing the whole brain of the rat for removal. This was performed using a curved tip spatula, cutting the optical nerves, placing the brain in a Petri dish with a filter paper and submerging it in an ice-cold Krebs solution (10 mM $C_6H_{12}O_6.H_2O$, 124 mM NaCl, 26 mM $NaHCO_3$, 3 mM KCl, 1.25 mM $NaH_2PO_4.H_2O$, 2 mM $CaCl_2$ e 1 mM $MgSO_4$) previously oxygenated with 5 % O_2/ 5 % CO_2. The two cerebral hemispheres were separated by the *corpus callosum*, using a blade under a magnifying glass (Olympus, Europe). The left and right hemisphere were then randomly assigned for fixation (see section 3.4.1 Histochemistry) or for hippocampal dissection. For histochemistry tissue samples were rinsed in oxigenated Krebs solution and then transferred to 10 % neutral buffered formalin. This later hemisphere was then placed with the inner face facing up, and a curved tip spatula was inserted in the lateral ventricular cleft between the hippocampus and the cortex, outlining it without disturbing the hippocampus. The cortical tissue was pushed and cut until it was possible to obtain a good hippocampus observation. With a microsurgery scissor the connection between the hippocampus and the *septum* was separated by cutting the tip from the fimbria that holds it. After that, using a spatula, the hippocampus was detached from its internal component, disconnecting it completely from the *encephalus* and all traces of cortical tissue removed. With the help of fine-tipped tweezers the visible blood vessels were removed to avoid homogenate contaminations and both hippocampi were immediately placed in criogenic tubes and frozen in liquid nitrogen.

3.3. Long-term potentiation studies

3.3.1. Hippocampal slices preparation

For electrophysiological recordings, hippocampal slices from 6-7 weeks-old rats were cut with a McIlwain tissue chopper from the isolated hippocampus. Slices (400 μm thick) were cut perpendicular to the long axis of the hippocampus and allowed to recover in a holding chamber for at least 1 h in gassed Krebs solution (10 mM $C_6H_{12}O_6.H_2O$, 124 mM NaCl, 26 mM $NaHCO_3$, 3 mM KCl, 1.25 mM $NaH_2PO_4.H_2O$, 2 mM $CaCl_2$ e 1 mM $MgSO_4$), at room temperature to allow the recovery of the damage made by the dissection procedure.

3.3.2. LTP induction and electrophysiological recordings

Hippocampal slices were introduced in an electrophysiology recording chamber previously perfused with Krebs solution and equilibrated at 30 °C. For the extracellular recording of the field excitatory post-synaptic potentials (fEPSPs), the stimulation electrode was placed in the Schaffer collateral fibers of the CA1 region of the hippocampus and the recording electrode also in CA1 area but in the contact zone between the Schaffer collateral fibers and the dendrites of pyramidal cells as seen in Figure 3.1- A. Then, hippocampal slices were subjected to basal stimulation once every 15 s for at least 20 min or until a stable baseline was observed. After this, LTP was induced in (θ), but not in control (C), slices with a moderate TBS (one episode of five bursts of four pulses at 100 Hz with intervals of 200 ms (5x4); Figure 3.1 - B) and the electrical activity of the slices monitored for 50 min under basal stimulation, after which slices were stored at -80 ºC until western-blot analysis. In each sample, 3-4 slices per condition were used.

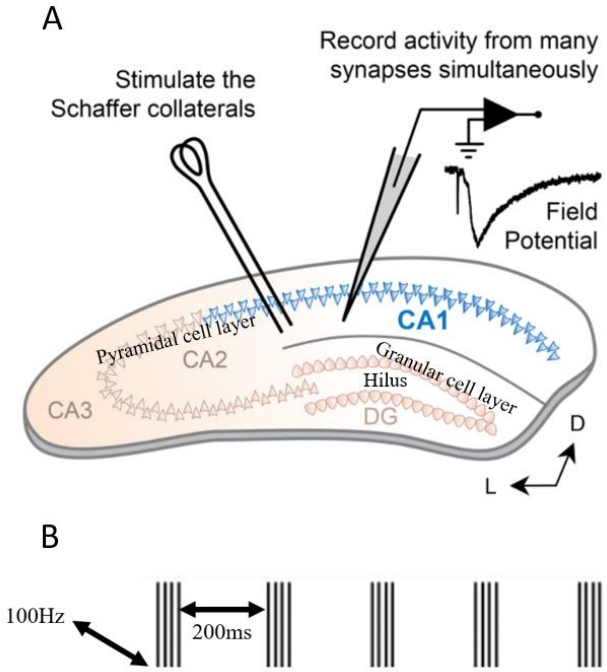

Figure 3.1. Schematic of the representation of the LTP induction procedure in rat hippocampal slices. The illustration shows the different hippocampal areas. (**A**) The stimulation electrode was placed in the Schaffer collateral fibers of the CA1 region of the hippocampus and the recording electrode also in CA1 area in the contact zone between the Schaffer collateral fibers and the dendrites of pyramidal cells. (**B**) TBS consisted of five bursts of four 100 Hz pulses delivered with intervals of 200 ms. Adapted from [118].

3.4. Lithium-Pilocarpine temporal lobe epilepsy rat model

3.4.1. Lithium-Pilocarpine treatment

Lithium chloride was injected at a dose of 100 mg/Kg, i. p., 24 hours prior to the administration of pilocarpine in 12-week-old rats. Furthermore, rats were pre-treated with α-methylscopolamine-bromide 1 mg/Kg, 1h prior to pilocarpine treatment to counteract its peripheral cholinomimetic effects. Pilocarpine was injected in intervals of 30 min at an initial dose of 10 mg/Kg and 5mg/Kg reinforcements were given when necessary until acute SE was observed. Once SE was induced, the rats were treated with 4 mg/Kg of Xylazine, i. m., to prevent tonic-clonic muscle contractions. After 30 min of SE, rats received 10 mg/Kg of Diazepam, i.p., to terminate seizures. Reinforcements were administered to the animals that continued to preset seizures to ensure the survival of the animals. Animals were killed at 12 months of age (9 months after SE). A diagram representing all the steps performed is shown in Figure 3.2.

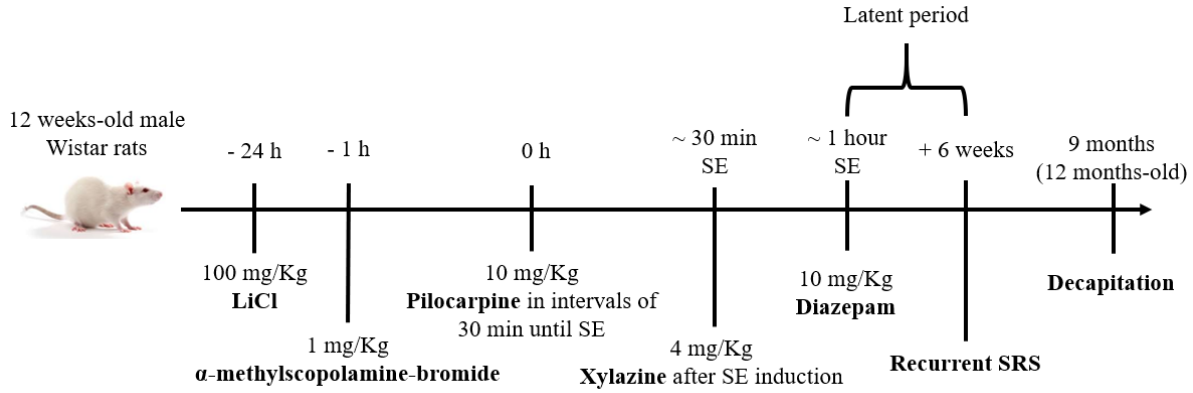

Figure 3.2. Procedure for the Li^{2+}-Pilo treatment performed in this work.

3.4.2. Histochemistry

Histochemistry and immunohistochemistry assays were performed by Pedro Pereira in Laboratório de Neuropatologia, Hospital Santa Maria, CHLN under my careful observation.

Tissue samples were kept in 10 % neutral buffered formalin for up to 3 days. Then the samples were post-fixed in glutaraldehyde solution (3 % glutaraldehyde, 1.5 M dextrose) for 1.5 hours and then back to the 10 % neutral buffered formalin for 24 hours. For embedding in paraffin, the samples were then transferred to 70 % ethanol for a minimum of 4 hours up to days, and then placed in 95 % ethanol overnight. Then the tissue was switched to absolute ethanol 2 times for 2 hours each, and then to chloroform where it stayed overnight. Finally, the tissue was placed in wax for 4 hours at 60ºC and preserved until use

The preserved tissue was cut in sections of 10-15 µm thick and placed in a water bath previously sprinkled with a small scoop of gelatin and chromium potassium sulfate, sparingly. The sections were mounted on positive slides which were then dried overnight in an incubator at 60ºC. Slides were finally dewaxed in xylene 2-3 times for 3 min each, and rehydrated in absolute ethanol, for 2 x 3min.

For the NeuN-labelling antigen retrieval was performed by microwave heating in citrate buffer (10mM Tris-sodium citrate dihydrated, 0.05 % Tween 20, pH 6.0). pH was then equalized with PBS for 5 min, and then the slices were incubated with the primary antibody for 1 hour. After being washed 2 times with PBS the tissue was incubated with secondary antibody (Dako Envision) for 1 hour. The slides were then washed 2 times with PBS and rinsed in DAB for 5 min, followed by a counterstain in Harris/Mayer's Hematoxylin. This was then washed 2 times with PBS and finally dehydrated with

absolute ethanol 2 x 3 min and mounted in Entellan. For NeuN-immunolabelling, neurons were counted using the Cell counter Plugin of ImageJ for each area of the hippocampus: CA1, CA3 and DG, whose region division was made as represented on Figure 3.1 - A.

For the Nissl-staining, the sections were stained with 0.1% of Cresyl Violet Acetate 0.2% in acetate buffer, and then rinsed in tap water to remove excess stain. After washed with 70% ethanol, the staining was checked on microscope and if required the sections were immersed for 2 min in differentiation solution (2 drops of glacial acetic acid in 95 % ethanol). Finally, the tissue was dehydrated with absolute ethanol 2 x 3 min, cleared with xylene 2 times, and mounted in Entellan.

In Timm-staining or Timm's sulphide silver method, metals are transformed in a metal sulphide which then catalyses the reduction of silver ions by a reducing agent to metallic grains that are visible under a light or electron microscope[119]. So, the method is sensitive to metals, especially zinc, which makes it a good approach to visualize cells and detect newly sprouted axons and axon terminals in the tissue. For this staining the slides were stained with Timm stain (30 % Gum Arabic, 132 mM citric acid, 90 mM sodium citrate, 155 mM hydroquinone, 5 mM silver nitrate) for 45 min in dark cupboard at room temperature, and then for 20 min at 60 ºC. The slides were then washed in de-ionized water and counterstained with cresyl violet working solution for 5min, followed by a dehydration with absolute ethanol 4 times for 1 min each. Cleaning the slides 3 times of 1 min each with xylene was followed by mounting in Cytoseal.

3.4.3. Isolation of total hippocampal membranes for western-blotting

Samples were homogenized in ice-cold sucrose-BSA-HEPES (320 mM sucrose, 1 mg/mL BSA, 10 mM HEPES, 1 mM EDTA, pH 7.4) with protease (complete, mini, EDTA-free Protease Inhibitor Cocktail, Sigma) and phosphatase (1 mM PMSF, 2 mM Na_3VO_4, and 10 mM NaF) inhibitors using a Potter-Elvejam homogenizer (B.Braun Melsungen). The suspension was then centrifuged at 1000 g for 10 min at 4 °C (eppendorf, MiniSpin). The supernatant was then collected and centrifuged at 14 000 g for 12 min at 4 °C (Eppendorf, centrifuge 5415D). The pellet was resuspended in aCSF (10 mM HEPES, 1 mM $MgCl_2$, 1.2 mM NaH_2PO_4, 120 mM NaCl, 2.7 mM KCl, 1.2 mM $CaCl_2$, 10 mM glucose, pH 7.4) and centrifuged at 14 000 g for 2 min at 4 °C (Eppendorf, centrifuge 5415D). Finally, the resulting pellet was resuspended in aCSF and stored at -80 °C.

3.4.4. Protein assays

3.4.4.1. Determination of protein concentration

The determination of the protein concentration was made following the Bradford method[120] because of its quickness and accuracy. First the standard curve was stablished with the concentrations of 0, 0.1, 0.2, 0.4, 0.7, 1.2 and 1.5 µg/mL of BSA diluted in Lysis buffer [45 mM Octylglucoside, 25 mM HEPES, 150 mM NaCl, 1 mM EDTA, 1 mM PMSF, 2 mM Na_3VO_4, 10 mM NaF, Protease inhibitors (complete, mini, EDTA-free Protease Inhibitor Cocktail, Sigma)]. The assays were performed in triplicate by adding 5 µL of the sample diluted 1:2 and 1:4 in Lysis buffer, and 245 µL of Bradford reagent (Coomassie Brilliant Blue G-250 0.1 g/L, Methanol 5 % (v/v), Orto-phosphoric acid 8.5 % (v/v)) to the wells of a microplate and left to incubate for 5 min. The absorbance was read in the spectrophotometer (TECAN, Sunrise; software: RdrOle4) at wavelength of 590 nm and 450 nm to calculate the ratio between the two.

The calibration curves can be found in the Appendix (Figure 8.1 and Figure 8.2).

3.4.4.2. Protein quantification using Western-blot

To identify and quantify specific proteins in each sample, western blot was performed (see [121] for review). The apparatus for gel preparation, electrophoresis and transfer steps were from BioRad.

3.4.4.2.1. Gel preparation

One small and one large (with integrated 1 mm spacers) glass plate, previously washed with Milli-Q water and ethanol, were dried and put together, in a support with the according casting block. To detect leaks a bit of ethanol was poured between the plates and then removed. 10 % running gel mix [10 % polyacrylamide, 375 mM Tris pH 8.8, 0.1 % SDS, 0.1 % APS, 0.1 %TEMED (this two were added last since they are the initiator peroxide and the catalyst respectively)] was then poured in between the glass plates (*circa* 5 mL); ethanol was placed on top of the polymerizing gel to prevent atmospheric oxygen from inhibiting polymerization.

Once the running gel was polymerized, the ethanol was poured off and 5 % stacking gel mix (5 % polyacrylamide, 250 mM Tris pH 6.8, 0.1 % SDS, 0.1 % APS, 0.1 % TEMED) was poured on the top of the running gel, quickly placing a plastic comb over the gel avoiding the formation of air bubbles that would cause wells to be ill-formed.

3.4.4.2.2. Sample preparation and loading

Samples were mixed with 1:4 volume of sample buffer (4x Laemmli Sample Buffer, BioRad), and heated for 5 min at 100 °C (VWR, analog heatblock) to denaturate the proteins in the sample.

The combs of the gel were carefully removed to prevent distortion of the wells. Gels were then placed in the holding block, which was placed in the electrophoresis tank. The space inside the block and the tank was filled with electrophoresis buffer (25 mM Tris, 192 mM Glycine, 0.1 % w/v SDS) making sure there was no leak and that all the wells were filled with the buffer and that no air bubbles remained in the wells.

Once all the samples (15 µL per well), and 4-5 µL of pre-stained standards (Precision Plus Protein Standards, BioRad) were loaded in the respective wells, the power was set to 80 V and the electrophoresis was initiated. After allowing for the time necessary for the samples to reach the running gel, the voltage was switched to 135 V and left to run until the samples reached the bottom of the gel.

3.4.4.2.3. Protein transfer to PVDF membranes and incubation with antibodies

The running gel was removed from the glass plates very carefully and left to equilibrate in transfer buffer (25 mM Tris, 192 mM Glycine, 20 % w/v methanol) for at least 15 min. The same was made to PVDF membranes [Immobilon-P transfer membrane PVDF (pore size 0.45 µm), Immobilon] that were first activated in methanol.

The transfer setting was then prepared by placing first the sandwich (black end down) following by a sponge, a filter, the gel, the membrane, again the filter and finally a sponge making sure that bubbles were removed using a roller at each step of stacking and that all the components enunciated were well moist with transfer buffer. The sandwich holder was then closed firmly and placed in a black/red holder inside the electrophoresis tank, filling the tank with a cold thermal bag (to make sure the high voltages don't overheat the system) and transfer buffer. The tank is next placed inside a box filled with ice. The current was set to 370 mA and transfer of the proteins was performed for 2h.

Upon separation from the gel, PVDF membranes (now containing the proteins) were then briefly washed with Milli-Q water to remove any gel debris, and blocked with TBST (20 mM Tris, 150 mM NaCl, 0.1 % Tween 20) mixed with either 3 % BSA or 5 % milk for 2 hours at 4 °C with constant agitation in a rocking platform, VWR which will block nonspecific antibody binding sites. The membrane was then washed with TBST 3 times for 10-15 min with mixing (rocking platform, VWR) and incubated overnight with constant agitation at 4 °C with primary antibody prepared with the appropriate dilution in 3 % BSA in TBST and 0.02 % NaN_3.

On the next day membranes were washed 3 times with TBST for 10 min with mixing, and then left to incubate for 2 hours with mixing at 4 °C with secondary antibody prepared with the appropriate dilution in 3 % BSA in TBST. The primary and secondary antibodies used, and their according dilution is shown on Table 3.1.

Table 3.1. Dilution of primary and secondary antibodies used and according blocking agent.

Primary antibody					**Secondary antibody**		
Target	*Source*	*Brand*	*Dilution*	*Blocked with*	*Antibody*	*Brand*	*Dilution*
GluA1	Rabbit, Polyclonal	Millipore	1:1000	BSA	Goat Anti-rabbit IgG (H+L), HRP*	proteintech®	1:10000
GluA1 PSer$_{831}$		Millipore	1:500	BSA			1:5000
GluA1 PSer$_{845}$		Millipore	1:500	BSA			1:10000
GluA2		proteintech®	1:1000	milk			1:40000
PSD-95		Cell Signaling Technology®	1:1000	BSA			1:15000
SNAP-25		Synaptic Systems	1:5000	BSA			1:10000
Kv4.2		Millipore	1:1000	BSA			1:10000
Caveolin-1		proteintech®	1:500	Milk			1:15000
Lamin-2B		Sigma	1:500	milk	Mouse anti-rabbit IgG-HRP*	SantaCruz Biotechnology	1:1000
Kv4.2PSer$_{438}$		SantaCruz Biotechnology	1:100	BSA			
Kv4.2PThr$_{607}$		SantaCruz Biotechnology		BSA			
GAPDH	Mouse, Monoclonal	proteintech®	1:5000	BSA	Goat Anti-mouse IgG (H+L), HRP*	proteintech®	1:10000
Flotillin-1	Mouse, Monoclonal	SantaCruz Biotechnology	1:750	milk	m-IgGκ BP-HRP*	SantaCruz Biotechnology	1:2000
β-Actin	Mouse, Monoclonal	SantaCruz Biotechnology	1:1000	BSA			
Gephyrin	Mouse Monoclonal	Synaptic Systems	1:3000	BSA			
Kv4.2PThr$_{602}$	Mouse Monoclonal	SantaCruz Biotechnology	1:2000	BSA			

*Horseradish peroxidase

Membranes were then washed 3 times for 10 min with mixing with TBST followed by two immediate washes with Tris-buffer saline (20 mM Tris, 150 mM NaCl), and then prepared for revelation. For that the membrane is incubated with enhanced chemiluminescence mixture (HRP, Millipore) for 5 min at room temperature and finally placed on the ImageQuant™ LAS 500 for revelation. Using ImageJ, the intensities of the signal for each protein target were obtained. The ratio of the signal from the different target proteins to the respective loading controls (GAPDH, Lamin-2B or β-actin) was used to normalize the signal intensities and correct for loading and sampling errors. All data are reported as percentage of Sham.

Membranes were dried and stored at 4ºC between filter papers, wrapped in aluminum foil.

3.4.4.3. Membrane stripping and re-probing

Following detection of protein, membranes were often stripped of bound antibodies and re-probed with a different one. First the dry membranes were activated in methanol and then submerged in stripping buffer (62.5 mM Tris-HCl, 100 mM 2-mercaptoethanol, 2 % SDS) in a Petri dish for 30 min at 55 °C with occasional shaking. Then the membrane was washed with TBST and Milli-Q water alternatively for 10-20 min, until the 2-mercaptoethanol characteristic odor was gone. Then the Western-blot steps were followed starting from the blocking of the membrane.

3.4.5. Lipid assays

1,2-dipalmitoyl-*sn*-glycero-3-phosphocholine (DPPC), 1,2-dioleoyl-*sn*-glycero-3-phosphocholine (DOPC), cholesterol and N-(lyssamine Rhodamine B sulfonyl)-1,2-dioleoyl-*sn*-glycero-3-phosphoethanolamine (Rhod-DOPE) were purchased from Avanti Polar Lipids, Inc.

3.4.5.1. Lipid dosing

Phospholipid quantification was made following the Rouser method[122], a procedure in which released inorganic phosphate reacts with ammonium molybdate to form a complex with a strong blue color. The following volumes of Na_2HPO_4 0.5 mM were added to glass vials in triplicate for the calibration curve: 0, 20, 40, 80, 100, 140, 160 µL, and left to dry at 170 °C in a heat block (Techne, Dri-block® DB3A). Separately, adequate volumes of the sample were added in triplicate to glass vials and dried under a nitrogen stream. Then, 300 µL of 70 % perchloric acid was added to all the vials at 170 °C in the heat block for 45 min to digest the samples and release the inorganic phosphate. Once all were at room temperature, 1 mL of water, 400 µL of ammonium molybdate (1.25 %) and 400 µL of ascorbic acid (5 %) were added in this order to all the vials and mixed. Then, all were heated in a water bath (Bioblock scientific, polystat 33) for 5 min at 100 °C. After quickly cooling the vials with running water, the absorbance was read at 797 nm.

3.4.5.2. Preparation of giant unilamellar vesicles

GUVs were prepared by electroformation as described by Angelova *et al.*[123]. Briefly, adequate volumes of lipids and probe (Rhod-DOPE) stock solutions were mixed to have a final lipid concentration of 1 mM, a lipid/probe ratio of 1:500 (mol/mol) and a chloroform/methanol ratio of 2:1 (v/v). Then, 25 µL of this mixture previously homogenized by vortexing, was spread with a gas-tight syringe on the titanium GUV chamber. The traces of organic solvent were removed through vacuum desiccation for 30 min. The titanium chambers were filled with 700 µL of sucrose solution 200 mM previously heated to 60 °C in a heat block (Techne, Dri-block® DB3A), sealed, connected to the signal generator and

placed in the block heater maintaining the system at 60 °C. A sinusoidal signal with a peak-to-peak voltage of 0.4 V and 10 Hz was applied and the voltage was increased to 2.0 V and maintained overnight. Then, the frequency was decreased to 4 Hz and the voltage increased to 2.6 V for 20 min Finally, the signal generator was turned off. The vesicle suspension was kept at room temperature (25 °C) in the dark until use.

3.4.5.3. GUV visualization with confocal microscopy

For GUV visualization 100 µL of each of the GUV suspension and 150 µL of glucose solution 200 mM, were added to a chamber of an eight-well plastic plate with glass like coverslip bottom.

Intensity images were taken using a Leica TCS SPE confocal microscope equipped with an X63 (1.4 N.A.) oil-immersion objective. Rhod-DOPE was excited at 543 nm using the HeNe laser and its emission was detected in the range of 570-670 nm, which was adjusted directly using the equipment software taking advantage of the Acousto Optical Tunable Filter (AOTF). Images with a frame size of 512 pixels x 512 pixels and 1024 x 1024 were acquired.

3.4.5.3.1. 3D viewing and determination of the mole fraction of each domain in the GUVs

The 3D projection of the GUVs was made by obtaining multiple images along different focal planes of the same sample (Z stacking), with an axial resolution (zz) of 0.344 µm, that was stacked together using FIJI software (3D Viewer), due to the optical sectioning capability of confocal microscopy. An approximate fraction area of each domain in 4 GUVs was estimated using the *Measure area* tool in ImageJ.

To estimate the fraction area of a spherical domain (l_o) it was assumed that the GUVs are perfectly spherical and that the boundary between the domains is circular (Figure 3.3). Considering the scheme in Figure 3.3, the area of the dark domain (A_{dark}) is given by the following equation:

$$A_{dark} = 2\pi \,.\, R \,.\, \overline{BC} \qquad \text{Eq 3.1.}$$

Since the OAC triangle is rectangle:

$$\overline{BC} = R - \sqrt{R^2 - \overline{AB}^2} \qquad \text{Eq 3.2.}$$

Replacing $\overline{BC}$ in the first equation results in:

$$A_{dark} = 2\pi \,.\, R \,.\, \left(R - \sqrt{R^2 - \overline{AB}^2}\right) \qquad \text{Eq 3.3.}$$

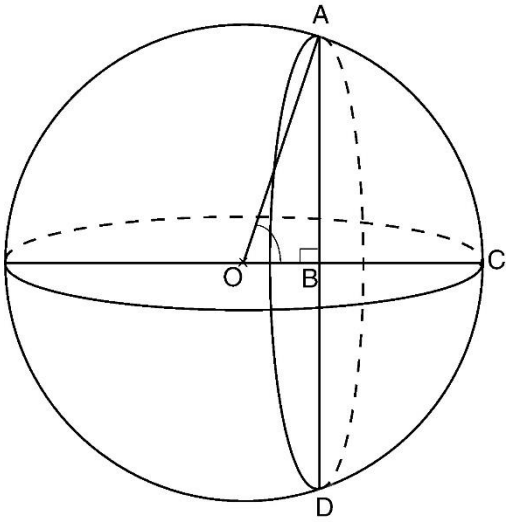

Figure 3.3. GUV representation for determination of domain area fraction. The right area is non-fluorescent representing a l_o domain. $\overline{OA}$ and $\overline{OC}$ are the GUV radius (R), while $\overline{AB}$ is the semi-major axis of the circular boundary that separates the domains.[124]

To calculate the percentage of each domain, for each GUV prepared with the ternary mixture, the $\overline{AB}$ from the dark areas and the radius of 12 vesicles prepared with DPPC/DOPC/chol were found and used in equation 3.3. If one GUV had more than one of these areas, then after estimating the area for all, these were summed up.

To determine the mole fraction associated to each area fraction estimated the expressions from Marquês *et al*. supplementary material[125] were used. If *x* and *y* are two different and coexisting domains from the same GUV, the mole fraction of the *x* domain is given by:

$$\frac{N_x}{N_t}$$

Eq 3.4.

in which N_x expresses the total number of molecules in the *x* phase and N_t the total number of molecules in the GUV.

Considering the following definitions:

$$a_x = \frac{A_x}{N_x} \Leftrightarrow N_x = \frac{A_x}{a_x}$$

Eq 3.5.

$$f_x = \frac{A_x}{A_t}$$

Eq 3.6

where a_x is the area per lipid, A_x stands for the total area *x* occupies, while A_t is the total superficial area of the GUV, and f_x the fraction area of *x*. Relating the two equations gives:

$$\frac{N_x}{N_Y} = \frac{A_x/a_x}{A_y/a_y} = \frac{f_x\,A_t/a_x}{f_y\,A_t/a_y} = \frac{f_x\,a_y}{f_y\,a_x}$$

Eq 3.7

Considering:

$$N_t = N_x + N_y$$

Eq 3.8

Then:

$$\frac{N_x}{N_t - N_y} = \frac{f_x\, a_y}{f_y\, a_x}$$

Eq 3.9

That results in:

$$\frac{N_x}{N_t} = \frac{f_x\, a_y}{f_y\, a_x - f_x\, a_y}$$

Eq 3.10

To perform these calculations, it was considered that for the DPPC/DOPC mixture a_{ld} = 65 Å and a_{so} = 48 Å [126]. For the DPPC/DOPC/chol mixture a_{ld} = 60 Å and a_{lo} = 43 Å [125].

3.5. Statistics

Statistical analysis was performed using GraphPad Prism 6 software. All results were expressed as mean ± standard error of the mean (SEM). Since data had normal distribution, parametric statistic method Student's *t*-test was applied to compare two samples. The differences were considered as statistically significant at p-value ≤ 0.05.

4. Results

4.1. Long-term potentiation by θ-burst stimulation *in vitro*

LTP was induced with a moderate TBS in hippocampal rat slices. Extracellular electrophysiological recordings and the time-course of these experiments are shown in Figure 4.1. - A. After 1 hour of stimulation the slope of the field excitatory post synaptic potentials (fEPSPs) increased by 27.4 ± 3.8 % (*n* = 6; Figure 4.1. - B).

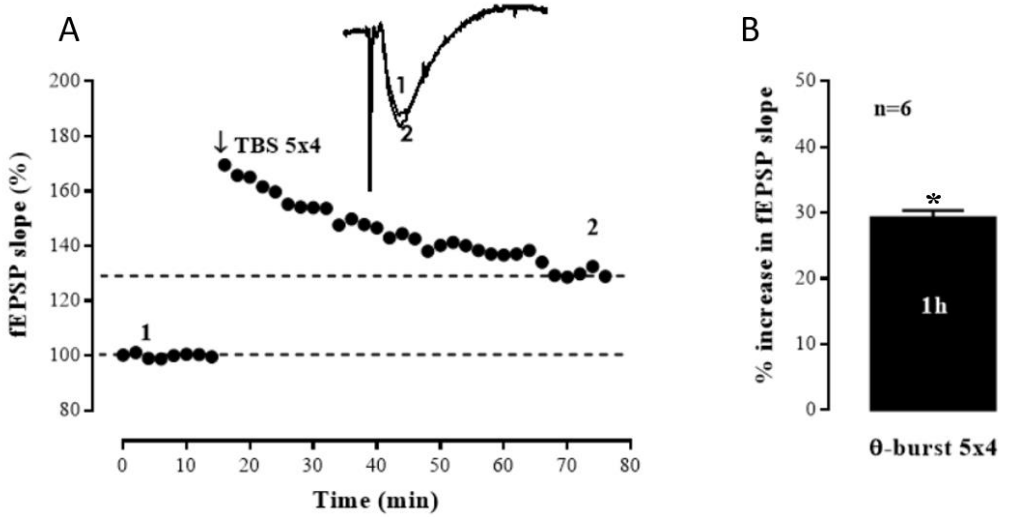

Figure 4.1. LTP induced by moderate TBS. (**A**) Extracellular electrophysiological recordings of fEPSPs (inset) and time-course of the slope of fEPSPs in the hippocampus, before (**1**), during and until 1 hour after (**2**) of LTP induction. (**B**) Enhancement in fEPSPs slope observed 1 hour after TBS. Values are the mean ± SEM of 6 experiments (n = 6; 6 hippocampal slices). *p-value < 0.5; Student's t-test.

Hippocampal membranes obtained from θ-burst stimulated (θ) and control (C) slices were used to evaluate Kv4.2 channel phosphorylation, PSD-95 and SNAP-25 levels by western-blot.

4.1.1. Kv4.2 channel phosphorylation following LTP induction

As previously mentioned, the activity and presence of Kv4.2 channel in the membrane is changed in LTP. However, it is still unclear if the modulation of the channel through phosphorylation is able to change its activity and/or play any role in LTP caused by moderate TBS. To investigate if the levels of phosphorylated Kv4.2 channel change following LTP induction with TBS, the western-blot technique was used.

In Figure 4.2 the raw data for the Kv4.2 channel phosphorylation experiments are depicted. Due to the limited amount of tissue available for these experiments, and to the low levels of phosphorylated channels under control and test conditions, it was not possible to obtain a reliable band intensity for band densitometry analysis for the Kv4.2 channel phosphorylated in Thr_{607} and some of the results could not be used. Quantification of the changes in channel phosphorylation in Thr_{602} was not possible since the majority of the control samples did not show any staining, although stimulated samples did show it with very low intensity (Figure 4.2 – Kv4.2PThr_{602}). Results for this phosphorylated form were interpreted qualitatively.

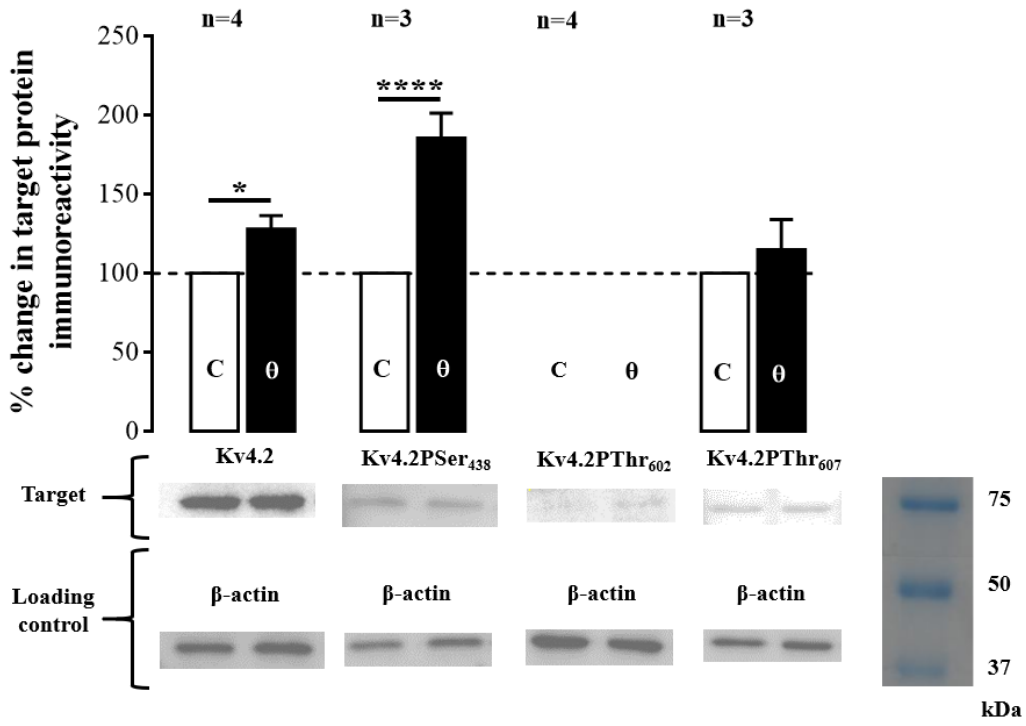

Figure 4.2. LTP induction with moderate TBS enhanced the levels of Kv4.2 channels and its phosphorylation on Ser$_{438}$, but not on Thr$_{602}$ and Thr$_{607}$. Average % change in band density (top) and representative western-blots (bottom) of the observed changes in the different forms of Kv4.2 and loading control. Experiments were performed in total hippocampal membranes isolated from stimulated (θ) and control (C) slices as described in *Methods*. Kv4.2 channel levels and its phosphorylation in Ser$_{438}$, Thr$_{602}$ and Thr$_{607}$ were probed with antibodies specific for this protein or its phosphorylated forms. Values are the mean ± SEM of 3 to 4 experiments (each n represents one animal, 3-4 slices per animal). *p-value < 0.05, ****p-value < 0.0001; Student's t-test.

The levels of Kv4.2 channel increased by 27.9 ± 8.6 % (n = 4) following LTP induction (Figure 4.2 – Kv4.2). As for the phosphorylation of the Kv4.2 channel, there were no changes in phosphorylation in Thr$_{607}$ between control samples with θ-burst stimulated ones (Figure 4.2 – Kv4.2PThr$_{607}$). But, Kv4.2 channel phosphorylation in Ser$_{438}$ increased significantly by 85.6 ± 7.6 % in θ samples (Figure 4.2 – Kv4.2PSer$_{438}$).

Although quantitative analysis for the Kv4.2 channel phosphorylated in Thr$_{602}$ was not possible, a qualitative analysis was made. Most of the control samples did not show any staining, *i.e.* there is no Kv4.2 phosphorylation in Thr$_{602}$ in the control samples. However, for samples stimulated with TBS Kv4.2 channel phosphorylation in Thr$_{602}$ was detected in all samples as evidenced by the presence of a very low intensity band in the respective western-blot results.

It is also important to express results for the phosphorylated forms as the percentage variation ratio to the change in Kv4.2 channel levels, to quantify the modification in Ser$_{438}$ without the contribution of the increase found for the total amount of the channel found in θ-burst stimulated samples.

When corrected for the enhancement in Kv4.2 levels, the changes in Kv4.2 phosphorylation were qualitatively similar to the ones described above. The phosphorylation of the channel in Thr$_{607}$ did not change, but phosphorylation in Ser$_{438}$ increased by 37.9 ± 1.1 % (n = 3; Figure 4.3).

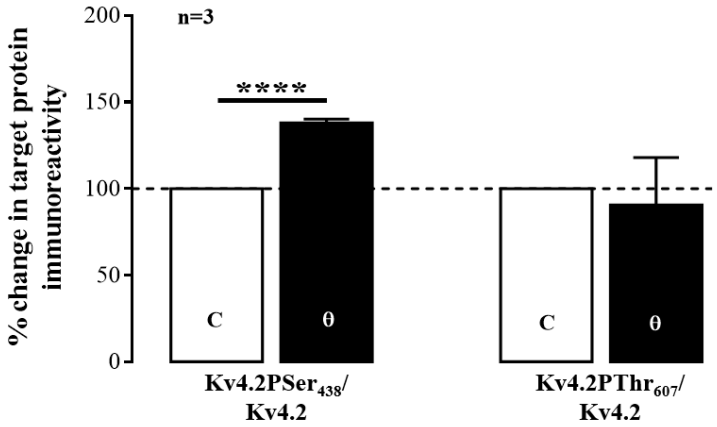

Figure 4.3. LTP induction with moderate TBS enhanced the percentage variation ratio to Kv4.2 channel of phosphorylation on Ser_{438}, but not on Thr_{607}. Average % change in the ratio of the different phosphorylated forms of Kv4.2 to the channel itself. Values are the mean ± SEM of 3 experiments (each n represents one animal, 3 slices per animal). **** p-value < 0.0001; Student's t-test.

4.1.2. PSD-95 and SNAP-25 levels following LTP induction

To make sure that there were no major structural changes at the synapse following LTP induction, the changes in the levels of two synaptic proteins were studied upon TBS: SNAP-25, a pre-synaptic protein, and PSD-95, a post-synaptic protein. As shown in Figure 4.4, the levels of these two proteins did not change.

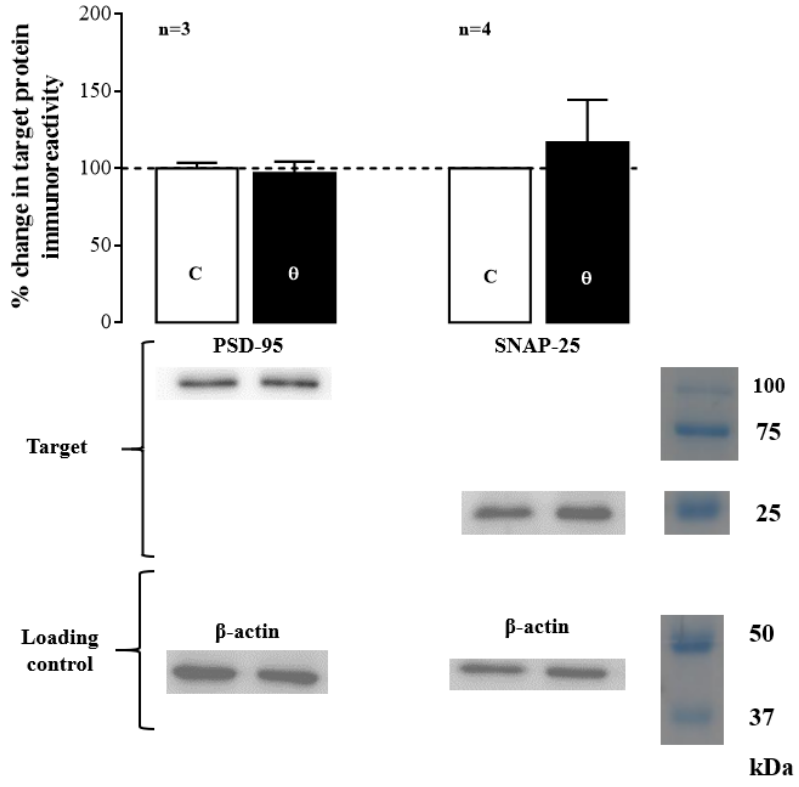

Figure 4.4. LTP induction with moderate TBS did not change PSD-95 and SNAP-25 expression. Average % change in band density (top) and representative western-blots (bottom) of the observed changes in PSD-95 and SNAP-25 levels. Experiments were performed in total hippocampal membranes isolated from stimulated (θ) and control (C) slices as described in *Methods*. Values are the mean ± SEM of 3 to 4 experiments (each *n* represents one animal, 3-4 slices per animal). Student's t-test.

4.2. Lithium-pilocarpine model of TLE

To understand the changes in l_o domains in the rat model of SRSs resembling human MTLE, a validation of the changes in neuronal survival and hippocampus organization, gliosis, synaptic proteins and synaptic plasticity associated channels was performed, that would allow lipid changes to be put in context. Results in chronic SRS rats (Epi) are compared with the ones obtained in rats used as control (*Sham*), which undergone the same procedures and have received the same treatment and drugs as the Epi rats except for the disease inductor, pilocarpine, that was replaced with a vehicle injection.

An interesting note is that the volume of the hippocampus of Epi rats was smaller than *Sham* and had more white nerve fibers on the Alveus surface.

4.2.1. Neuronal survival and hippocampus organization

The extent of neuronal survival and changes in hippocampal architecture in the Li^{2+}-Pilo rat model were evaluated by immunohistochemistry against neuronal nuclear protein (NeuN)-labelling and by Nissl- and Timm-staining ($n = 3$).

Overall, cerebral structures of Epi rats were not as well defined as for *Sham* rats, being harder to obtain a clear image of the hippocampus without artefacts from the fixation for the former group. In some cases, part of the hippocampus was missing. This was probably due to hippocampal atrophy that caused a greater detachment of the hippocampus of Epi rats from the surrounding cerebral tissue, making it very flexible and more sensible to the cutting and fixation process.

4.2.1.1. NeuN immunolabelling

NeuN – neuronal nuclear protein – a specific neuronal marker, was used to investigate the general cellular organization of the hippocampal layers and areas of Epi rats, as compared to *Sham*.

For all the *Sham* rats, the three main areas of the hippocampus, CA1, CA3 and DG, had the expected appearance of and healthy hippocampus (Figure 4.5 – *Sham*). However, the same was not observed for all the three Epi rats, although large differences were noticed between the three individuals. These differences in Epi rats can be due to differences between seizures frequency and total number as well as time passed since chronic seizure onset. Noticeably, one of the rats started to have seizures earlier than the other two.

In Epi rats, more neurons are detected in the *stratum radiatum* and *stratum lacunosum-moleculare* than in *Sham* rats (Figure 4.5 – A vs D), also the pyramidal cell layer of the CA1 region was thinner than the same layer in Sham rats. The pyramidal cell layer of the CA3 region of Epi rats had less neurons than *Sham* rats (Figure 4.5 – B vs E). Finally, the DG granular cell layer did not have a uniform thickness along the layer and had a different architecture in Epi rats (Figure 4.5 – C vs F). Also, the DG granular cell layer showed a more angular shape in Epi than in *Sham* rats and had less neurons in the *hilus*.

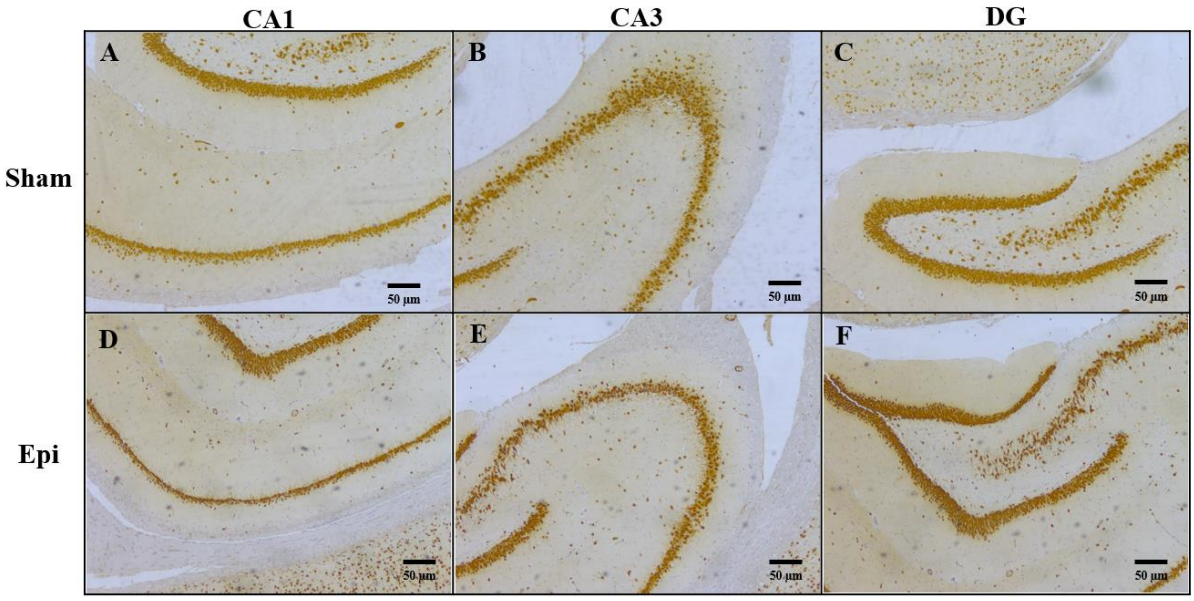

Figure 4.5. Loss and dispersion of CA1 and CA3 pyramidal cells in the hippocampus of Epi rats. Representative immunohistochemistry images of NeuN+ cells in *Sham* (**A-C**) and Epi rats (**D-F**) in the hippocampal CA1 (**A, D**), CA3 **(B, E)** and DG (**C, F**) regions. Brain samples were subjected to formalin fixation and paraffin embedding. Scale bars represent 50 µm.

A neuron count for each hippocampal region was performed for all animals (Figure 4.6). In CA1 and CA3 hippocampal region no significant differences were observed between Epi and Sham rats, due to the fact histological differences were inconsistent between Epi rats. However, in the DG, histological differences were more consistent, and Epi rats showed on average 24.5 ± 6.4 % (n = 3) fewer neurons than *Sham*.

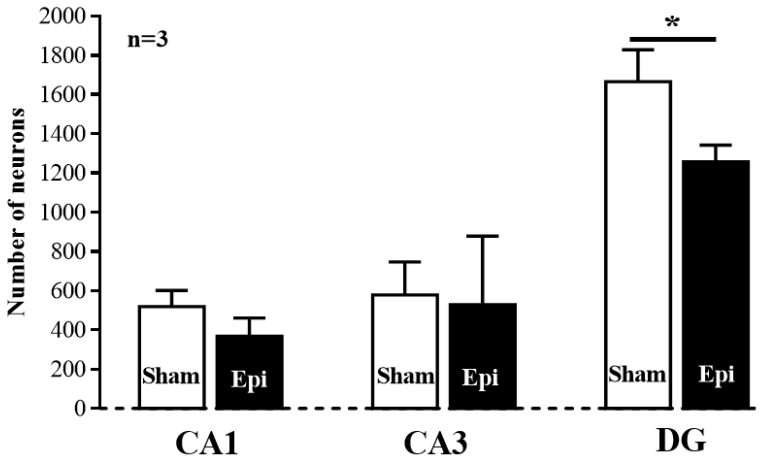

Figure 4.6. Epi rats have less neurons in the DG than *Sham* rats. Change in the number of neurons in the CA1, CA3 and DG regions of the hippocampus for Epi and *Sham* rats. Values are the mean ± SEM of 3 experiments (n represents the number of animals). *****p-value < 0.05; Student's t-test.

4.2.1.2. Nissl-staining

Nissl staining is a selective method for detecting Nissl bodies - large granules of endoplasmic reticulum - making it highly useful for localizing the cell body of both neurons and glia.

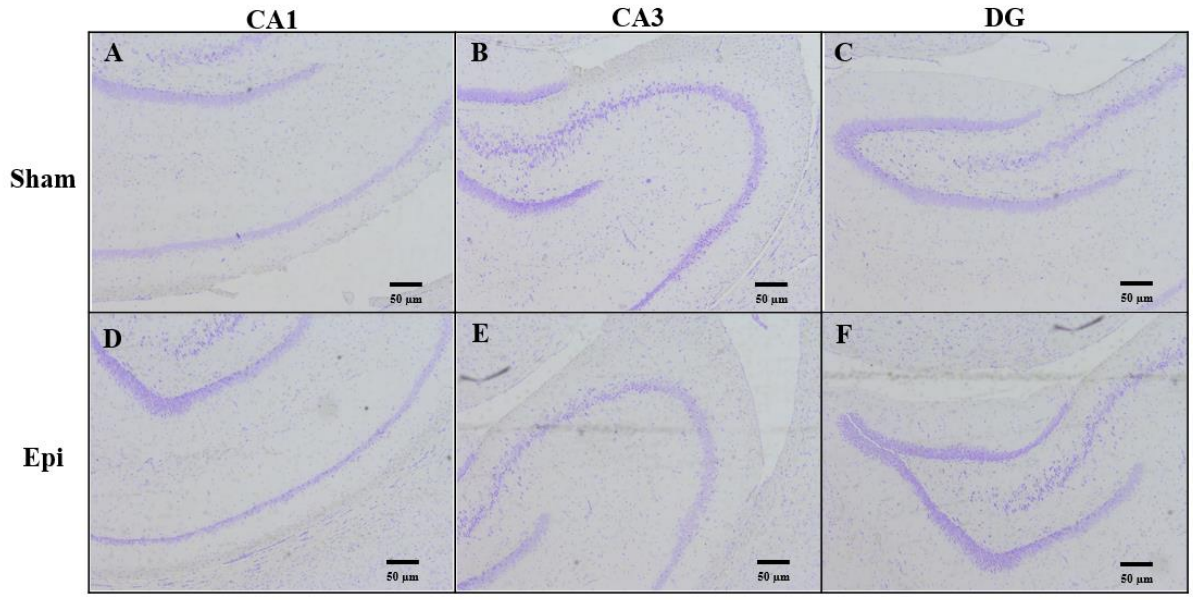

Figure 4.7. Loss of CA1 pyramidal cells in the hippocampus of Epi rats. Representative images of Nissl-stained cells in *Sham* (**A-C**) and Epi rats (**D-F**) in the hippocampal CA1 (**A, D**), CA3 **(B, E)** and DG (**C, F**) regions. Brain samples were subjected to formalin fixation and paraffin embedding. Scale bars represent 50 µm.

Results for Nissl-staining show that in all Epi rats the CA1 pyramidal cell layer is narrower than in *Sham* (Figure 4.7 - Sham), but neuron scattering is not obvious from this coloration as it is with NeuN-labelling. The CA3 area of Epi rats is very similar to the one of *Sham rats* (Figure 4.7 – B and E). Epi rats have a different architecture of the DG as described for the NeuN labelling results: the granular cell layer has variations in the thickness and its shape is more angular. However, differences in neuron number in the *hilus* are not obvious from this coloration and no changes for this area are detected.

4.2.1.3. Timm-staining

Timm-staining revealed a denser staining in the principal cell layers, especially in the granular cell layer of the DG and more fainted in the pyramidal cell's layers of CA1 and CA3 (Figure 4.8). In the *stratum* radiatum of the CA1 region of Epi rats, an enhancement in the number of axons is detected, suggesting axon sprouting occurred. Overall Epi rats' hippocampal neurons are more stained than *Sham*'s.

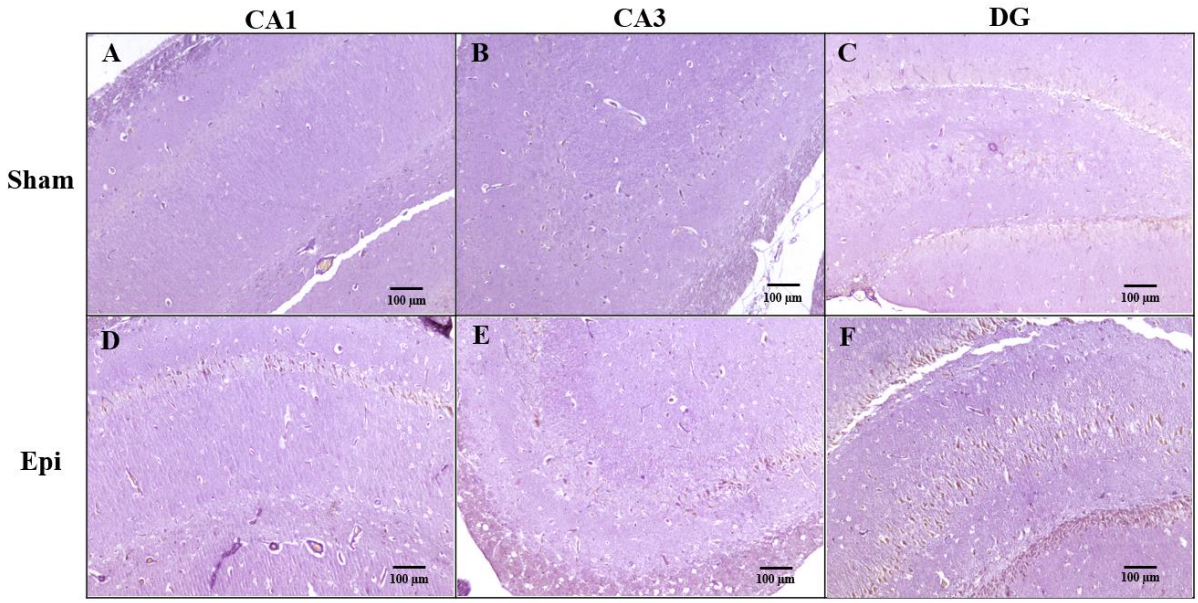

Figure 4.8. Axon sprouting in the hippocampus of Epi rats. Representative images of Timm-stained cells in *Sham* (**A-C**) and Epi rats (**D-F**) in the hippocampal CA1 (**A, D**), CA3 **(B, E)** and DG (**C, F**) regions. Brain samples were subjected to formalin fixation and paraffin embedding. Scale bars represent 100 µm.

4.2.2. Proteins involved in synaptic plasticity and in lipid raft structure

Changes in synaptic plasticity in SRSs rats (TLE model) were evaluated by western blot in isolated hippocampal membranes of *Sham* and Epi rats. Samples were probed for different target proteins and their post-translational modifications: AMPAR subunits GluA1 and GluA2, (and GluA1 phosphorylation in Ser_{831} and in Ser_{845}), PSD-95 and gephyrin, SNAP-25, Kv4.2 channel, and flotillin-1 and caveolin-1.

4.2.2.1. AMPA receptor subunits GluA1 and GluA2

Changes in AMPARs levels, phosphorylation and activity have been described in association with human TLE and in animal models of the disease, affecting its permeability to Ca^{2+} ions. The levels of GluA1 and GluA2 subunits were first evaluated, to determine GluA1/GluA2 ratio which reveals changes in the receptor subunit stoichiometry.

GluA1 and GluA2 levels were lower in Epi rats when compared to *Sham*. GluA1 levels decreased by 42.8 ± 17.5 (n = 4) and GluA2 levels by 50.2 ± 6.8 % (n = 3) respectively (Figure 4.9). The GluA1/GluA2 ratio increased by 20.5 ± 5.5 % (n = 3, Figure 4.9).

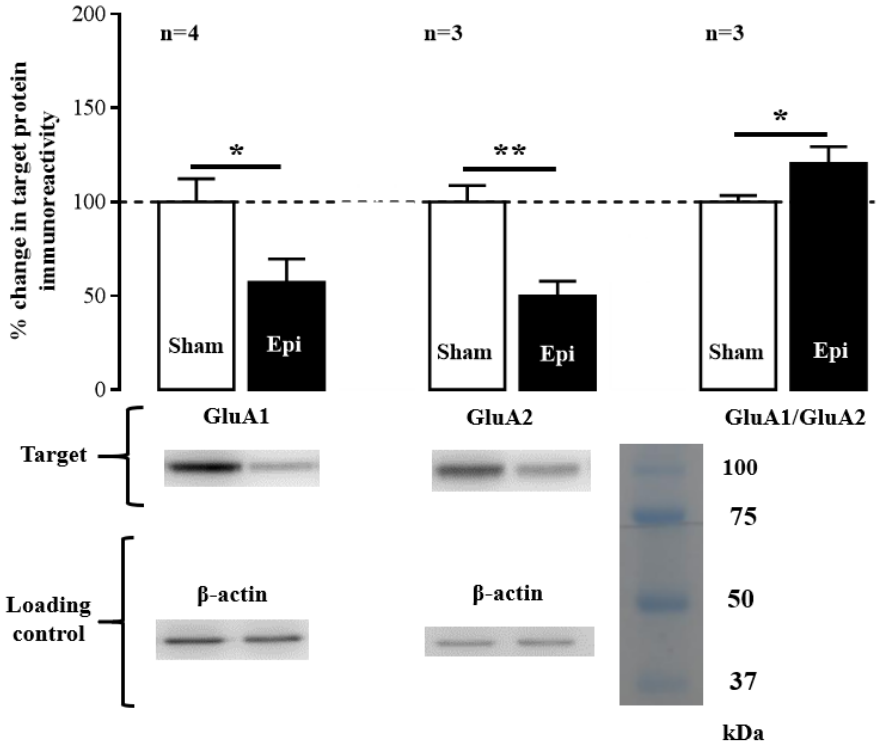

Figure 4.9. Epi rats have lower levels of GluA1 and GluA2 but higher GluA1/GluA2 ratio then *Sham* rats. % change in band density (top) and representative western-blots (bottom) of the observed changes in GluA1 and GluA2 subunit and respective ratio. Experiments were performed in total hippocampal membranes isolated from Epi and *Sham* rats, as described in *Methods*. GluA1 and GluA2 levels were probed with antibodies specific for each of these proteins. Values are the mean ± SEM of 3 to 4 experiments (n represents the number of animals). *p-value < 0.05, **p-value < 0.01; Student's t-test.

4.2.2.2. AMPA receptor subunit GluA1 phosphorylation

AMPAR activity is not only modulated by stoichiometry, but also by phosphorylation of its component subunits. Phosphorylation of GluA1 AMPAR subunit is of particular relevance in synaptic plasticity. By performing western-blot studies using phospho-specific antibodies the phosphorylation of GluA1 on Ser_{831} and Ser_{845} was accessed.

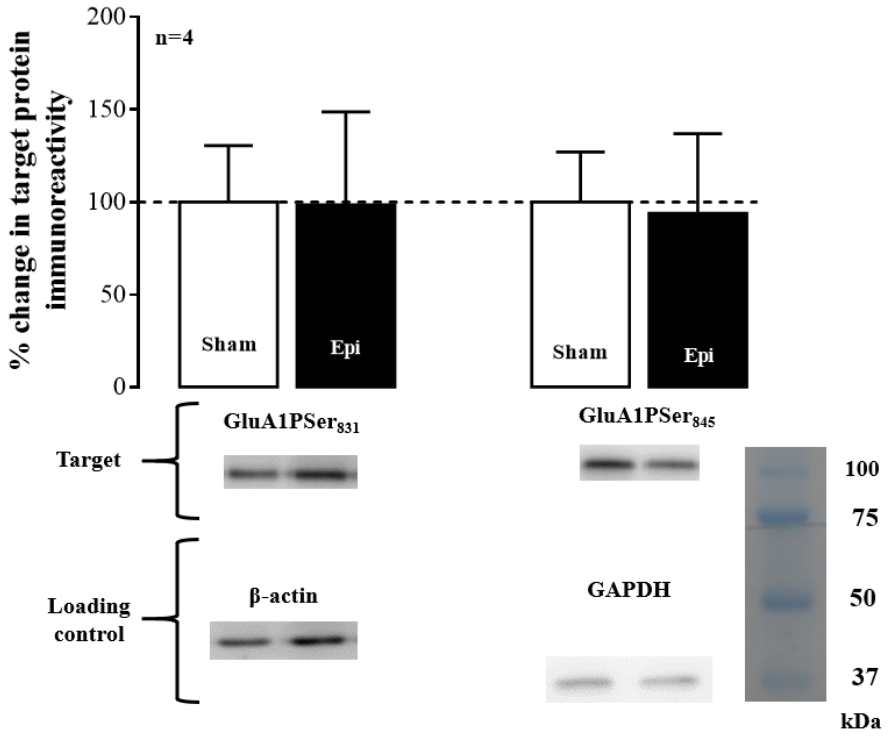

Figure 4.10. GluA1 phosphorylation in Ser$_{831}$ and in Ser$_{845}$ did not change between *Sham* and Epi rats. Average % change in band density (top) and representative western-blots (bottom) of the observed changes in GluA1 phosphorylation in Ser$_{831}$ and Ser$_{845}$. Experiments were performed in total hippocampal membranes isolated from Epi and *Sham* rats, as described in *Methods*. GluA1 phosphorylated in Ser$_{831}$ and Ser$_{845}$ levels were probed with antibodies specific for each of these two forms. Values are the mean ± SEM of 4 experiments (n represents the number of rats). Student's *t*-test did not reveal significant differences.

The levels of phosphorylated GluA1 subunit were not different between *Sham* and Epi rats (Figure 4.10) which could indicate that these modifications have no relevance in TLE. However, it is important to correct the results for phosphorylation of GluA1 to the variation of GluA1 levels between Epi and *Sham* rats, that also contributes to changes in band density. When this is considered (Figure 4.11), phosphorylation of GluA1 on both Ser$_{831}$ and Ser$_{845}$ is increased by 63.5 ± 19.8 (n = 4) and 59.9 ± 16.4 % (n = 4), respectively.

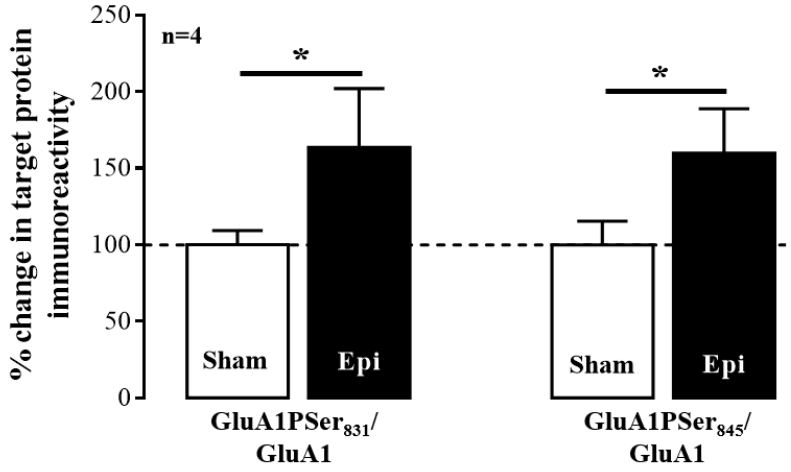

Figure 4.11. Epi rats have higher levels of GluA1 phosphorylated in Ser$_{831}$ and in Ser$_{845}$ when total amount of GluA1 subunit is considered. Average % change in the ratio of both phosphorylated forms of GluA1 subunit, Ser$_{831}$ and Ser$_{845}$, with GluA1 itself. Values are the mean ± SEM of 4 experiments (n represents the number of rats). *p-value < 0.5; Student's t-test.

4.2.2.3. Pre and post-synaptic markers

Other targets studied with western-blot were PSD-95 and gephyrin, two proteins that are specifically located at the glutamatergic and the GABAergic PSD, respectively. Besides these two proteins, pre-synaptic protein SNAP-25 levels were also studied. Although SNAP-25 levels did not change in Epi rats when compared with *Sham*, PSD-95 levels decreased in Epi rats by 53.5 ± 13.9 % (*n* = 4) while gephyrin levels increased by 24.4 ± 5.2 % (*n* = 3; Figure 4.12).

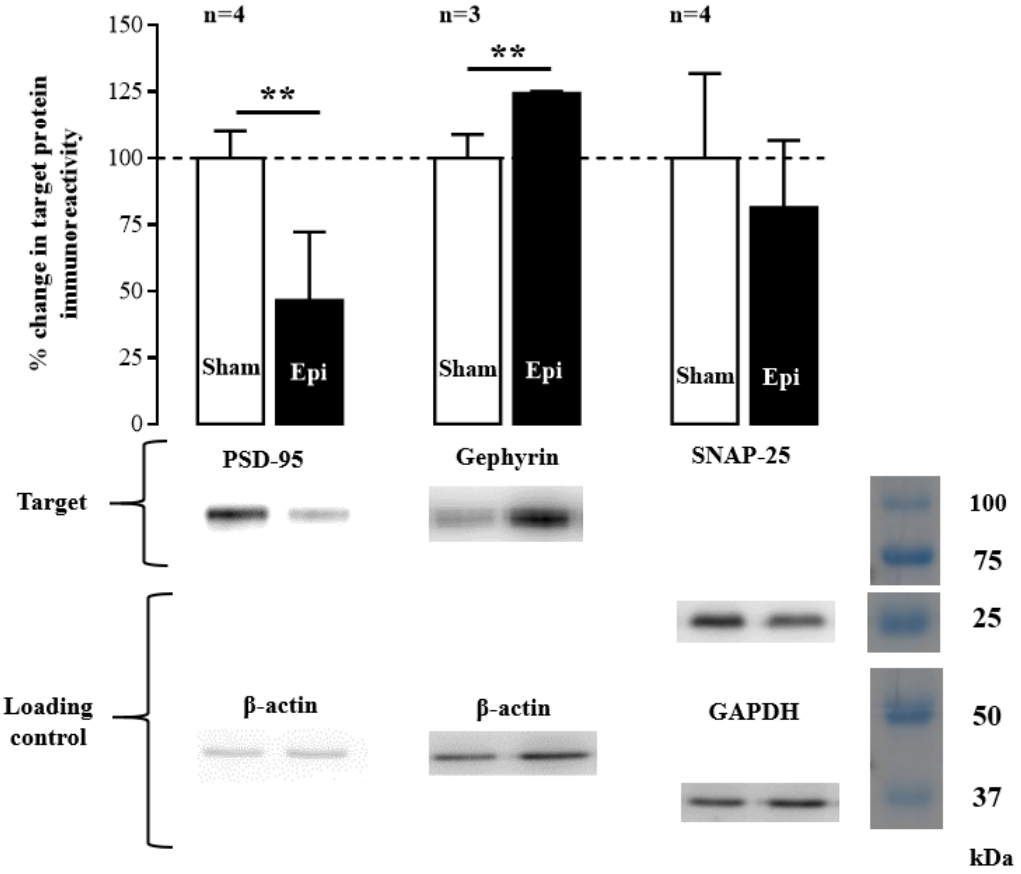

Figure 4.12. PSD-95 levels in Epi rats is lower than in *Sham* rats, and gephyrin levels are increased in Epi rats, while SNAP-25 levels are not changed. Average % change in band density (top) and representative western-blots (bottom) of the observed changes in PSD-95, gephyrin and SNAP-25. Experiments were performed in total hippocampal membranes isolated from Epi and *Sham* rats as described in *Methods*. PSD-95, gephyrin and SNAP-25 levels were probed with antibodies specific for each of these proteins. Values are the mean ± SEM of 3 or 4 experiments (n represents the number of rats). **p-value < 0.01; Student's t-test.

To evaluate how post-synaptic changes relate to the pre-synaptic proteins in Epi rats, the ratio between the post-synaptic proteins, PSD-95 and gephyrin, with SNAP-25 was calculated (Figure 4.13 – PSD-95/SNAP-25 and gephyrin/SNAP-25). The percentage variation ratio of PSD-95 to SNAP-25 revealed a decrease of 48.8 ± 14.5 % (*n* = 4) relative to the presynaptic marker while gephyrin increased by 39.6 ± 12.3 % (*n* = 3) in relation to SNAP-25.

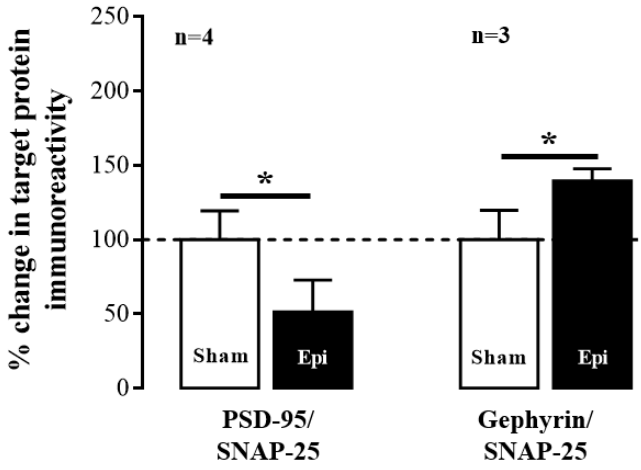

Figure 4.13. The ratio of PSD-95 and gephyrin with SNAP-25 decreased and increased respectively in Epi rats when compared with *Sham* rats. Average % change in the ratio of PSD-95 and gephyrin with SNAP-25. Values are the mean ± SEM of 3 or 4 experiments (n represents the number of rats). *p-value < 0.5; Student's t-test.

4.2.2.4. Kv4.2 channel

As with LTP evoked by TBS (chapter 4.1.1.), the influence of SRSs on Kv4.2 channel expression was also studied by western-blot. Although it would have been interesting to study also the phosphorylation as previous studies have shown these modifications in TLE rodent models, this was not considered crucial for the characterization of our model.

The expression levels of the channel, were not significantly changed in Epi rats (Figure 4.14), but increasing the number of animals may be required.

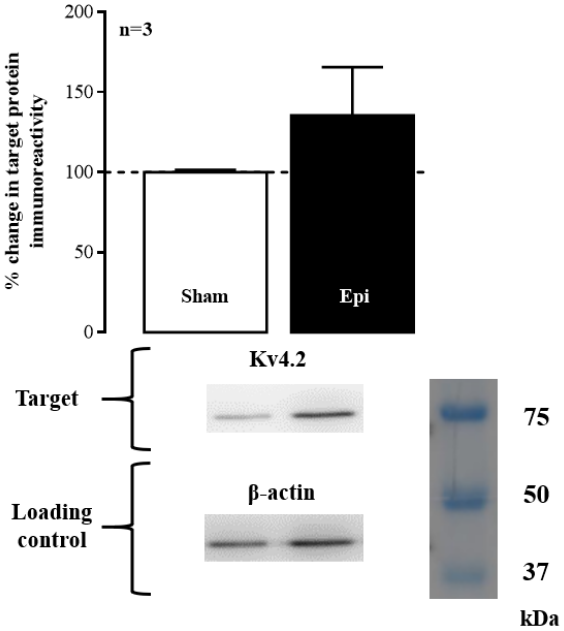

Figure 4.14. Kv4.2 channel levels did not change between Epi and *Sham* rats. Average % change in band density (top) and representative western-blots (bottom) of the observed changes in Kv4.2 channel. Experiments were performed in total hippocampal membranes isolated from Epi and *Sham* rats as described in *Methods*. Kv4.2 channel was probed with a Kv4.2 specific antibody. Values are the mean ± SEM of 3 experiments (n represents the number of rats). Student's t-test.

4.2.2.5. Lipid rafts proteins: flotillin-1 and caveolin-1

Finally, the levels of lipid rafts stabilization proteins flotillin-1 and caveolin-1 levels were also investigated, to find out if these microdomains suffer alterations in TLE. When the level of these proteins increases, it is expected that there is also an increase in the abundance of the membrane domains in which each one is preferentially localized.

The results in Figure 4.15 show that, although flotillin-1 levels did not change between samples, caveolin-1 levels increased by 57.2 ± 9.0 % (n = 3) in Epi rats.

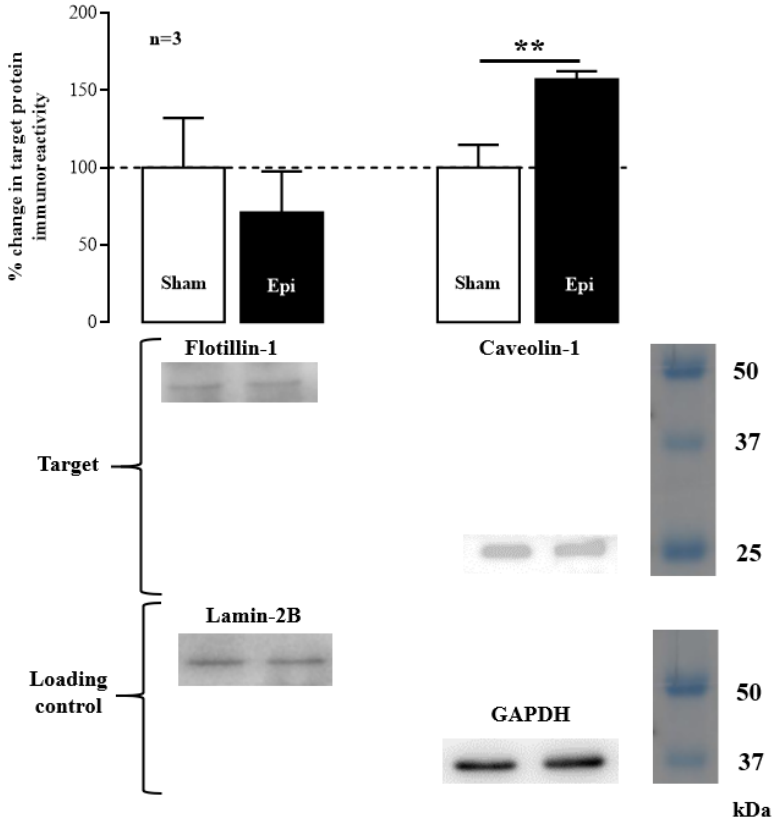

Figure 4.15. Flotillin-1 levels did not change, and caveolin-1 levels are increased in Epi rats when compared with *Sham* rats. Average % change in band density (top) and representative western-blots (bottom) of the observed changes in flotillin-1 and caveolin-1. Experiments were performed in total hippocampal membranes isolated from Epi and *Sham* rats as described in *Methods*. Flotillin-1 and caveolin-1 levels were probed with antibodies specific for each of these proteins. Values are the mean ± SEM of 3 experiments (n represents the number of rats). **p-value < 0.01; Student's t-test.

4.3. Imaging and quantification of lipid domains in GUVs

In the present study, analysis of GUVs prepared with lipids extracted from Epi and *Sham* rat synaptosomes would be important to know if there are any differences between these two samples at synapses, regarding lipid rafts presence and stability. However, the number of biological samples was scarce and limited, and from each synaptosomes preparation only a small amount of lipid could be extracted. Therefore, before working in Epi and *Sham* samples, it was imperative that all the methodologies and techniques inherent to the preparation, imaging and analysis of the domains of GUVs with complex composition were well optimized, to avoid any possible waste of sample. So, optimization of all the procedure and equipment was made by preparing GUVs by electroformation with binary and ternary mixtures of highly pure synthetic lipids which phase behaviour is well known and there are no limitations regarding sample quantity. Optimization of the preparation procedure took longer than

initially anticipated. So, the results presented here are only the ones obtained for the optimization of the procedure.

For that purpose, two lipid mixtures labelled with Rhod-DOPE were prepared with equimolar proportions of the lipid components: DPPC/DOPC and DPPC/DOPC/cholesterol (chol).

Since Rhod-DOPE was used as a membrane probe, all the GUV regions with stronger fluorescence correspond to the presence of l_d domains. Any weakly or non-fluorescent zones that appear in the membrane could be any of the other domains, *i.e.*, ordered domains. L_o domains have a spherical shape and there are usually more than one, while s_o usually have a thread disformed-like appearance.

Looking at the miscibility phase diagrams (Figure 1.10) of the mixtures used in this work at room temperature only two phases for each mixture are expected: for the binary l_d-s_o and for the ternary l_d-l_o.

For the lipid systems used in this work, previous studies of these systems allowed to draw the respective tie-lines, and by using these it is possible to have an estimate of the molar percentage expected for each type of domain (Table 4.1- Lit).

For the binary mixture of DPPC/DOPC (Figure 4.16) the GUVs obtained were small with around 10-15 μm in diameter. However, after careful observation of each one it was possible to notice non-fluorescent zones in the surface of the vesicles that had a shape of a thread, in particular in Figure 4.16 – C.

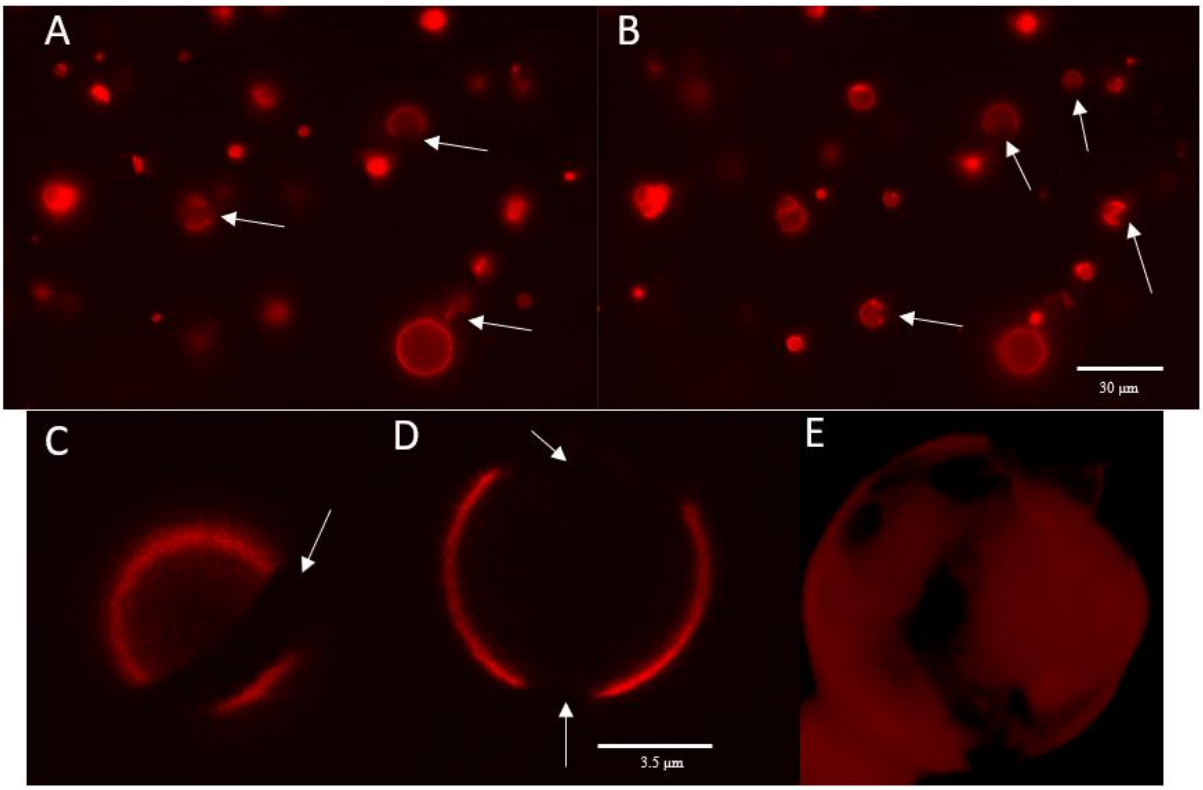

Figure 4.16. Confocal microscopy of GUVs prepared with DPPC/DOPC (equimolar) and Rhod-DOPE as a fluorescent probe reveals the coexistence of s_o and l_d phases. (**A, B**) Two different planes of the same preparation, where several GUVs with s_o domains are identified with white arrows. (**C, D**) A GUV with around 10 μm in diameter, observed in two different focal planes and its three-dimensional representation obtained through a 3D projection of confocal sections (**E**). The non-fluorescent zones pointed by white arrows represent non-l_d domains, that have a snake-like shape which means it corresponds to s_o domains.

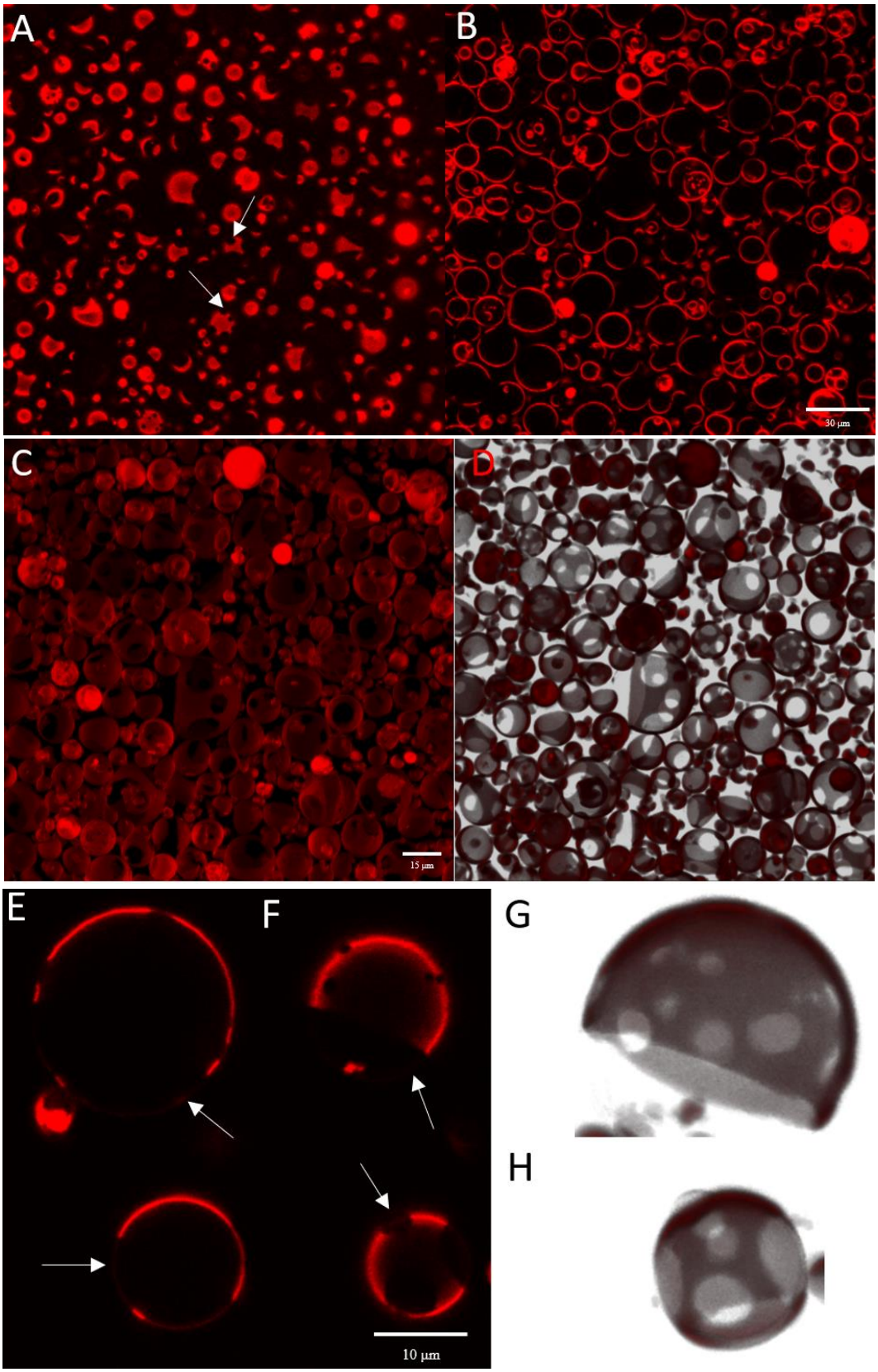

Figure 4.17. Confocal microscopy of GUVs prepared with DPPC/DOPC/chol (equimolar) and Rhod-DOPE as a fluorescent probe reveals the presence of l_d and l_o, *i.e.*, raft-like domains. (**A, B**) Two different planes of the same preparation and its three-dimensional representation obtained through a 3D projection of confocal sections in black (**C**) and white (**D**) background. (**E, F**) Two selected GUVs in two different planes and their three-dimensional representation obtained through a 3D projection of confocal sections (**G, H**). The non-fluorescent zones pointed by white arrows represent non-l_d domains, that have a circular shape which means it corresponds to l_o domains.

As for the ternary mixture which has the same components as the binary and, in addition, cholesterol, all in equimolar amounts, it was easier to obtain bigger GUVs in larger number (Figure 4.17 – A and B) than for the binary mixture. Each GUV had around 20 μm in diameter with the biggest one having more than 30 μm. Zooming in, the presence of round shaped non-fluorescent zones is very distinct in all the GUVs as seen in Figure 4.17 – E and F, which suggests the presence of l_o domains.

The overall phase behaviour of each of the mixtures studied was confirmed. Nonetheless, it can be advantageous to obtain an estimate of the percentage that each type of domain occupies in the GUVs for the two mixtures, *i.e*, to obtain a value that can be used to estimate the mole fraction of each phase. A good approach for determining this is to obtain a 3D reconstruction of the vesicles. Moreover, having the 3D projection allows the possibility to better analyse the different shape of the domains. By comparing the results for the two mixtures using the image corresponding to only one focal plane (Figure 4.16 - C, D with Figure 4.17 – E, F) it is not very easy to distinguish between circular and non-circular domains. But using 3D reconstruction for the same comparison there are no doubts that the domains are different in shape for the two mixtures.

3D view of the GUVs prepared from the binary mixture DPPC/DOPC (Figure 4.16 - E) show the presence of a big non-round non-fluorescent region that represents around 20 % of all surface area of the GUV. The shape of this zone suggests what already was mentioned for the observation of two-dimensional images, that it corresponds to a s_o domain. Therefore, 20 % of each of the GUVs prepared with the binary mixture is s_o domain, and 80 % is l_d.

As for the ternary mixture (Figure 4.17 – G and H), GUVs have more than one perfectly round dark regions that in total make 49 % of the surface area of the GUVs. Not only the shape corresponds to the presence of l_o domain, but also the fact that there are more than one of these circular zones confirms the presence of this phase. So, more than 49 % of each of the GUVs prepared with the ternary mixture of DPPC/DOPC/chol corresponds to l_o domains, and the other 51 % is l_d.

These values were obtained by using the *Measure area* tool of ImageJ which measures areas in 2D but in the 3D projection, which makes them only a rough estimate. A method described by Fidorra *et al.* can determine the lipid surface areas in GUVs independently on the shape of the domains[127]. However, this requires a specific software which was not available. However, since l_o domains have a circular shape, using the mathematical approach described in the methods, it is possible to obtain a more rigorous estimate of the relative surface area of each domain, *i.e.* the percentage each domain occupies in the GUV, in the situation of l_d-l_o phase separation. Results for these calculations are in Table 4.1 (Math).

Knowing the area fraction of each domain in the GUVs and the mean molecular area per lipid in each domain it is possible to calculate the mole fraction of each domain in the GUVs (Table 4.1. – mole fraction), which is comparable to the values obtained from literature (Table 4.1 - Lit).

Table 4.1. Percentage of each domain for the GUVs prepared for binary and ternary mixtures. The values were obtained by using ImageJ *Measure area tool* (ImageJ), mathematical calculations (Math), and from literature (Lit). Values are the mean ± SEM; *n* represents each GUV.

Mixture	Domain	ImageJ		Math		Lit
		area fraction	mole fraction	area fraction	mole fraction	
Binary	l_d	80 ± 1.4 (*n* = 4)	75 ± 1.7 (*n* = 4)	/	/	75*
	s_o	20 ± 1.4 (*n* = 4)	25 ± 1.7 (*n* = 4)	/	/	25*
Ternary	l_d	51 ± 2.2 (*n* = 4)	43 ± 2.1 (*n* = 4)	55.7 ± 4.9 (*n* = 12)	47 ± 4.9 (*n* = 12)	50**
	l_o	49 ± 2.2 (*n* = 4)	57 ± 2.1 (*n* = 4)	44.3 ± 4.9 (*n* = 12)	53 ± 4.9 (*n* = 12)	50**

* Values estimated using the tie-lines and phase diagram from [117] for DPPC/DOPC equimolar.

** Values estimated using the tie-line and phase diagram from [116,128] for DPPC/DOPC equimolar with 30 % of chol.

5. Discussion

5.1. Molecular changes in LTP induced with moderate θ-burst stimulation

5.1.1. Kv4.2 channel association with LTP modulation

In this work western-blot was performed to evaluate possible molecular changes in Kv4.2 channel and its phosphorylation following LTP induction with a moderate TBS in hippocampal rat slices. A quantitative analysis revealed that LTP induction caused an increase in Kv4.2 channel expression and phosphorylation at Ser_{438}, while no changes were observed for the phosphorylation at Thr_{607}. A qualitative analysis of the phosphorylation at Thr_{602} showed no detectable phosphorylation in control slices however, a clear phosphorylation Kv4.2 channel was observed in θ-burst stimulated slices.

TBS is the LTP induction stimulation pattern that better mimics the physiologically neuronal activity in the hippocampus during learning tasks[16,17]. However, depending on the intensity and duration of pattern of stimulation, LTP induction with TBS can be dependent on NMDA receptors and/or L-type voltage-dependent calcium channels[16]. These two forms of LTP coexist in the CA1 area of the hippocampus and it was suggested that each of them has independent roles in learning and memory[16]. Also, NMDA receptor-dependent LTP can be either PKA-dependent or not[42]. Moderate TBS, such as the one used in our study is NMDA receptor dependent[16] but not PKA-dependent[42], which is confirmed by previous results of our lab (Figure 1.4).

As mentioned earlier, NMDA receptor activation leads to a Ca^{2+} influx that activates CaMKII. Enhancement of CaMKII activity can be the cause for the enhanced Kv4.2 channel phosphorylation at Ser_{438} found in this work, since phosphorylation at this residue is catalysed by CaMKII. This post-translational modification leads to an increase in the cell-surface expression of the channel[66], which can explain the increase of the channel levels found in this work. Since the increase of the channel expression leads to an increase of I_A[129] and consequently to the decrease of dendritic excitability, the increased expression of this channel does not seem to contribute to LTP expression, but rather opposing it. This result is in agreement with the up-regulation of dendritic Kv4.2 mRNA observed in another work, which was NMDA receptor- and Ca^{2+}-dependent, indicating that Kv4.2 mRNA levels are regulated in response to synaptic activity[130].

Another study has showed that Kv4.2 internalization contributes to LTP induced chemically with glycine, and also suggest that the channel internalization contributes to LTP induced with a low frequency stimulation[68]. The phosphorylation of Kv4.2 channel at Thr_{602} is associated with Kv4.2 channel internalization and I_A decrease[63]. Therefore, the increase in the levels of phosphorylation of the Kv4.2 channel at Thr_{602} found in the present work might be contributing to LTP expression, through the internalization of the Kv4.2 channel that would lead to a decrease in I_A.

In this work we observed an enhancement in the Kv4.2 channel phosphorylation simultaneously at Ser_{438} and at Thr_{602}, and the consequence previously described for each of these phosphorylations is opposed. However, one must consider that no differentiation between the different cellular regions of the membrane of the neurons was possible in this work since the whole hippocampal slice was analysed, and therefore each phosphorylation can be associated to different regions of the neuron. It is known that along the dendrites of neurons of the CA1 region of the hippocampus (pyramidal cells) the density of Kv4.2 channel is different[60]. One possible explanation for the results of this work on Kv4.2 phosphorylation is that the regulation of the channel is different along the dendrites in response to the stimulation that induced LTP, *i.e.* in certain segments of the dendrites Kv4.2 channel may be phosphorylated in Ser_{438} and in other segments the channel may be phosphorylated in Thr_{602}. This hypothesis would imply that the overall enhancement of Kv4.2 expression in response to TBS is not representative of the specific changes in Kv4.2 signalling at the synapse.

Our results suggest that LTP involves regulation of Kv4.2 channel, which agrees with results that show that these channels modulate spatial memory formation in rats[131].

5.1.2. PSD-95 and SNAP-25 expression was not affected by θ-burst stimulation

Western-blot was also used to evaluate the levels of PSD-95 and SNAP-25 following LTP induction with moderate TBS in rat hippocampal slices. The levels of PSD-95 and SNAP-25 did not change following LTP induction. However, this does not mean that these proteins do not have a role in LTP expression or maintenance.

According to Ehrlich *et al*. PSD-95 is not necessary for the induction and early expression of LTP, so no alterations in the proteins levels are expected, which agrees with the results obtained in this work[132]. However, after the expression of LTP this scaffolding protein is required for synapse stabilization. The mechanism suggested for this is through regulation of the AMPAR trafficking. El-Husseini *et al*. have showed that the rapid internalization of this receptor requires depalmitoylation of PSD-95 and suggest that regulation of the palmitate cycle on PSD-95 can regulate synaptic strength through changes in AMPAR trafficking upon which synaptic plasticity depends[133].

The same can be concluded in relation to SNAP-25 results. Although it has been suggested that this protein may be involved in memory consolidation in the CA1 region of the hippocampus[134], no changes in its levels have been reported after LTP induction in this work. In another work, also no changes were detected in SNAP-25 levels following LTP induced with high-frequency stimulation (tetanic simulation) in the Schaffer collateral CA1 synapses[135]. However, LTP induction with strong TBS leads to SNAP-25 phosphorylation[75] which promotes insertion of NMDA receptors responsible for LTP expression[136]. This suggests a possible role of SNAP-25 which expression does not change but, which function can be regulated through fast post-translational mechanisms. This possible role of SNAP-25 can be associated not only with pre-synaptic vesicle fusion, but also with post-synaptic functions, since recently has been found that SNAP-25 is also present in postsynaptic spines, being suggested that this protein has a function in post-synaptic vesicle exocytosis[135].

The fact that no changes were obtained in the levels of these two proteins following LTP induction, that all have been in some way connected to LTP, and that following LTP induction kinases responsible for post-translational modification, such as CaMKII, are highly activated, suggests that the stimulation pattern applied in this study activates mainly rapid regulation mechanisms such as phosphorylation or depalmitoylation which are important to the expression and/or maintenance of LTP.

5.2. Changes in lithium-pilocarpine model of TLE

5.2.1. Neuronal death and reorganization in the *dentate gyrus*

NeuN immunolabelling was performed to study neuronal organization in the hippocampus of rats showing SRSs induced with Li^{2+}-Pilo. Results for NeuN staining were not consistent between epileptic rats. Overall the CA1, CA3 and the DG *hilus* of the hippocampus had less neurons, but statistical significance was only found in the DG. The DG of Epi rats also had a distinct angular shape in the granular cell layer.

These differences between epileptic rats could be due to differences between seizures frequency and number. In fact, one of the rats that showed different neuronal pathology started to have seizures earlier than the others and had seizures more frequently, suggesting that progression of the disease was faster in this animal, thus leading to more damage. Moreover, recent evidence showed that neuronal survival correlates negatively with seizure frequency[137].

Also, Nissl-staining method was performed, and showed that the CA1 area of the hippocampus of epileptic rats, had less cells than control rats and the granular cell layer of the DG had an angular shape.

Neuronal death in the *hilus* of the DG area of the hippocampus detected for all the rats in NeuN-labelling results characterizes TLE, alongside a not so highlighted neuronal loss in the pyramidal cell layer of the CA1 and CA3 area[138,139].

Neuronal death in the *hilus* can be the cause of the angular shape found for the granular cell layer observed in the DG for all epileptic rats with both NeuN immuolabelling and Nissl-staining. The loss of *hilar* neurons could lead to the collapse of the granular cell layer of the DG to the interior (in the direction of the CA3) as seen in the results of this work.

Timm-staining results show that epileptic rats had higher staining than *Sham* rats, especially in the granular cell layer of the DG and in the CA4 area, but also in CA1 and CA3 areas. This higher staining indicates that mossy fiber (the axons granule cells) sprouting occurred in the DG. It is proposed that neuronal loss in the *hilus* of the DG area of the hippocampus (also observed in the present work), leads to this mossy fiber sprouting and re-innervation of new regions of the DG[140]. Higher mossy fiber sprouting is also found in the DG of both human TLE patients [140,141] and in several rat models of TLE[142,143], and it is thought to underlie the creation of aberrant circuitry which promotes the generation and/or spread of SRSs[143].

5.2.2. AMPA receptor subunit regulation leads to hyperexcitability that characterizes TLE

Evaluation of the AMPAR composition in isolated hippocampal membranes of rats showing SRSs revealed that the AMPAR subunits GluA1 and GluA2 levels decreased, and the GluA1/GluA2 ratio increased. Also, an increase in the phosphorylation of GluA1 in Ser_{831} and Ser_{845} residues was observed.

Eight weeks following SE induction with KA, a down-regulation of GluA2 subunit is observed in rats hippocampus[96], a result that agrees with the decrease of GluA2 here described.

Lopes *et al.* have shown that 50 days after SE induced with pilocarpine GluA1 levels do not change[55] in the hippocampus of rats, which is not agreement with our observation of decreased GluA1 levels. In the same work no changes in GluA1 phosphorylation in Ser_{831} are detected while, the level of hippocampal GluA1 phosphorylation at Ser_{845} is decreased [8]. The same group described that 60 days after SE induced in rats with pilocarpine, GluA1 phosphorylation on Ser_{845} was decreased in the dorsal hippocampus, while GluA1 in the ventral hippocampus was instead less phosphorylated in Ser_{831} residue. Those results are not in agreement with what was found in this work: an enhancement in GluA1 phosphorylation in Ser_{831} and Ser_{845}. However, in our study, rats are also in a chronic phase of the disease, not only with 50 days after SE, but 9 months after SE induced with Li^{2+}-Pilo. This suggests that there are differences in GluA1 phosphorylation along the chronic period in SRS rats, *i.e.*, with the progression of the disease.

The increase in the phosphorylation of GluA1 at Ser_{845} observed in this work, suggests that an increase of the open probability of the channel of AMPAR and in the recruitment of this receptor from intracellular compartments to the extra-synaptic region. In addition, Ser_{831} phosphorylation leads to an increase of the conductance state of the AMPAR and of the recruitment of the receptor to the synaptic region. These relations suggest that, overall, in the chronic period of TLE, there are more AMPARs in the synaptic region with channels in higher conductance states. This leads to the existence of larger EPSPs, and consequently, neurons are easier to stimulate. So, these post-translational modifications possibly contribute to the disease. Since PKA is the only known kinase that catalyses phosphorylation in Ser_{845}, this result suggests that this kinase has a higher activity and/or a role in the chronic period of TLE. However, for phosphorylation in Ser_{831}, there are two possible enzymes that catalyse the modification: CaMKII and PKC; which makes it unpredictable which one of the two, or even if both these enzymes have higher activity in this model of TLE.

The increase in GluA1/GluA2 ratio found in this work, suggests that the pool of GluA2-lacking receptors is increased in rats with SRSs. This pool is permeable to Ca^{2+}, which hints that there is a higher influx of Ca^{2+} following depolarization, that can both activate kinases, such as CaMKII and increase the excitability of the neurons thus leading to excitotoxicity and contributing to the progression of the

disease. The present work was the first to study the GluA1/GluA2 ratio in the chronic period of rodent models of TLE.

Probably, the enhancement in GluA1 phosphorylation in Ser_{831} and Ser_{845} and the increase in the number of Ca^{2+}-permeable AMPARs, happens at the same time, or at time scales that are not distinguishable, as a result from overly excitation of the neurons that occurs during seizures. This in turn leads also to Ca^{2+} influx through, among other, NMDA receptors[96]. This influx activates kinases, such as CaMKII and PKA, that regulate, the interaction of the receptor with associated proteins that modulate the membrane trafficking and synaptic targeting of the AMPARs[144]. This NMDA receptor and PKA dependent mechanism agrees with what is seen in LTP induced with high frequency stimulation patterns[42,47].

5.2.3. PSD-95 and gephyrin expression is altered in the chronic period of TLE: a new adaptive mechanism that guarantees animal survival?

In this work, the PSD-95 and gephyrin levels showed opposite changes in the model of chronic period of TLE studied: PSD-95 expression decreased while gephyrin expression increased. These results were maintained when the levels of PSD-95 and gephyrin were normalized to the variation the levels of SNAP-25, taken as a marker of the total number of synapses, *i. e.*, the ratio of PSD-95 to SNAP-25 expression decreases, while the ratio of gephyrin to SNAP-25 levels increases.

A decrease in the levels of PSD-95 was also observed in a previous study in the hippocampus of rats 4 to 6 weeks after SE was induced with KA[10].

Immunohistochemistry studies from Fang *et al.* (2011) show that gephyrin levels are decreased in the hippocampus of rats in the latent and chronic period of TLE, from 24 hours to 2 months after the first grade of seizures induced with Li^{2+}-Pilo[89]. This decrease in gephyrin does not agree with the increase found in our work, however, this difference is probably due to the fact that our study was performed 9 months after SE, while in the work of Fang *et al.* the study is conducted 24 hours to 2 months after SE was induced, an early stage of the disease. Also, in the present work Wistar rats were used, while the work of Fang *et al.* was conducted using Sprague-Dawley.

PSD-95 is a scaffolding PSD protein that promotes maturation and strengthening of excitatory synapses[145] and regulates AMPAR trafficking *in vitro* and *in vivo*[79,146–148]. These roles lead to regulation of synaptic strength such as the ones that underlie synaptic plasticity mechanisms. Taking this into account, the decrease found in PSD-95 levels will consequently lead to a dampening of excitatory synapses, reducing neuronal excitability.

Gephyrin controls the number of postsynaptic $GABA_A$ receptors[88] and its recruitment to the PSD leads to the immobilization of $GABA_A$ receptors at synapses[149]. These receptors mediate inhibitory transmission, so an increase in gephyrin, likely reflects an increase in synaptic targeting of $GABA_A$ receptors and consequent increase in inhibitory transmission, that may have a role in the control of excessive pyramidal/principal cell excitability in TLE.

The change in gephyrin and PSD-95 levels here reported suggest that this alteration must be an adaptative mechanism that neurons have to reduce the hyperexcitability imposed by other molecular mechanism such as the ones mentioned in the previous chapter (5.2.2) that involved AMPAR, *i.e.* a neuronal protection to the excitotoxic conditions.

5.2.4. Kv4.2 channel is not changed in the chronic period of TLE

No significant difference on the Kv4.2 channel levels were found in the chronic period of the Li^{2+}-Pilo rat model of TLE when compared with the controls. In a previous study, 50 days after SE induced in rats with Li^{2+}-Pilo, a decrease in the Kv4.2 channel was observed in the hippocampus[11], which is not

in agreement with our results. However, as already discussed in a previous chapter (5.2.2), since our rats were studied 9 months (270 days) after SE induction, and not 50 days, there may be differences along the chronic period of TLE in the expression of this channel.

It is important to note that the dispersion of the results for SRS rats was very large, influencing the result for the Kv4.2 channel. A non-statistical analysis by simple observation suggests that the Kv4.2 channel levels tend to increase. A confirmation of these results would require an increase in the number of the samples probed for this channel.

5.2.5. Temporal lobe epilepsy and lipid rafts

In this work we have shown that caveolin-1 levels are increased in hippocampal membranes of rats with SRSs, but flotillin-1 levels did not change. This was the first time that the level of proteins that are associated with lipid rafts, flotillin-1 and caveolin-1 was studied in the context of TLE.

Whether the increase of caveolin-1 found in this work constitutes an additional mechanism of neuronal protection, to counteract hyperexcitability, or is itself contributing to the disease would require extending the studies in the present work. However, one may wonder what is changed with the alteration in this protein. In neurons, caveolin is involved in trafficking of signalling complexes, neuronal differentiation, regulation of neurotransmitter binding[106], and neuroprotection[150,151]. Caveolin-1 can inhibit the binding of ligands to AMPARs by inhibiting phospholipase A_2[109]. This enzyme, when activated, can change the lipid environment of AMPARs increasing its affinity to ligands[109]. It is possible that the high neuronal influx on Ca^{2+} that characterizes repeated firing and depolarization in TLE can activates this enzyme leading to higher AMPARs affinity for glutamate, that in turn may contribute to hyperexcitability. Considering this possibility, and the role of caveolin in neuroprotection, the enhancement in caveolin-1 levels in the hippocampus of rats with SRSs, reported in this work could be another neuronal protective mechanism, by promoting inhibition phospholipase A_2, and consequently neuronal excitability.

As for flotillin-1, a planar lipid raft associated protein, its levels did not change in the hippocampus of rats with SRSs. Swanwick *et al.* have shown through immunocytochemical and electrophysiological assays that flotillin-1 promotes the formation of glutamatergic, but not GABAergic, synapses in the hippocampus[152]. As suggested by the authors, flotillin-1 enhances the formation of glutamatergic synapses probably by accelerating dendritic spine formation and maturation, since it induces filopodia formation[152]. PSD proteins are highly connected with lipid rafts, *e.g.* PSD-95. The increase of PSD-95 and flotillin-1 separately increases glutamatergic transmission. Furthermore, raft depletion reduces the density of PSD-95 along dendrites[153]. No significant changes were found for flotillin-1 levels in the chronic period of TLE, probably because of the high error associated with the results, associated to poor antibody staining. If statistics are not considered, the levels of the protein seem to decrease in diseased animals. If this is true, then it suggests that, due to flotillin-1 role in promoting glutamatergic synapse formation, this decrease is contributing to reduce glutamatergic transmission. This would again suggest a neuroprotective role for flotillin-1 in the chronic period of TLE, alongside caveolin-1, PSD-95 and gephyrin. However, enhancing the size of the sample with a more sensitive antibody would be important to accurately address this question.

5.3. GUV preparation by electroformation was optimized

GUVs observation and preparation with artificial mixtures by the electroformation method was successfully achieved in this work.

The number of GUVs prepared from the DPPC/DOPC/chol mixture was larger and produced bigger GUVs than the ones obtained with the DPPC/DOPC mixture. This is probably due to the presence of

the gel domain, that in the binary mixture decreases the GUV stability, or renders their formation more difficult, hence the smaller number of GUVs obtained for this mixture.

The mole fraction of each phase in the GUVs prepared with the binary mixture estimated with visual cues was equal to the one obtained by other studies using tie-lines and phase diagrams[117]. For the ternary mixture, the mole fraction of each phase estimated with both the visual cues and through a mathematical approach was very close to what is found in literature[116,128], with the mathematical approach having closer values. This suggests that both methods used are good approaches to estimate phase coexistence, with the mathematical one being slightly better than the one that uses visual cues.

6. Conclusion and future perspectives

This work characterized the hippocampal membranes of a rat SRS model of TLE obtained by the lithium-pilocarpine injection procedure. In this model it was observed that:

- The *dentate gyrus* suffers more damage than the other hippocampal regions;
- An enhancement of AMPAR GluA1 subunit phosphorylation and changes in AMPAR subunit composition leads to hyperexcitability that characterizes TLE, contributing to the maintenance of the disease;
- PSD-95 levels are decreased and gephyrin expression is enhanced in a way that is consistent with a role in promoting animal neuroprotection from excessive neuronal activity;
- Caveolin-1 expression is enhanced suggesting an involvement of lipid raft changes in the disease, which is probably also neuroprotective;
- There are likely changes along the timeline of the chronic period of TLE in the expression of several synaptic/molecular markers.

In this work it was also studied the possible role of Kv4.2 channel phosphorylation, in the expression of LTP induced with a moderate θ-burst stimulation. It was concluded that modulation of the Kv4.2 channel has a role in LTP induced with a moderate θ-burst stimulation, through phosphorylation in Ser_{438} and Thr_{602} but not in Thr_{607}.

Although the present work has demonstrated some molecular mechanisms that underlie both LTP expression and synaptic and molecular membrane changes in TLE, more studies are needed to fully understand their precise role in disease pathology. An important study would be to have different rats along the timeline of the lithium-pilocarpine model, *i.e.* to study the SE, the latent period and the chronic period of this TLE model, in each of the different regions of the hippocampus and in the temporal cortex, regarding the levels of the same proteins approached in this work, and their phosphorylation and palmitoylation. Also, using the same timeline approach, the presence of lipid rafts and their stability in the disease needs to be studied, to better understand how the change found for caveolin-1 expression could be related to TLE. One possible study is the analysis of GUVs prepared with lipids extracted from lithium-pilocarpine and *Sham* rats synaptosomes, together with lipidomic studies. This type of approach would be important to unravel the molecular changes that happen along the progression of the disease, and define differences between epileptogenesis, its consequence along time and the adaptive mechanisms that try to guarantee the animal survival. A matter of finding what is cause, and what is consequence.

7. References

1. WHO. Fact sheet: Epilepsy. (2018).
2. Herman, S. T. Epilepsy after brain insult: targeting epileptogenesis. *Neurology* **59,** S21-6 (2002).
3. Malkin, S. L. *et al.* Changes of AMPA receptor properties in the neocortex and hippocampus following pilocarpine-induced status epilepticus in rats. *Neuroscience* **327,** 146–155 (2016).
4. Temporal Lobe Epilepsy (TLE) | Epilepsy Foundation. Available at: https://www.epilepsy.com/learn/types-epilepsy-syndromes/temporal-lobe-epilepsy-aka-tle. (Accessed: 21st July 2018)
5. Gu, B. & Dalton, K. A. Models and detection of spontaneous recurrent seizures in laboratory rodents. *Zool. Res.* **38,** 171–179 (2017).
6. Raimondo, J. V. *et al.* Methodological standards for in vitro models of epilepsy and epileptic seizures. A TASK1-WG4 report of the AES/ILAE Translational Task Force of the ILAE. *Epilepsia* **58,** 40–52 (2017).
7. Kandratavicius, L. *et al.* Animal models of epilepsy: use and limitations. *Neuropsychiatr. Dis. Treat.* **10,** 1693–705 (2014).
8. Lopes, M. W. *et al.* Region-specific alterations of AMPA receptor phosphorylation and signaling pathways in the pilocarpine model of epilepsy. *Neurochem. Int.* **87,** 22–33 (2015).
9. Curia, G., Longo, D., Biagini, G., Jones, R. S. G. & Avoli, M. The pilocarpine model of temporal lobe epilepsy. *J. Neurosci. Methods* **172,** 143–57 (2008).
10. Sun, Q.-J. *et al.* Alterations of NR2B and PSD-95 expression in hippocampus of kainic acid-exposed rats with behavioural deficits. *Behav. Brain Res.* **201,** 292–299 (2009).
11. Su, T. *et al.* Altered expression of voltage-gated potassium channel 4.2. and voltage-gated potassium channel 4-interacting protein, and changes in intracellular calcium levels following lithium-pilocarpine-induced status epilepticus. *Neuroscience* **157,** 566–576 (2008).
12. Mansvelder, H. D., Verhoog, M. B. & Goriounova, N. A. Synaptic plasticity in human cortical circuits: cellular mechanisms of learning and memory in the human brain? *Curr. Opin. Neurobiol.* (2018).
13. McNamara, J. O., Huang, Y. Z. & Leonard, A. S. Molecular signaling mechanisms underlying epileptogenesis. *Sci. STKE* **2006,** re12 (2006).
14. Volianskis, A. *et al.* Long-term potentiation and the role of N-methyl-d-aspartate receptors. *Brain Res.* **1621,** 5–16 (2015).
15. Citri, A. & Malenka, R. C. Synaptic plasticity: multiple forms, functions, and mechanisms. *Neuropsychopharmacology* **33,** 18–41 (2008).
16. Morgan, S. L. & Teyler, T. J. Electrical Stimuli Patterned After the Theta-Rhythm Induce Multiple Forms of LTP. *J. Neurophysiol.* **86,** 1289–1296 (2001).
17. Larson, J. & Munkácsy, E. Theta-burst LTP. *Brain Res.* **1621,** 38–50 (2015).
18. Collingridge, G. L., Kehl, S. J. & McLennan, H. Excitatory amino acids in synaptic transmission in the Schaffer collateral-commissural pathway of the rat hippocampus. *J. Physiol.* **334,** 33–46 (1983).
19. Ascher, P. & Nowak, L. The role of divalent cations in the N-methyl-D-aspartate responses of mouse central neurones in culture. *J. Physiol.* **399,** 247–66 (1988).
20. Miller, S. G. & Kennedy, M. B. Regulation of brain type II Ca2+/calmodulin-dependent protein kinase by autophosphorylation: a Ca2+-triggered molecular switch. *Cell* **44,** 861–70 (1986).
21. Benke, T. A., Lüthi, A., Isaac, J. T. R. & Collingridge, G. L. Modulation of AMPA receptor unitary conductance by synaptic activity. *Nature* **393,** 793–797 (1998).
22. Mammen, A. L., Kameyama, K., Roche, K. W. & Huganir, R. L. Phosphorylation of the alpha-amino-3-hydroxy-5-methylisoxazole4-propionic acid receptor GluR1 subunit by calcium/calmodulin-dependent kinase II. *J. Biol. Chem.* **272,** 32528–33 (1997).
23. Chater, T. E. & Goda, Y. The role of AMPA receptors in postsynaptic mechanisms of synaptic plasticity. *Front. Cell. Neurosci.* **8,** 401 (2014).
24. Johnston, D. *et al.* Active dendrites, potassium channels and synaptic plasticity. *Philos. Trans. R. Soc. B Biol. Sci.* **358,** 667–674 (2003).
25. Monday, H. R., Younts, T. J. & Castillo, P. E. Long-Term Plasticity of Neurotransmitter Release: Emerging Mechanisms and Contributions to Brain Function and Disease. *Annu. Rev. Neurosci.*

41, 299–322 (2018).
26. Lamprecht, R. & LeDoux, J. Structural plasticity and memory. *Nat. Rev. Neurosci.* **5,** 45–54 (2004).
27. Feng, Z., Zeng, M., Chen, X. & Zhang, M. Neuronal Synapses: Microscale Signal Processing Machineries Formed by Phase Separation? *Biochemistry* **57,** 2530–2539 (2018).
28. Steiner, P. *et al.* Destabilization of the postsynaptic density by PSD-95 serine 73 phosphorylation inhibits spine growth and synaptic plasticity. *Neuron* **60,** 788–802 (2008).
29. Li, J. *et al.* Long-term potentiation modulates synaptic phosphorylation networks and reshapes the structure of the postsynaptic interactome. *Sci. Signal.* **9,** rs8-rs8 (2016).
30. Watson, N. V. & Breedlove, S. M. *The Mind's Machine: Foundations of Brain and Behavior*. (Sinauer Associates, Inc, 2015).
31. Santos, S. D., Carvalho, A. L., Caldeira, M. V. & Duarte, C. B. Regulation of AMPA receptors and synaptic plasticity. *Neuroscience* **158,** 105–125 (2009).
32. Granger, A. J., Gray, J. A., Lu, W. & Nicoll, R. A. Genetic analysis of neuronal ionotropic glutamate receptor subunits. *J. Physiol.* **589,** 4095–4101 (2011).
33. Collingridge, G. L., Olsen, R. W., Peters, J. & Spedding, M. A nomenclature for ligand-gated ion channels. *Neuropharmacology* **56,** 2–5 (2009).
34. Collingridge, G. L., Isaac, J. T. R. & Wang, Y. T. Receptor trafficking and synaptic plasticity. *Nat. Rev. Neurosci.* **5,** 952–962 (2004).
35. Wenthold, R. J., Petralia, R. S., Blahos J, I. I. & Niedzielski, A. S. Evidence for multiple AMPA receptor complexes in hippocampal CA1/CA2 neurons. *J. Neurosci.* **16,** 1982–9 (1996).
36. Schwenk, J. *et al.* High-Resolution Proteomics Unravel Architecture and Molecular Diversity of Native AMPA Receptor Complexes. *Neuron* **74,** 621–633 (2012).
37. Cull-Candy, S., Kelly, L. & Farrant, M. Regulation of Ca2+-permeable AMPA receptors: synaptic plasticity and beyond. *Curr. Opin. Neurobiol.* **16,** 288–297 (2006).
38. Fernández, I. S. & Loddenkemper, T. Subunit composition of neurotransmitter receptors in the immature and in the epileptic brain. *Biomed Res. Int.* **2014,** 1–11 (2014).
39. Friedman, L. K. & Koudinov, A. R. Unilateral GluR2(B) hippocampal knockdown: a novel partial seizure model in the developing rat. *J. Neurosci.* **19,** 9412–25 (1999).
40. Talos, D. M. *et al.* Developmental regulation of α-amino-3-hydroxy-5-methyl-4-isoxazole-propionic acid receptor subunit expression in forebrain and relationship to regional susceptibility to hypoxic/ischemic injury. I. Rodent cerebral white matter and cortex. *J. Comp. Neurol.* **497,** 42–60 (2006).
41. Talos, D. M. *et al.* Developmental regulation of α-amino-3-hydroxy-5-methyl-4-isoxazole-propionic acid receptor subunit expression in forebrain and relationship to regional susceptibility to hypoxic/ischemic injury. II. Human cerebral white matter and cortex. *J. Comp. Neurol.* **497,** 61–77 (2006).
42. Park, P. *et al.* Calcium-Permeable AMPA Receptors Mediate the Induction of the Protein Kinase A-Dependent Component of Long-Term Potentiation in the Hippocampus. *J Neurosci* **36,** 622–631 (2016).
43. Plant, K. *et al.* Transient incorporation of native GluR2-lacking AMPA receptors during hippocampal long-term potentiation. *Nat. Neurosci.* **9,** 602–604 (2006).
44. Adesnik, H. & Nicoll, R. A. Conservation of Glutamate Receptor 2-Containing AMPA Receptors during Long-Term Potentiation. *J. Neurosci.* **27,** 4598–4602 (2007).
45. Mathern, G. W., Pretorius, J. K., Mendoza, D., Lozada, A. & Kornblum, H. I. Hippocampal AMPA and NMDA mRNA levels correlate with aberrant fascia dentata mossy fiber sprouting in the pilocarpine model of spontaneous limbic epilepsy. *J. Neurosci. Res.* **54,** 734–753 (1998).
46. Porter, B. E., Cui, X.-N. & Brooks-Kayal, A. R. Status epilepticus differentially alters AMPA and kainate receptor subunit expression in mature and immature dentate granule neurons. *Eur. J. Neurosci.* **23,** 2857–2863 (2006).
47. Lee, H.-K., Barbarosie, M., Kameyama, K., Bear, M. F. & Huganir, R. L. Regulation of distinct AMPA receptor phosphorylation sites during bidirectional synaptic plasticity. *Nature* **405,** 955–959 (2000).
48. Rodrigues, N. C. A. Vias de transdução envolvidas no efeito do VIP na LTP na área CA1 do hipocampo. (Faculdade de Ciências e Tecnologia, Universidade de Coimbra, 2009).

49. Park, P. *et al.* Calcium-permeable AMPA receptors mediate the induction of the protein kinase A-dependent component of long-term potentiation in the hippocampus. *J. Neurosci.* **36,** 622–631 (2016).
50. Roche, K. W., O'Brien, R. J., Mammen, A. L., Bernhardt, J. & Huganir, R. L. Characterization of multiple phosphorylation sites on the AMPA receptor GluR1 subunit. *Neuron* **16,** 1179–88 (1996).
51. Derkach, V., Barria, A. & Soderling, T. R. Ca2+/calmodulin-kinase II enhances channel conductance of alpha-amino-3-hydroxy-5-methyl-4-isoxazolepropionate type glutamate receptors. *Proc. Natl. Acad. Sci. U. S. A.* **96,** 3269–74 (1999).
52. Esteban, J. A. *et al.* PKA phosphorylation of AMPA receptor subunits controls synaptic trafficking underlying plasticity. *Nat. Neurosci.* **6,** 136–143 (2003).
53. Sanderson, J. L. & Dell'Acqua, M. L. AKAP Signaling Complexes in Regulation of Excitatory Synaptic Plasticity. *Neurosci.* **17,** 321–336 (2011).
54. Banke, T. G. *et al.* Control of GluR1 AMPA receptor function by cAMP-dependent protein kinase. *J. Neurosci.* **20,** 89–102 (2000).
55. Lopes, M. W. *et al.* Time-dependent modulation of AMPA receptor phosphorylation and mRNA expression of NMDA receptors and glial glutamate transporters in the rat hippocampus and cerebral cortex in a pilocarpine model of epilepsy. *Exp. Brain Res.* **226,** 153–163 (2013).
56. Tempel, B. L., Jan, Y. N. & Jan, L. Y. Cloning of a probable potassium channel gene from mouse brain. *Nature* **332,** 837–9 (1988).
57. Beck, H. & Yaari, Y. Plasticity of intrinsic neuronal properties in CNS disorders. *Nat. Rev. Neurosci.* **9,** 357–369 (2008).
58. Miller, C. An overview of the potassium channel family. *Genome Biol.* **1,** reviews0004.1 (2000).
59. Hoffman, D. A., Magee, J. C., Colbert, C. M. & Johnston, D. K+ channel regulation of signal propagation in dendrites of hippocampal pyramidal neurons. *Nature* **387,** 869–875 (1997).
60. Kerti, K., Lorincz, A. & Nusser, Z. Unique somato-dendritic distribution pattern of Kv4.2 channels on hippocampal CA1 pyramidal cells. *Eur. J. Neurosci.* **35,** 66–75 (2012).
61. Sansom, M. S. Potassium channels: watching a voltage-sensor tilt and twist. *Curr. Biol.* **10,** R206-9 (2000).
62. Varga, A. W., Anderson, A. E., Adams, J. P., Vogel, H. & Sweatt, J. D. Input-specific immunolocalization of differentially phosphorylated Kv4.2 in the mouse brain. *Learn. Mem.* **7,** 321–32 (2000).
63. Schrader, L. A. *et al.* ERK/MAPK regulates the Kv4.2 potassium channel by direct phosphorylation of the pore-forming subunit. *Am. J. Physiol. Physiol.* **290,** C852–C861 (2006).
64. Hu, H.-J. *et al.* The Kv4.2 Potassium Channel Subunit Is Required for Pain Plasticity. *Neuron* **50,** 89–100 (2006).
65. Hammond, R. S., Lin, L., Sidorov, M. S., Wikenheiser, A. M. & Hoffman, D. A. Protein kinase a mediates activity-dependent Kv4.2 channel trafficking. *J. Neurosci.* **28,** 7513–9 (2008).
66. Varga, A. W. *et al.* Calcium-Calmodulin-Dependent Kinase II Modulates Kv4.2 Channel Expression and Upregulates Neuronal A-Type Potassium Currents. *J. Neurosci.* **24,** 3643–3654 (2004).
67. Kim, J. & Hoffman, D. A. Potassium Channels: Newly Found Players in Synaptic Plasticity. *Neurosci.* **14,** 276–286 (2008).
68. Kim, J., Jung, S.-C., Clemens, A. M., Petralia, R. S. & Hoffman, D. A. Regulation of Dendritic Excitability by Activity-Dependent Trafficking of the A-Type K+ Channel Subunit Kv4.2 in Hippocampal Neurons. *Neuron* **54,** 933–947 (2007).
69. Juhng, K. N. *et al.* Induction of seizures by the potent K+ channel-blocking scorpion venom peptide toxins tityustoxin-K(alpha) and pandinustoxin-K(alpha). *Epilepsy Res.* **34,** 177–86 (1999).
70. Bernard, C. *et al.* Acquired Dendritic Channelopathy in Temporal Lobe Epilepsy. *Science (80-.).* **305,** 532–535 (2004).
71. UniProtKB - P60880 (SNP25_HUMAN). Available at: https://www.uniprot.org/uniprot/P60880. (Accessed: 24th October 2018)
72. Greaves, J. & Chamberlain, L. H. Differential palmitoylation regulates intracellular patterning of SNAP25. *J. Cell Sci.* **124,** 1351–60 (2011).

73. Aicart-Ramos, C., Valero, R. A. & Rodriguez-Crespo, I. Protein palmitoylation and subcellular trafficking. *Biochim. Biophys. Acta - Biomembr.* **1808,** 2981–2994 (2011).
74. Roberts, L. A., Morris, B. J. & O'Shaughnessy, C. T. Involvement of two isoforms of SNAP-25 in the expression of long-term potentiation in the rat hippocampus. *Neuroreport* **9,** 33–6 (1998).
75. Genoud, S. *et al.* Activity-dependent phosphorylation of SNAP-25 in hippocampal organotypic cultures. *J. Neurochem.* **72,** 1699–706 (1999).
76. Kennedy, M. B. Signal-processing machines at the postsynaptic density. *Science* **290,** 750–4 (2000).
77. Zacchi, P., Antonelli, R. & Cherubini, E. Gephyrin phosphorylation in the functional organization and plasticity of GABAergic synapses. *Front. Cell. Neurosci.* **8,** 103 (2014).
78. Kennedy, M. B. The postsynaptic density at glutamatergic synapses. *Trends Neurosci.* **20,** 264–8 (1997).
79. El-Husseini, A. E., Schnell, E., Chetkovich, D. M., Nicoll, R. A. & Bredt, D. S. PSD-95 involvement in maturation of excitatory synapses. *Science* **290,** 1364–8 (2000).
80. Zaręba-Kozioł, M., Figiel, I., Bartkowiak-Kaczmarek, A. & Włodarczyk, J. Insights Into Protein S-Palmitoylation in Synaptic Plasticity and Neurological Disorders: Potential and Limitations of Methods for Detection and Analysis. *Front. Mol. Neurosci.* **11,** 175 (2018).
81. Tulodziecka, K. *et al.* Remodeling of the postsynaptic plasma membrane during neural development. *Mol. Biol. Cell* **27,** 3480–3489 (2016).
82. Jeyifous, O. *et al.* Palmitoylation regulates glutamate receptor distributions in postsynaptic densities through control of PSD95 conformation and orientation. *Proc. Natl. Acad. Sci. U. S. A.* **113,** E8482–E8491 (2016).
83. Ehrlich, I. & Malinow, R. Postsynaptic Density 95 controls AMPA Receptor Incorporation during Long-Term Potentiation and Experience-Driven Synaptic Plasticity. *J. Neurosci.* **24,** 916–927 (2004).
84. Ogino, K. *et al.* Duplicated Gephyrin Genes Showing Distinct Tissue Distribution and Alternative Splicing Patterns Mediate Molybdenum Cofactor Biosynthesis, Glycine Receptor Clustering, and Escape Behavior in Zebrafish. *J. Biol. Chem.* **286,** 806–817 (2011).
85. Fritschy, J.-M., Harvey, R. J. & Schwarz, G. Gephyrin: where do we stand, where do we go? *Trends Neurosci.* **31,** 257–264 (2008).
86. Tretter, V. *et al.* Gephyrin, the enigmatic organizer at GABAergic synapses. *Front. Cell. Neurosci.* **6,** 23 (2012).
87. Tyagarajan, S. K. & Fritschy, J.-M. Gephyrin: a master regulator of neuronal function? *Nat. Rev. Neurosci.* **15,** 141–156 (2014).
88. Förstera, B. *et al.* Irregular RNA splicing curtails postsynaptic gephyrin in the cornu ammonis of patients with epilepsy. *Brain* **133,** 3778–3794 (2010).
89. Fang, M. *et al.* Downregulation of Gephyrin in Temporal Lobe Epilepsy Neurons in Humans and a Rat Model. *Synapse* **65,** 1006–1014 (2011).
90. Blümcke, I. *et al.* Altered distribution of the alpha-amino-3-hydroxy-5-methyl-4-isoxazole propionate receptor subunit GluR2(4) and the N-methyl-D-aspartate receptor subunit NMDAR1 in the hippocampus of patients with temporal lobe epilepsy. *Acta Neuropathol.* **92,** 576–87 (1996).
91. Mathern, G. W. *et al.* Hippocampal AMPA and NMDA mRNA levels and subunit immunoreactivity in human temporal lobe epilepsy patients and a rodent model of chronic mesial limbic epilepsy. *Epilepsy Res.* **32,** 154–71 (1998).
92. Palomero-Gallagher, N. *et al.* Multireceptor analysis in human neocortex reveals complex alterations of receptor ligand binding in focal epilepsies. *Epilepsia* **53,** 1987–1997 (2012).
93. Ying, Z., Bingaman, W. & Najm, I. M. Increased Numbers of Coassembled PSD-95 to NMDA-receptor Subunits NR2B and NR1 in Human Epileptic Cortical Dysplasia. *Epilepsia* **45,** 314–321 (2004).
94. Condorelli, D. F. *et al.* Changes in gene expression of AMPA-selective glutamate receptor subunits induced by status epilepticus in rat brain. *Neurochem. Int.* **25,** 367–76 (1994).
95. Rajasekaran, K., Todorovic, M. & Kapur, J. Calcium-permeable AMPA receptors are expressed in a rodent model of status epilepticus. *Ann. Neurol.* **72,** 91–102 (2012).
96. Lorgen, J.-Ø., Egbenya, D. L., Hammer, J. & Davanger, S. PICK1 facilitates lasting reduction in

GluA2 concentration in the hippocampus during chronic epilepsy. *Epilepsy Res.* **137,** 25–32 (2017).
97. Russo, I., Bonini, D., La Via, L., Barlati, S. & Barbon, A. AMPA receptor properties are modulated in the early stages following pilocarpine-induced status epilepticus. *Neuronal Med* **15,** 324–338 (2013).
98. Singer, S. J. & Nicolson, G. L. The fluid mosaic model of the structure of cell membranes. *Science* **175,** 720–31 (1972).
99. Nickels, J. D., Smith, J. C. & Cheng, X. Lateral organization, bilayer asymmetry, and inter-leaflet coupling of biological membranes. *Chem. Phys. Lipids* **192,** 87–99 (2015).
100. Marquês, J. T., Antunes, C. A. C., Santos, F. C. & de Almeida, R. F. M. Biomembrane Organization and Function: The Decisive Role of Ordered Lipid Domains. *Adv. Planar Lipid Bilayers Liposomes* **22,** 65–96 (2015).
101. Aureli, M., Grassi, S., Prioni, S., Sonnino, S. & Prinetti, A. Lipid membrane domains in the brain. *Biochim. Biophys. Acta - Mol. Cell Biol. Lipids* **1851,** 1006–1016 (2015).
102. Sebastiao, A. M., Colino-Oliveira, M., Assaife-Lopes, N., Dias, R. B. & Ribeiro, J. A. Lipid rafts, synaptic transmission and plasticity: Impact in age-related neurodegenerative diseases. *Neuropharmacology* **64,** 97–107 (2013).
103. Edidin, M. Lipids on the frontier: a century of cell-membrane bilayers. *Nat. Rev. Mol. Cell Biol.* **4,** 414–418 (2003).
104. Simons, K. & Ikonen, E. Functional rafts in cell membranes. *Nature* **387,** 569–572 (1997).
105. Pike, L. J. Rafts defined: a report on the Keystone symposium on lipid rafts and cell function. *J. Lipid Res.* **47,** 1597–1598 (2006).
106. Allen, J. A., Halverson-Tamboli, R. A. & Rasenick, M. M. Lipid raft microdomains and neurotransmitter signalling. *Nat. Rev.* **8,** 128–140 (2007).
107. Korade, Z. & Kenworthy, A. K. Lipid rafts, cholesterol, and the brain. *Neuropharmacology* **55,** 1265–73 (2008).
108. Burger, K., Gimpl, G. & Fahrenholz, F. Regulation of receptor function by cholesterol. *Cell. Mol. Life Sci.* **57,** 1577–92 (2000).
109. Gaudreault, S. B., Chabot, C., Gratton, J.-P. & Poirier, J. The caveolin scaffolding domain modifies 2-amino-3-hydroxy-5-methyl-4-isoxazole propionate receptor binding properties by inhibiting phospholipase A2 activity. *J. Biol. Chem.* **279,** 356–62 (2004).
110. Sooksawate, T. & Simmonds, M. A. Effects of membrane cholesterol on the sensitivity of the GABA(A) receptor to GABA in acutely dissociated rat hippocampal neurones. *Neuropharmacology* **40,** 178–84 (2001).
111. Colin, J. *et al.* Membrane raft domains and remodeling in aging brain. *Biochimie* **130,** 178–187 (2016).
112. Loura, L. M. S. & Almeida, R. F. M. de. *Tópicos de biofísica de membranas*. (Lidel, 2004).
113. Santos, F. C. *et al.* Reorganization of plasma membrane lipid domains during conidial germination. *Biochim. Biophys. Acta - Mol. Cell Biol. Lipids* **1862,** 156–166 (2017).
114. de Almeida, R. F. M. & Joly, E. Crystallization around solid-like nanosized docks can explain the specificity, diversity, and stability of membrane microdomains. *Front. Plant Sci.* **5,** 72 (2014).
115. de Almeida, R. F., Loura, L. M. & Prieto, M. Membrane lipid domains and rafts: current applications of fluorescence lifetime spectroscopy and imaging. *Chem. Phys. Lipids* **157,** 61–77 (2009).
116. de Almeida, R. F. M., Borst, J., Fedorov, A., Prieto, M. & Visser, A. J. W. G. Complexity of lipid domains and rafts in giant unilamellar vesicles revealed by combining imaging and microscopic and macroscopic time-resolved. *Biophys. J.* **93,** 539–553 (2007).
117. Uppamoochikkal, P., Tristram-Nagle, S. & Nagle, J. F. Orientation of Tie-Lines in the Phase Diagram of DOPC:DPPC:Cholesterol Model Biomembranes. *Langmuir* **26,** 17363 (2010).
118. PlasticityLab. Available at: https://www.plasticitylab.com/methods/. (Accessed: 26th October 2018)
119. Smejda Haug, F. M. Heavy metals in the brain. A light microscope study of the rat with Timm's sulphide silver method. Methodological considerations and cytological and regional staining patterns. *Adv. Anat. Embryol. Cell Biol.* **47,** 1–71 (1973).

120. Bradford, M. M. A rapid and sensitive method for the quantitation of microgram quantities of protein utilizing the principle of protein-dye binding. *Anal. Biochem.* **72,** 248–254 (1976).
121. Bass, J. J. *et al.* An overview of technical considerations for Western blotting applications to physiological research. *Scand. J. Med. Sci. Sports* **27,** 4–25 (2017).
122. Rouser, G., Fkeischer, S. & Yamamoto, A. Two dimensional thin layer chromatographic separation of polar lipids and determination of phospholipids by phosphorus analysis of spots. *Lipids* **5,** 494–6 (1970).
123. Angelova, M. I., Soléau, S., Méléard, P., Faucon, F. & Bothorel, P. Preparation of giant vesicles by external AC electric fields. Kinetics and applications. in *Trends in Colloid and Interface Science VI* 127–131 (Steinkopff, 1992). doi:10.1007/BFb0116295
124. Juhasz, J., Sharom, F. J. & Davis, J. H. Quantitative characterization of coexisting phases in DOPC/DPPC/cholesterol mixtures: Comparing confocal fluorescence microscopy and deuterium nuclear magnetic resonance. *Biochim. Biophys. Acta - Biomembr.* **1788,** 2541–2552 (2009).
125. Marquês, J. T., Viana, A. S. & de Almeida, R. F. M. A Biomimetic Platform to Study the Interactions of Bioelectroactive Molecules with Lipid Nanodomains. *Langmuir* **30,** 12627–12637 (2014).
126. Marsh, D. *Handbook of Lipid Bilayers*. (CRC Press, 2013).
127. Fidorra, M., Garcia, A., Ipsen, J. H., Härtel, S. & Bagatolli, L. A. Lipid domains in giant unilamellar vesicles and their correspondence with equilibrium thermodynamic phases: A quantitative fluorescence microscopy imaging approach. *Biochim. Biophys. Acta - Biomembr.* **1788,** 2142–2149 (2009).
128. Veatch, S. L., Polozov, I. V, Gawrisch, K. & Keller, S. L. Liquid domains in vesicles investigated by NMR and fluorescence microscopy. *Biophys. J.* **86,** 2910–22 (2004).
129. Jung, S.-C., Kim, J. & Hoffman, D. A. Rapid, Bidirectional Remodeling of Synaptic NMDA Receptor Subunit Composition by A-type K+ Channel Activity in Hippocampal CA1 Pyramidal Neurons. *Neuron* **60,** 657–671 (2008).
130. Jo, A. & Kim, H. K. Up-regulation of dendritic Kv4. 2 mRNA by activation of the NMDA receptor. *Neurosci. Lett.* **496,** 129–134 (2011).
131. Truchet, B. *et al.* Kv4 potassium channels modulate hippocampal EPSP-spike potentiation and spatial memory in rats. *Learn. Mem.* **19,** 282–93 (2012).
132. Ehrlich, I., Klein, M., Rumpel, S. & Malinow, R. PSD-95 is required for activity-driven synapse stabilization. *Proc. Natl. Acad. Sci. U. S. A.* **104,** 4176–81 (2007).
133. El-Husseini, A. E.-D. *et al.* Synaptic strength regulated by palmitate cycling on PSD-95. *Cell* **108,** 849–63 (2002).
134. Hou, Q. *et al.* SNAP-25 in hippocampal CA1 region is involved in memory consolidation. *Eur. J. Neurosci.* **20,** 1593–1603 (2004).
135. Hussain, S. *et al.* A possible postsynaptic role for SNAP-25 in hippocampal synapses. *Brain Struct. Funct.* (2018). doi:10.1007/s00429-018-1782-2
136. Antonucci, F. *et al.* SNAP-25, a Known Presynaptic Protein with Emerging Postsynaptic Functions. *Front. Synaptic Neurosci.* **8,** 7 (2016).
137. Lopim, G. M. *et al.* Relationship between seizure frequency and number of neuronal and non-neuronal cells in the hippocampus throughout the life of rats with epilepsy. *Brain Res.* **1634,** 179–186 (2016).
138. Mello, L. E. A. M. *et al.* Circuit Mechanisms of Seizures in the Pilocarpine Model of Chronic Epilepsy: Cell Loss and Mossy Fiber Sprouting. *Epilepsia* **34,** 985–995 (1993).
139. do Nascimento, A. L. *et al.* Neuronal degeneration and gliosis time-course in the mouse hippocampal formation after pilocarpine-induced status epilepticus. *Brain Res.* **1470,** 98–110 (2012).
140. Proper, E. A. *et al.* Immunohistochemical characterization of mossy fibre sprouting in the hippocampus of patients with pharmaco-resistant temporal lobe epilepsy. *Brain* **123 (Pt 1),** 19–30 (2000).
141. Mathern, G. W., Pretorius, J. K. & Babb, T. L. Quantified patterns of mossy fiber sprouting and neuron densities in hippocampal and lesional seizures. *J. Neurosurg.* **82,** 211–219 (1995).
142. Inostroza, M. *et al.* Hippocampal-Dependent Spatial Memory in the Water Maze is Preserved in

an Experimental Model of Temporal Lobe Epilepsy in Rats. *PLoS One* **6,** e22372 (2011).
143. Althaus, A. L., Zhang, H. & Parent, J. M. Axonal plasticity of age-defined dentate granule cells in a rat model of mesial temporal lobe epilepsy. *Neurobiol. Dis.* **86,** 187–196 (2016).
144. Song, I. & Huganir, R. L. Regulation of AMPA receptors during synaptic plasticity. *TRENDS Neurosci.* **25,** 578–88 (2002).
145. Kim, M. J. *et al.* Synaptic Accumulation of PSD-95 and Synaptic Function Regulated by Phosphorylation of Serine-295 of PSD-95. *Neuron* **56,** 488–502 (2007).
146. Béïque, J.-C. & Andrade, R. PSD-95 regulates synaptic transmission and plasticity in rat cerebral cortex. *J. Physiol.* **546,** 859–67 (2003).
147. Carlisle, H. J., Fink, A. E., Grant, S. G. N. & O'Dell, T. J. Opposing effects of PSD-93 and PSD-95 on long-term potentiation and spike timing-dependent plasticity. *J. Physiol.* **586,** 5885–5900 (2008).
148. Stein, V., House, D. R. C., Bredt, D. S. & Nicoll, R. A. Postsynaptic density-95 mimics and occludes hippocampal long-term potentiation and enhances long-term depression. *J. Neurosci.* **23,** 5503–6 (2003).
149. Petrini, E. M. *et al.* Synaptic recruitment of gephyrin regulates surface GABAA receptor dynamics for the expression of inhibitory LTP. *Nat. Commun.* **5,** 3921 (2014).
150. Head, B. P. *et al.* Loss of Caveolin-1 Accelerates Neurodegeneration and Aging. *PLoS One* **5,** e15697 (2010).
151. Gaudreault, S. B., Blain, J.-F., Gratton, J.-P. & Poirier, J. A role for caveolin-1 in post-injury reactive neuronal plasticity. *J. Neurochem.* **92,** 831–839 (2005).
152. Swanwick, C. C., Shapiro, M. E., Vicini, S. & Wenthold, R. J. Flotillin-1 promotes formation of glutamatergic synapses in hippocampal neurons. *Dev. Neurobiol.* **70,** 875–83 (2010).
153. Hering, H., Lin, C.-C. & Sheng, M. Lipid rafts in the maintenance of synapses, dendritic spines, and surface AMPA receptor stability. *J. Neurosci.* **23,** 3262–71 (2003).

8. Appendix

8.1. Calibration curves for the Bradford method

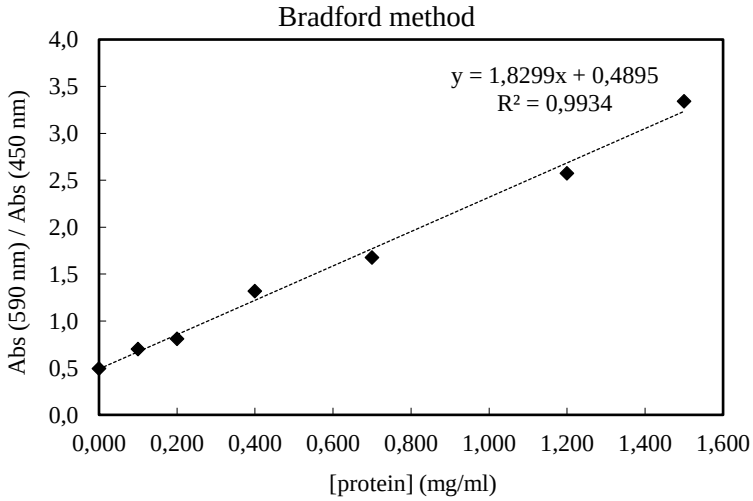

Figure 8.1. Calibration curve for the Bradford method[120], for determination of protein concentration of C and θ samples. The dashed line represents the linear adjustment for the ratio of the absorbances read at 590 nm and 450 nm obtained for each protein concentration. R^2 is the coefficient of determination, which reflects the quality of the linear regression (the closer to 1 the better the adjustment).

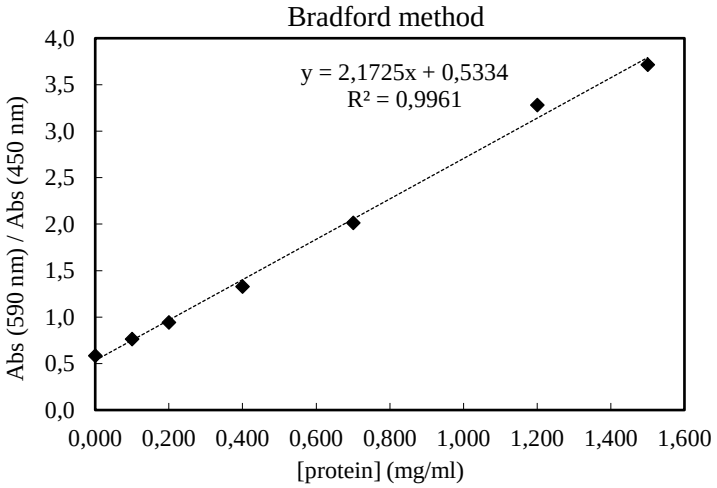

Figure 8.2. Calibration curve for the Bradford method[120] for determination of protein concentration of *Sham* and Epi samples. The dashed line represents the linear adjustment for the ratio of the absorbances read at 590 nm and 450 nm obtained for each protein concentration. R^2 is the coefficient of determination.

8.2. Calibration curve for the Rouser method

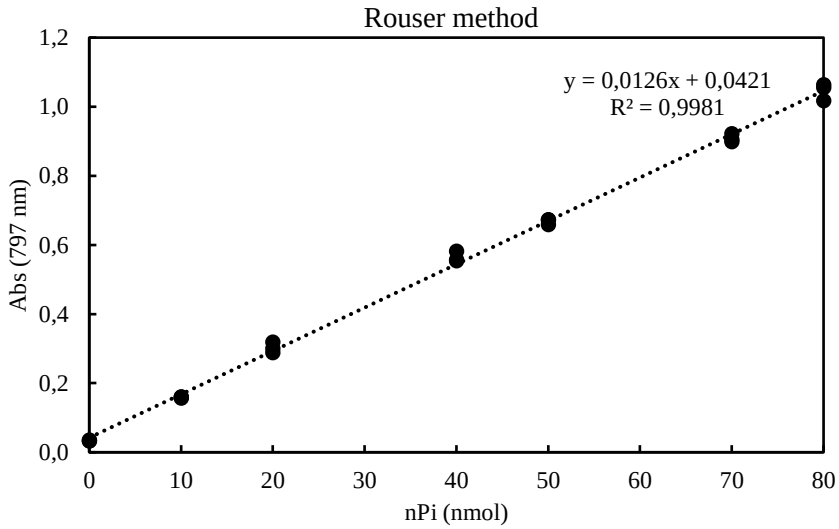

Figure 8.3. Calibration curve for the phospholipid quantification by Rouser method [122], used to quantify DPPC and DOPC. The dashed line represents the linear fit for the three replicates obtained for each phosphate (Pi) quantity. R^2 is the coefficient of determination.

8.3. Rhod-DOPE absorption spectrum

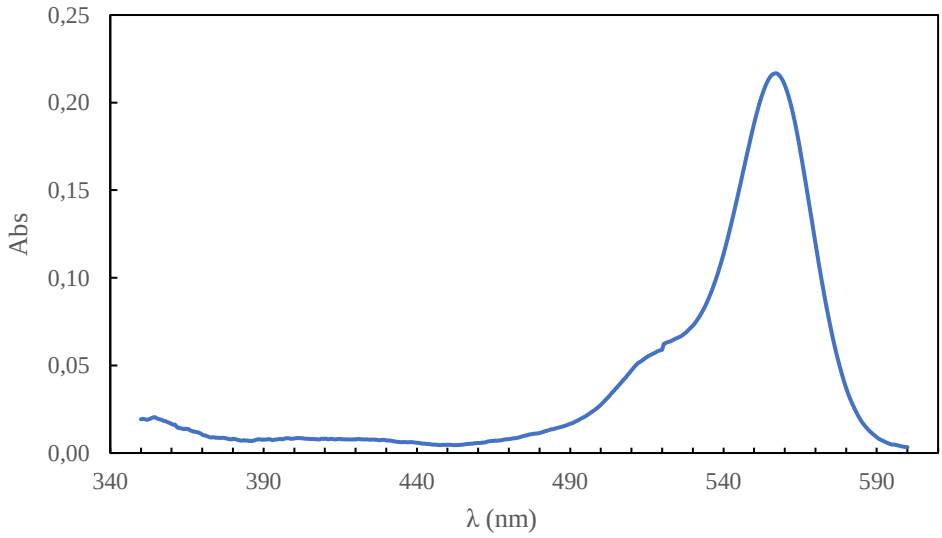

Figure 8.4. Absorption spectrum of Rhod-DOPE in chloroform at room temperature. The maximum of absorbance occurs at 559 nm with a value of 0.2136. Rhod-DOPE was at 0.1 mM.